

AN INVESTIGATION OF JAMMING TECHNIQUES THROUGH A RADAR
RECEIVER SIMULATION

A THESIS SUBMITTED TO
THE GRADUATE SCHOOL OF NATURAL AND APPLIED SCIENCES
OF
MIDDLE EAST TECHNICAL UNIVERSITY

BY

ATİYE ASLI KIRKPANTUR-ÇADALLI

IN PARTIAL FULFILLMENT OF THE REQUIREMENTS
FOR
THE DEGREE OF MASTER OF SCIENCE
IN
ELECTRICAL AND ELECTRONICS ENGINEERING

DECEMBER 2007

Approval of the thesis:

**AN INVESTIGATION OF JAMMING TECHNIQUES THROUGH A
RADAR RECEIVER SIMULATION**

submitted by **ATIYE ASLI KIRKPANTUR-ÇADALLI** in partial fulfillment of
the requirements for the degree of **Master of Science in Electrical and Electronics
Engineering Department, Middle East Technical University** by,

Prof. Dr. Canan Özgen _____
Dean, Graduate School of **Natural and Applied Sciences**

Prof. Dr. İsmet Erkmek _____
Head of Department, **Electrical and Electronics Engineering**

Assoc. Prof. Dr. Sencer Koç _____
Supervisor, **Electrical and Electronics Engineering Dept., METU**

Prof. Dr. Yalçın Tanık _____
Co-Supervisor, **Electrical and Electronics Engineering Dept., METU**

Examining Committee Members:

Prof. Dr. Fatih Canatan _____
Electrical and Electronics Engineering Dept., METU

Assoc. Prof. Dr. Sencer Koç _____
Electrical and Electronics Engineering Dept., METU

Prof. Dr. Yalçın Tanık _____
Electrical and Electronics Engineering Dept., METU

Assist. Prof. Dr. Çağatay Candan _____
Electrical and Electronics Engineering Dept., METU

Dr. Mehmet Ali Tuğay _____
Engineering Director, MİKES

Date: 6 December 2007

I hereby declare that all information in this document has been obtained and presented in accordance with academic rules and ethical conduct. I also declare that, as required by these rules and conduct, I have fully cited and referenced all material and results that are not original to this work.

Name, Last Name : Atiye Aslı Kırkpantur-Çadallı

Signature :

ABSTRACT

AN INVESTIGATION OF JAMMING TECHNIQUES THROUGH A RADAR RECEIVER SIMULATION

Kırkpantur-Çadallı, Atiye Aslı

M.S., Department of Electrical and Electronics Engineering

Supervisor : Assoc. Prof. Dr. Sencer Koç

Co- Supervisor: Prof. Dr. Yalçın Tanık

December 2007, 120 pages

In this study, various jamming techniques and their effects on detection and tracking performance have been investigated through a radar receiver simulation that models a search radar for target acquisition and single-target tracking radar during track operation. The radar is modeled as looking at airborne targets, and hence clutter is not considered. Customized algorithms have been developed for the detection of target azimuth angle, range and Doppler velocity within the modeled geometry and chosen radar parameters. The effects of varying parameters like jamming-to-signal ratio (JSR) and jamming signal's Doppler shift have been examined in the analysis of jamming effectiveness.

Keywords: Radar Receiver, Detection, Target Tracking, RGPO, Jamming Effectiveness

ÖZ

RADAR KARIŐTIRMA YÖNTEMLERİNİN BİR RADAR ALMAÇ BENZETİMİ ÜZERİNDE İNCELENMESİ

Kırkpantur-Çadallı, Atiye Aslı

Yüksek Lisans Tezi, Elektrik ve Elektronik Mühendisliđi Bölümü

Tez Yöneticisi : Doç. Dr. Sencer Koç

Ortak Tez Yöneticisi: Prof. Dr. Yalçın Tanık

Aralık 2007, 120 sayfa

Bu çalışmada, deđişik karıştırma teknikleri ile bu tekniklerin radar hedef tespit ve izleme başarımına etkileri, hedef arama modunda tarama radarı olarak çalışan ve hedef takip modunda, tek hedef takibi yapan bir radar almaç benzetimi üzerinde incelenmiştir. Benzetimi yapılan radar modeli, hava hedeflerini ve hava platformunu kapsamaktadır. Bu nedenle yüzey kargaşasının benzetimi gerekli görülmemiştir. Model yapısı ve seçilen radar parametreleri dikkate alınarak hedefin açısal koordinatının, menziline ve Doppler frekans kaymasının tespiti için uygun algoritmalar geliştirilmiştir. Karıştırma-sinyal oranı ve karıştırma sinyalinin frekans kayması gibi parametreler deđiştirilerek karıştırma etkinliđi incelenmiştir.

Anahtar Kelimeler: Radar Almaç, Tespit, Hedef İzleme, RGPO, karıştırma etkinliđi

To My Parents and My Husband

ACKNOWLEDGEMENTS

I would like to express my deepest gratitude to my supervisor Assoc. Prof. Dr. Sencer Koç and co-supervisor Prof. Dr. Yalçın Tanık for their guidance, insightful advice and criticism, and constant encouragement throughout this research.

I would like to thank my colleagues at MİKES Inc. for their support on every phase of this work.

I would like to thank my whole family for their constant care and understanding throughout my life and their sincere trust that I could accomplish this task.

I would like to thank my husband for his support and tolerance during my thesis study.

TABLE OF CONTENTS

ABSTRACT	iv
ÖZ	v
ACKNOWLEDGEMENTS	vii
TABLE OF CONTENTS	viii
CHAPTER	
1. INTRODUCTION	1
2. BASIC PRINCIPLES OF RADAR	3
2.1 Classification of Radars	3
2.2 The Radar Equation	4
2.3 Basic Pulsed Radar Block Diagram	4
2.3.1 Pulse-Doppler radar	6
2.4 Radar Block Diagram Basic Elements	8
2.4.1 Synchronizer	8
2.4.2 Modulator	8
2.4.3 Transmitter	8
2.4.4 Duplexer	8
2.4.5 Antenna	8
2.4.6 Receiver protection device	9
2.4.7 Receiver	9
2.4.8 Indicator	10
2.4.9 Antenna servo	10
2.5 Target Tracking	11
2.5.1 Single target tracking (continuous tracking)	11
2.5.1.1 Angle tracking	11
2.5.1.2 Range tracking	12
2.5.2 Multiple target tracking	13
3. RADAR SIMULATION	15
3.1 Transmitter-Receiver Simulation	15

3.2	Delay-Doppler Detection.....	22
3.2.1	Computation of the power spectral density.....	22
3.2.2	Detection using PSD.....	24
3.3	Azimuth Angle Detection.....	28
3.4	Tracking.....	30
3.4.1	Tracking Filter.....	32
3.5	Tracking Performance under No Jamming.....	37
4.	JAMMING AND ITS EFFECTIVENESS.....	48
4.1	The Jamming Concept.....	48
4.1.1	Noise Technique.....	48
4.1.2	Range Gate Pull Off (RGPO).....	49
4.1.2.1	Jamming procedure.....	51
4.1.2.2	ECM parameters.....	53
4.1.2.3	Required radar signal parameters.....	53
4.1.3	Related Techniques.....	54
4.1.3.1	RGPI.....	54
4.1.3.2	Overlapped RGPO.....	55
4.1.3.3	RGPO with hold out (hook).....	55
4.2	Tracking Performance under Jamming.....	56
4.2.1	Spot-Noise Jamming.....	56
4.2.2	RGPO.....	64
4.2.3	RGPI.....	79
4.2.4	Overlapped RGPO.....	86
4.2.5	RGPO with hold-out.....	92
5.	CONCLUSIONS.....	100
	REFERENCES.....	103

LIST OF FIGURES

Figure 2-1: Basic pulse radar block diagram.....	5
Figure 2-2: Radar receiver block diagram.....	10
Figure 3-1: Depiction of the simulated radar scenario.....	17
Figure 3-2: Target range within the search period.....	19
Figure 3-3: Received power in the search period.	19
Figure 3-4: Scanning antenna pattern gain in the search period.	20
Figure 3-5: Received radar signal with white Gaussian noise.	22
Figure 3-6: Power spectral density of the received pulses as a function of delay and Doppler frequency.	23
Figure 3-7: Projection of PSD along the Doppler axis onto the delay axis.	25
Figure 3-8: Magnified version of Figure 3-7. Detection threshold is indicated.....	25
Figure 3-9: Doppler frequency reading from the cross section of PSD.....	26
Figure 3-10: Received signal as a function of the radar scan angle is used for angle detection.	29
Figure 3-11: Angle detection is performed using curve fitting.	29
Figure 3-12: Data collection of the radar in the search and track modes.....	32
Figure 3-13: Pole-zero plot of the tracking filter with $\xi = 0.8$	35
Figure 3-14: Range performance of the tracking filter; update interval is 0.05 s; smoothing coefficient is 0.8.	36
Figure 3-15: Velocity performance of the tracking filter; update interval is 0.05 s; smoothing coefficient is 0.8.	37
Figure 3-16: Received signal and thermal noise during the first snapshot.	38
Figure 3-17: PSD of the return signal within the range gate, and its projection on delay axis.....	40
Figure 3-18: Doppler measurement within the first snapshot.	40
Figure 3-19: CFAR noise power estimate throughout the snapshots.	41
Figure 3-20: Range estimates/measurements for no-jamming tracking scenario.	43
Figure 3-21: Velocity estimates/measurements for no-jamming tracking scenario.	43

Figure 3-22: Error of range measurements/estimates for no-jamming tracking scenario.	44
Figure 3-23: Error of velocity measurements/estimates for no-jamming tracking scenario.	44
Figure 3-24: Range estimates/measurements for a stationary target at 10050 m.	45
Figure 3-25: Range estimates/measurements for a stationary target at 10075 m.	46
Figure 3-26: Velocity estimates/measurements for a target with no velocity representation error.	47
Figure 4-1: RGPO Video Programming Waveforms	52
Figure 4-2: RGPO pulse generation.....	52
Figure 4-3: Target return and the jamming noise for the last snapshot (Snapshot 100) and the received signal throughout snapshots. Spot-noise, $JSR_{spn} = 6$ dB.	57
Figure 4-4: Target range, jammer transmit/received power. Spot-noise, $JSR_{spn} = 6$ dB.	57
Figure 4-5: CFAR noise power estimate throughout the snapshots. Spot-noise, $JSR_{spn} = 6$ dB.	58
Figure 4-6: PSD for the last snapshot of spot-noise jamming simulation for $JSR_{spn} = 6$ dB.	58
Figure 4-7: Spot-noise jamming, $JSR_{spn} = 6$ dB. Range measurements/estimates. ...	60
Figure 4-8: Spot-noise jamming, $JSR_{spn} = 6$ dB. Velocity measurements/estimates.	60
Figure 4-9: Spot-noise jamming, $JSR_{spn} = 6$ dB. Error of range measurements/estimates.	61
Figure 4-10: Spot-noise jamming, $JSR_{spn} = 6$ dB. Error of velocity measurements/estimates.	61
Figure 4-11: Spot-noise jamming, $JSR_{spn} = 8$ dB. Range measurements/estimates.	62
Figure 4-12: Spot-noise jamming, $JSR_{spn} = 8$ dB. Velocity measurements/estimates.	62
Figure 4-13: Spot-noise jamming, $JSR_{spn} = 8$ dB. Error of range measurements/estimates.	63

Figure 4-14: Spot-noise jamming, $JSR_{spn} = 8$ dB. Error of velocity measurements/estimates.	63
Figure 4-15: Spot-noise jamming, $JSR_{spn} = 9$ dB. Range measurements/estimates. Track is dropped due to the lack of measurement updates.	64
Figure 4-16: RGPO offset and gain profiles.	65
Figure 4-17: A typical RGPO sample-offset profile.	66
Figure 4-18: RGPO. Snapshot 1, cover pulse. Spot-noise present. $s_{RGPO} = 1.3$ samples/s.	68
Figure 4-19: RGPO. Snapshot 108, jamming pulse starts pull-off. Spot-noise present. $s_{RGPO} = 1.3$ samples/s.	68
Figure 4-20: RGPO. Snapshot 203, further in pull-off. Spot-noise not present. $s_{RGPO} = 1.3$ samples/s.	69
Figure 4-21: RGPO. Snapshot 384, hold period. Spot-noise not present. $s_{RGPO} = 1.3$ samples/s.	69
Figure 4-22: RGPO. CFAR noise power estimate. $s_{RGPO} = 1.3$ samples/s.	70
Figure 4-23: RGPO. Range measurements/estimates. $JSR_{spn} = 6$ dB, $JSR = 6$ dB, $s_{RGPO} = 1.3$ samples/s.	71
Figure 4-24: RGPO. Velocity measurements/estimates. $JSR_{spn} = 6$ dB, $JSR = 6$ dB, $s_{RGPO} = 1.3$ samples/s.	72
Figure 4-25: RGPO. Range measurements/estimates. $JSR_{spn} = 6$ dB, $JSR = -6$ dB, $s_{RGPO} = 1.3$ samples/s.	73
Figure 4-26: Close-up of Figure 4-25.	74
Figure 4-27: RGPO. Velocity measurements/estimates. $JSR_{spn} = 6$ dB, $JSR = -6$ dB, $s_{RGPO} = 1.3$ samples/s.	75
Figure 4-28: RGPO. Range measurements/estimates. $JSR_{spn} = 6$ dB, $JSR = -7$ dB, $s_{RGPO} = 1.3$ samples/s.	76
Figure 4-29: RGPO. Velocity measurements/estimates. $JSR_{spn} = 6$ dB, $JSR = -7$ dB, $s_{RGPO} = 1.3$ samples/s.	77
Figure 4-30: RGPO. Range measurements/estimates. $JSR_{spn} = 6$ dB, $JSR = -3$ dB, $s_{RGPO} = 2.7$ samples/s.	78
Figure 4-31: RGPI offset and gain profiles.	81

Figure 4-32: RGPI. Snapshot 108, jamming pulse starts pulling in. Spot-noise present. $s_{RGPI} = -1.3$ samples/s.	81
Figure 4-33: RGPI. Snapshot 170, further in pull-in. Spot-noise present. $s_{RGPI} = -1.3$ samples/s.	82
Figure 4-34: RGPI. Snapshot 384, hold period. Spot-noise not present. $s_{RGPI} = -1.3$ samples/s.	82
Figure 4-35: RGPI. Range measurements/estimates. $JSR_{spn} = 6$ dB, $JSR = 6$ dB, $s_{RGPI} = -1.3$ samples/s.	83
Figure 4-36: RGPI. Velocity measurements/estimates. $JSR_{spn} = 6$ dB, $JSR = 6$ dB, $s_{RGPI} = -1.3$ samples/s.	84
Figure 4-37: RGPI. Range measurements/estimates. $JSR_{spn} = 6$ dB, $JSR = -5$ dB, $s_{RGPI} = -1.3$ samples/s.	85
Figure 4-38: RGPI. Range measurements/estimates. $JSR_{spn} = 6$ dB, $JSR = -6$ dB, $s_{RGPI} = -1.3$ samples/s.	86
Figure 4-39: RGPO offset and gain profiles. $s_{RGPO} = 2.7$ samples/s.	87
Figure 4-40: Overlapping RGPO pulse's offset and gain profiles. $s_{OVLP-RGPO} = 1.3$ samples/s.	87
Figure 4-41: Overlapped RGPO. Range measurements/estimates. $JSR_{spn} = 6$ dB, $JSR = 6$ dB, $s_{RGPO} = 2.7$ samples/s, $s_{OVLP-RGPO} = 1.3$ samples/s.	89
Figure 4-42: Overlapped RGPO. Velocity measurements/estimates. $JSR_{spn} = 6$ dB, $JSR = 6$ dB, $s_{OVLP-RGPO} = 2.7$ samples/s. $s_{RGPO} = 1.3$ samples/s.	90
Figure 4-43: Overlapped RGPO. Range measurements/estimates. $JSR_{spn} = 6$ dB, $JSR = -6$ dB, $s_{RGPO} = 2.7$ samples/s, $s_{OVLP-RGPO} = 1.3$ samples/s.	91
Figure 4-44: Overlapped RGPO. Range measurements/estimates. $JSR_{spn} = 6$ dB, $JSR = -7$ dB, $s_{RGPO} = 2.7$ samples/s, $s_{OVLP-RGPO} = 1.3$ samples/s.	92
Figure 4-45: RGPO with hold-out. RGPO offset and gain profiles. $s_{RGPO} = 1.3$ samples/s.	93
Figure 4-46: RGPO with hold-out. Hold-out offset and gain profiles.	93
Figure 4-47: RGPO with hold-out. Range measurements/estimates. $JSR_{spn} = 6$ dB, $JSR = 6$ dB, $s_{RGPO} = 1.3$ samples/s.	95

Figure 4-48: RGPO with hold-out. Velocity measurements/estimates. $JSR_{spn} = 6$ dB, $JSR = 6$ dB, $s_{RGPO} = 1.3$ samples/s.....	96
Figure 4-49: RGPO with hold-out. Range measurements/estimates. $JSR_{spn} = 6$ dB, $JSR = -6$ dB, $s_{RGPO} = 1.3$ samples/s.	97
Figure 4-50: RGPO with hold-out. Range measurements/estimates. $JSR_{spn} = 6$ dB, $JSR = -7$ dB, $s_{RGPO} = 1.3$ samples/s.	98
Figure 4-51: RGPO with hold-out. Range measurements/estimates. $JSR_{spn} = 6$ dB, $JSR = -3$ dB, $s_{RGPO} = 2.7$ samples/s.	99

LIST OF ABBREVIATIONS

RF	: Radio frequency
PRF	: Pulse repetition frequency
PRI	: Pulse repetition interval
PW	: Pulse width
AM	: Amplitude Modulation
JSR	: Jamming to signal ratio
RCS	: Radar Cross Section
RGPO	: Range Gate Pull Off
RGPI	: Range Gate Pull In
DRFM	: Digital Radio Frequency Memory
SNR	: Signal to Noise Ratio
TWS	: Track While Scan
CW	: Continuous Wave
IF	: Intermediate frequency
MTI	: Moving Target Indicator
LO	: Local Oscillator
PSD	: Power Spectral Density
P_{FA}	: Probability of False Alarm

CHAPTER 1

INTRODUCTION

Important functions of a radar system include detection and tracking of targets. Since some radar systems can be used for guiding missiles, it is important to disrupt the tracking lock on a target. Jamming techniques can be used for such purposes. The main focus of this thesis is to find out the effectiveness of various jamming techniques by using a simulated radar receiver.

The radar receiver model assumes an air-to-air target and platform environment. For instance, the scenario can be as follows: the radar platform is an aggressor (a high performance attack aircraft such as MIG, Mirage, F-16 etc.) that has fire control radar. The target is a defending aircraft with an embedded self-protection electronic warfare (EW) system that can utilize jamming to avoid fire from the aggressor. The aggressor aircraft tries to detect and track and send missiles onward. The defending aircraft on the other hand tries various jamming techniques to break the tracking lock or to deceive the aggressor from locking onto the defending aircraft itself.

The radar receiver simulation here uses a medium-PRF pulse-Doppler radar model, in order to provide less range ambiguity than high-PRF and less Doppler ambiguity than low-PRF pulse-Doppler radars, for searching targets. The detection of targets is performed in azimuth angle, range and Doppler velocity dimensions within a single swing of the radar antenna through the scan sector. The elevation angle is not taken into account.

After detection of targets, the receiver switches to a single-target-track mode for continuous tracking of a selected target with the beam of the radar directed towards the respective azimuth angle. For the purposes of this thesis, multiple target tracking has not been investigated.

For the purposes of this thesis, it is assumed that the targets move with a constant radial velocity, with their velocity defined relative to the receiver platform. Due to the assumption of air-to-air propagation, clutter has not been taken into account in the simulations either.

As the radar tracks a target, the radar receiver takes not only actual returns from the target but also jamming pulses as well. Here, jamming techniques against the utilized radar model are simulated. Jamming techniques are examined according to several varying parameters like JSR, jamming signal Doppler frequency, etc.

The algorithm development has been carried out in Matlab. The developed program enables the simulation of target returns, jamming signals, jamming noise and thermal noise according to given radar and jamming parameters. The program is very useful for performing the analyses that are the subject of this thesis. It is also very extensible for future developments.

The thesis is organized as follows: Chapter 2 provides background for the basic principles of radar. The details of the radar receiver simulation and the tracking filter are given in Chapter 3. That chapter includes also reference simulations for tracking a target in absence of jamming. Then in Chapter 4, principles of jamming techniques investigated in this thesis are presented together with simulations performed for various scenarios of the respective jamming techniques. Chapter 5 includes the conclusions of this study.

CHAPTER 2

BASIC PRINCIPLES OF RADAR

2.1 Classification of Radars

Radars can be classified as ground based, airborne, space borne, or ship based. Another classification is based on the radar functions as search, acquisition, track, track-while-scan, fire control, early warning, over the horizon, terrain following, and terrain avoidance. In addition, radars are generally classified into two groups according to the types of waveforms like continuous wave (CW) and pulse radars.

CW radars, emitting electromagnetic energy continuously, generally use separate transmit and receive antennas. By using unmodulated CW radars, only Doppler shift (target's radial velocity) and angular position can be measured. In order to measure target range information, some kind of modulation is added. Unmodulated CW radars are used in target velocity search, track, and in missile guidance.

Pulsed radars use trains of pulsed waveforms, usually, with modulation. Pulsed radars can be classified as low PRF, high PRF and medium PRF radars. Low PRF radars are used for unambiguous range measurement while high PRF ones are used for unambiguous Doppler measurements.

In tracking radar applications; S, C, X, Ku, Ka, V and W frequency bands are used [6]. S and C bands are used especially for long range tracking, and the others are

used for short range tracking. The operating frequency determines the antenna beam width, as the lower the frequency the broader the beam width for an aperture with a given size. Also the beam width is inversely proportional to the size of the antenna aperture.

2.2 The Radar Equation

The general radar range equation is

$$R_{\max} = \left(\frac{P_t G^2 \lambda^2 \sigma}{(4\pi)^3 k T_e B F (SNR)_{o,\min}} \right)^{1/4} \quad (2.1)$$

where P_t is the transmit radar signal power in Watts; G is the transmit and receive antenna gains; λ is the radar signal wavelength in meters; σ is the radar cross section (RCS) in meters square; k is the Boltzman constant, 1.38×10^{-23} joule/degree Kelvin; T_e is the effective noise temperature in degrees Kelvin; B is the receiver bandwidth in Hz; F is the receiver's noise figure and $SNR_{o,\min}$ is the minimum output signal-to-noise ratio, SNR. The Radar Cross Section (RCS) is defined by the intensity of the backscattered energy with the same polarization as the radar receive antenna.

2.3 Basic Pulsed Radar Block Diagram

The basic pulsed radar block diagram is shown in Figure 2-1. Basic radar circuitry consists of a timing circuit, which defines the pulse repetition interval and measures the time-of-arrival (TOA) values for the transmit and receive pulses; a waveform generator which generates the required waveform with required frequency; a transmitter which provides the required amplification for the transmit pulses; a duplexer for the usage of the same antenna both for transmission and reception which acts as a switch; an antenna used both for transmission and reception; a receiver which is used for the reception of echo pulses and reduction to IF in order to make the echo signal ready for signal processing applications; a signal processing circuitry which is used for the application of signal processing algorithms in order

to obtain the range and velocity information and angular position of a target; and a display which is used for providing an interface for the operator.

The pulsed radar uses modulated pulse train transmission and reception. The range is calculated by using the time difference between the transmitted and received pulses. Doppler measurement is performed by the Doppler filter banks. The carrier frequency, f_c , pulse width T_p , modulation, and pulse repetition frequency f_{PR} (PRF) are the basic operational parameters for the pulsed radars.

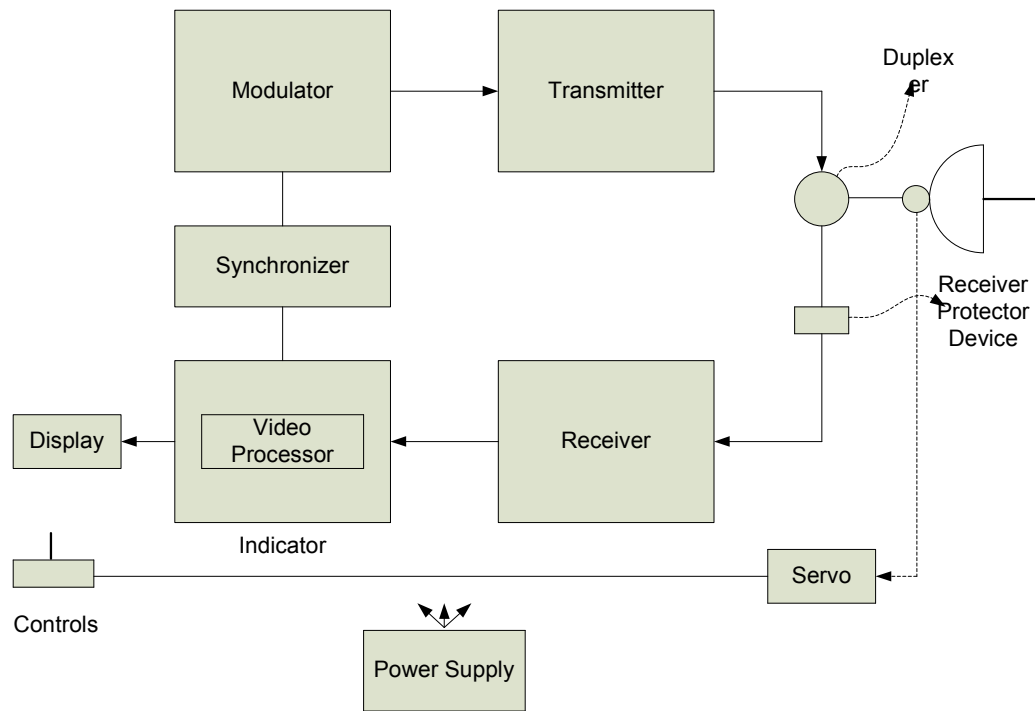


Figure 2-1: Basic pulse radar block diagram

There exist three types of pulse radars which are different by their PRFs regimes and caused ambiguities. These are:

- High PRF pulse-Doppler radar with range ambiguity and with no Doppler ambiguity.

- Medium PRF Pulse-Doppler radar both with tolerable range and Doppler ambiguities.
- Low PRF, MTI radar with Doppler ambiguity and with no range ambiguity.

The maximum unambiguous range can be specified as:

$$R_{\max} = \frac{c T_{PR}}{2} \quad (2.2)$$

Here, T_{PR} is the pulse repetition interval and c is the speed of light. The range resolution is formulated as

$$\Delta R = \frac{c T_p}{2} \quad (2.3)$$

Here, T_p , is the pulse width.

2.3.1 Pulse-Doppler radar

Radars with high enough PRF can decrease the number of blind speeds [6]. Such radars are called pulse-Doppler radars. The pulse-Doppler radar is based on the fact that the targets moving with a nonzero radial velocity will result in a frequency shift between the transmitter master oscillator and the carrier component in the returned echoes. This provides detection of moving targets. Especially if the radar's operating frequency increases, a decrease in the first blind speed takes place, without changing the pulse repetition frequency, as seen in the blind speed calculation equation as follows.

$$v_n = \frac{n\lambda}{2T_{PR}}, \quad n = 1, 2, 3 \quad (2.4)$$

where v_n is the n'th blind speed; λ is the radar's transmit wavelength.

The blind speeds can cause actual target misses during the radar's detection process. If the PRF of a transmitted radar signal is increased, the first blind speed increases which supports the detection of moving targets. However, an increase in PRF will result in range ambiguity.

The main advantage of the high PRF pulse-Doppler radars is that they provide superior average transmitted power, and excellent clutter rejection. On the other hand, they are ambiguous in range. In addition, the concept of high PRF indication depends on the maximum detection range. The same PRF value can be introduced as medium or high according to the maximum detection range.

In order to solve the range ambiguity problem in high PRF Pulse-Doppler Radars, multiple PRFs can be used. Three different PRFs are used instead of two in order to increase the unambiguous range and reduce the possibility of ghost targets. Target detection and range measurement are performed on each of the three PRFs. For this purpose, a high PRF pulse-Doppler radar requires very high peak transmit power. High PRF and high duty cycle also result in poor resolution of multiple targets. On the other hand, high PRF pulse-Doppler radars provide excellent Doppler measurement, and hence excellent measurement of target's radial velocity.

On the other hand, the medium PRF pulse-Doppler radar is the one whose PRF value is between the high PRF pulse-Doppler radar and the MTI radar [8]. For this reason, both Doppler and range ambiguities take place. Less clutter effect is observed in medium PRF Pulse-Doppler radar than that in the low PRF pulse-Doppler radar.

To solve the range ambiguity problem in medium PRF pulse-Doppler radars, three PRFs can be used as in high PRF pulse-Doppler. However, usually seven or eight different PRFs are used to ensure that a target will have a proper Doppler frequency to be detected on at least three PRFs in order to resolve range ambiguities.

2.4 Radar Block Diagram Basic Elements

2.4.1 Synchronizer

Synchronizer performs the exact timing of the operation of the transmitter and the indicator by generating a continuous stream of very short, evenly spaced pulses. These pulses designate the time at which successive radar pulses are to be transmitted and are supplied to the modulator and indicator.

2.4.2 Modulator

Modulator produces a high power pulse of direct current energy and supplies it to the transmitter upon receipt of each timing pulse from the synchronizer.

2.4.3 Transmitter

Transmitter is a high power oscillator, generally a magnetron or a traveling wave tube amplifier (TWTA). The transmitter generates a high power RF wave for the duration of the input pulse from the modulator. This wave with a specified wavelength is radiated into the waveguide which conveys it to the duplexer.

2.4.4 Duplexer

Duplexer is a waveguide switch that connects the transmitter and the receiver to the antenna. It is sensitive to the direction of flow of the radio waves allowing the waves coming from the transmitter to pass with negligible attenuation to the antenna, while blocking their flow to the receiver. In addition, the duplexer allows the waves coming from the antenna to pass with negligible attenuation to the receiver, while blocking their way to the transmitter.

2.4.5 Antenna

The antenna consists of a radiator and a parabolic reflector (dish) mounted on a common support in simple radar models. The radiator is little more than a horn-

shaped nozzle on the end of the waveguide coming from the duplexer. The horn directs the radio wave arriving from the transmitter onto the dish which reflects the wave in the form of a narrow beam. Echoes intercepted by the dish are reflected into the horn and conveyed by the same waveguide back to the duplexer, hence to the receiver. Some pulse radars use a simple version of planar array antenna. The antenna is generally mounted in the gimbals which allow it to be pivoted about both azimuth and elevation axes. To isolate the antenna from the roll of the aircraft, a third gimbal may be provided. In order to provide the indicator with signals proportional to the displacement of the antenna about each axis, transducers on the gimbals are used.

2.4.6 Receiver protection device

Due to the electrical discontinuities (mismatch of impedances) between the antenna and the waveguide, some of the energy of the radio waves is reflected from the antenna back to the duplexer. Since the duplexer performs its switching function on the basis of direction of flow, there is nothing to prevent this reflected energy from flowing on to the receiver, just as the radar echoes do. The reflected energy amounts to only a very small fraction of the transmitter's output. But because of the transmitter's high power, the reflections are strong enough to damage the receiver. To prevent the reflections from reaching the receiver, as well as to block any of the transmitter's energy that has leaked through the duplexer, a protection device is provided. This device is essentially a high-speed microwave switch, which automatically blocks any radio waves strong enough to damage the receiver.

2.4.7 Receiver

The most popular receiver type is the super-heterodyne receiver. In order to apply filtering and amplification conveniently, the receiver lowers the frequency of the received echo. For this purpose, a mixer is used which beats the received signal against the output of a low-power oscillator (Local Oscillator, LO). Here, the resultant frequency is the difference of the radar echo frequency and LO frequency

which is called the intermediate frequency (IF). Then this output signal is amplified by an IF amplifier. The IF amplifier also filters out interfering signals and noise which lies outside the received signal's frequency band. Finally, the amplified signal is applied to a detector which produces an output voltage corresponding to the peak amplitude (or envelope) of the signal. The detector output (video signal) is applied to the indicator.

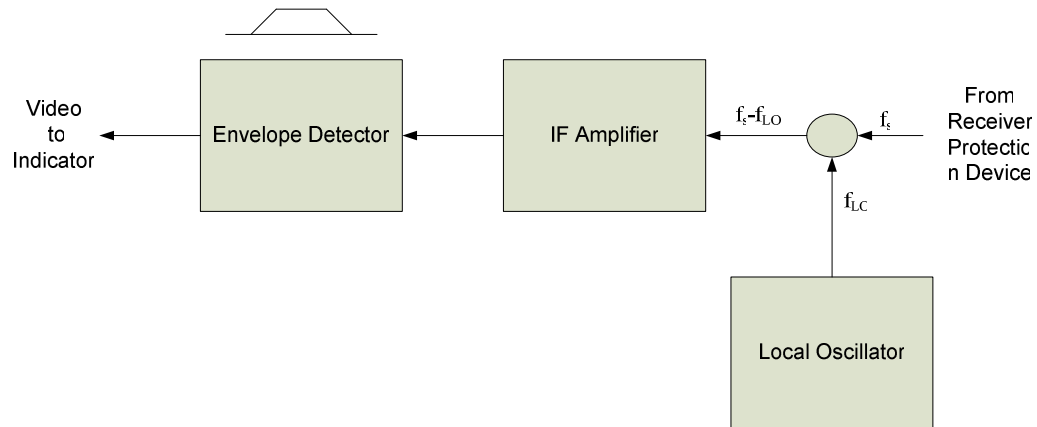


Figure 2-2: Radar receiver block diagram

2.4.8 Indicator

Indicator provides the display of received echoes in a format that will satisfy the operator's requirements; control the automatic searching and tracking functions; and extract the desired target data when tracking a target.

2.4.9 Antenna servo

Antenna servo positions the antenna according to the control signals which can be provided by the search scan circuitry in the indicator; a hand control with which the operator can point the antenna manually; the angle tracking system. A separate servo channel is assigned for each gimbal. The voltage obtained from the transducer on the gimbal is subtracted from the control signal. So an error signal is produced proportional to the error in the antenna's position. This error signal is then amplified

and applied to a motor which rotates the antenna about the gimbal axis in such a way as to reduce the error to zero. So the search scan, being usually much wider in azimuth than in elevation, will not be affected by the attitude of the aircraft. In addition, stabilization may be provided. To correct the roll position of an antenna, a vertical gyro provided reference signal is used for comparison. The resulting error signal is used to correct the roll position of the antenna. Otherwise, the azimuth and elevation error signals are resolved into horizontal and vertical components by using the reference provided by the gyro.

2.5 Target Tracking

Tracking radars are used to track targets in their course, as they update their measurements and estimates about the target's relative position (range, velocity, azimuth angle and elevation angle).

Tracking radars are classified into two groups as continuous-single-target tracking radars and multi-target track-while-scan (TWS) radars. Tracking techniques are also classified as angle, and range/velocity tracking. Tracking radars utilize pencil beam antennas. For this reason, separate search radar should be utilized for detection and acquisition purpose. Tracking radars use sector, raster, helical, spiral search scan patterns for target acquisition.

2.5.1 Single target tracking (continuous tracking)

2.5.1.1 Angle tracking

Angle tracking is based on the continuous measurement of target's angular position in azimuth and elevation. In order to generate an error signal, tracking radars use the angular deviation from the antenna main axis of the target within the beam. The resultant error signal defines how much the target has deviated from the beam's main axis. Then, the beam position is continuously updated in order to produce a zero error signal.

There are three techniques of angular tracking as ‘sequential lobing’, ‘conical scan’, and ‘monopulse’. The monopulse method is also divided into two groups as ‘amplitude comparison monopulse’ and ‘phase comparison monopulse’.

Sequential lobing or lobe switching is achieved by continuously switching the pencil beam between two predetermined symmetrical positions around the antenna’s Line of Sight (LOS) axis in order to track in one axis.

Conical scan is achieved by continuously rotating the antenna at an offset angle, or rotating a feed about the antenna’s main axis.

Amplitude comparison monopulse has four simultaneously generated beams in order to make angular measurement at a single pulse basis. It operates like sequential lobing with a difference of simultaneously generated four beams instead of sequentially generated beam positions.

Phase comparison monopulse operation principle is similar to amplitude comparison monopulse only with some main differences. Both of them use sum and difference channels for angular measurement. On the other hand, the four signals generated in amplitude comparison monopulse have different amplitudes and same phases while in the phase comparison monopulse the signals have same amplitudes and different phases.

2.5.1.2 Range tracking

Range measurement is based on the estimation of round-trip delay of the transmitted pulses. The time delay t_d , between the transmission and the reception of a radar signal maintains the range R as

$$R = \frac{t_d \cdot c}{2} \quad (2.5)$$

In order to provide continuous range tracking for moving targets, a tracker should be employed.

Split gate tracking is a range tracking method which employs early and late gates. The gate durations are half the pulse width. The early gate is started at echo TOAs and the late gate is started at echo centres. The voltage outputs of late and early gates have opposite signs. These outputs are subtracted from each other and the resultant signal is fed to the integrator in order to produce an error signal. The sign of the error determines in which direction the gates should be moved in time in order to make the error signal zero.

2.5.2 Multiple target tracking

The Track-While-Scan (TWS) radar sample each target once during its scan interval. It uses smoothing and prediction filters for estimating target position information from scan to scan. For this purpose; alpha-beta ($\alpha\beta$), alpha-beta-gamma ($\alpha\beta\gamma$) (constant coefficient filters), and Kalman filters (adaptive filters) are used in radar receiver circuitry. First of all, the radar receiver circuitry takes enough number of pulses in order to measure the position information (range, velocity, acceleration, angle, etc. information) of the target. After that process, measured position information is used by the filters in order to estimate the target's future position information. Then a special track file for this target is set in order to provide continuous tracking of target's position information. In a case when a new target is detected, a separate track file is assigned for this target.

The radar measurements are based on position (range, velocity, acceleration) and angle measurements. After these sufficient measurements the TWS system places a gate around the target's position and attempts to track the signal within this gate. This gate is set for the angle and range bins. In order to provide continuous track from scan to scan, the gate should be wide enough to prevent missing target returns. After the target has been observed for several scans the size of the gate is reduced.

Gating provides distinction between different target returns; however in single target situation it reduces the amount of processed data. The gating algorithms are

based on the computation of statistical error between measured and estimated radar observation. The amount of the error should be bounded with a specified maximum value. The error which does not correlate with the existing ones, according to the specified maximum, cause new track file generation for this target (new target). The correlation between observations and all existing track files is defined by a correlation matrix whose rows represent radar observations while columns represent track files.

CHAPTER 3

RADAR SIMULATION

3.1 Transmitter-Receiver Simulation

In this thesis, the radar transmitter is modeled as a pulse-Doppler radar using various radar parameters, which include radar's operating RF, PRI, PW, pulse amplitude, transmitter power, transmit antenna gain and sampling frequency. The radar operates at 10 GHz making it an X band Airborne Intercept (AI) radar. The PRI is set to 100 μ s and the PW is set to 1 μ s, making the duty cycle about 1%. The RF, PRI and, PW types are chosen as stable. There is no modulation on the transmit signal since a baseband receiver model is assumed. The received signal has amplitude modulation due to the antenna beam pattern and the scanning of the receive antenna. The transmitter power is set to 1 kW as a typical value. The sampling frequency f_s is set to the Nyquist rate at 2 MHz as dictated by the following equation,

$$f_s \geq 2 \frac{1}{T_p} \quad (3.1)$$

where T_p is the pulse width. For the purposes of the analysis in this thesis, targets are modeled to have only a radial velocity component that produces a Doppler shift on receive. The scenario starts with a search operation where the target antenna scans a sector of azimuth angle range from -30 to 30 degrees within 6 ms using 60

transmit pulses with 100 μ s PRI, T_{PR} . At the end of the scan, the received signal is processed for detection of range, Doppler velocity and azimuth angle of each target.

With the simulation settings, the maximum unambiguous range is

$$R_{\max} = \frac{c T_{PR}}{2} = \frac{3 \times 10^8 \times 100 \times 10^{-6}}{2} = 15000 \text{ m} \quad (3.2)$$

and the range resolution (size of a range cell) is

$$\Delta R = \frac{c T_p}{2} = \frac{3 \times 10^8 \times 1 \times 10^{-6}}{2} = 150 \text{ m} \quad (3.3)$$

The PRF is

$$PRF = \frac{1}{T_{PR}} = \frac{1}{100 \times 10^{-6}} = 10 \text{ kHz} \quad (3.4)$$

With such a PRF setting, the simulated radar can be classified as medium-PRF radar.

The frequency sample resolution in the Doppler dimension is inversely proportional to the number of FFT bins used in the detection stage:

$$\Delta f_d = \frac{PRF}{FFT \text{ length}} = \frac{10 \times 10^3}{256} = 39.0625 \text{ Hz} \quad (3.5)$$

Corresponding Doppler velocity can be calculated as

$$\Delta V = \frac{\Delta f_d \lambda}{2} = \frac{39.0625 \times 0.03}{2} = 0.5859 \text{ m/s} \quad (3.6)$$

Note that Δf_d is the sample resolution in the frequency domain; it is not the Doppler resolution, which is the frequency distance that is needed to separate two targets in the frequency domain, and is to be explained later in this thesis.

Consider the following scenario as depicted in Figure 3-1. There are two targets with radar cross sections set to 10 m^2 each; at azimuth angles of -10 and 5 degrees; at a range of 10000 m and 12000 m ; with radial velocities 50 m/s and 70 m/s , respectively. Note that the speed values and other parameters are quantities relative to the receiver platform. Figure 3-2 shows the target ranges for both targets as a function of time as the antenna scans the sector from -30 to 30 degrees within 6 ms .

Note that the change in range during the 6 ms search scan period is small compared to the initial values of the range and the velocity. Thus the change is not noticeable from the figure. The change of range for Target 1 is about 30 cm and for Target 2 is about 42 cm .

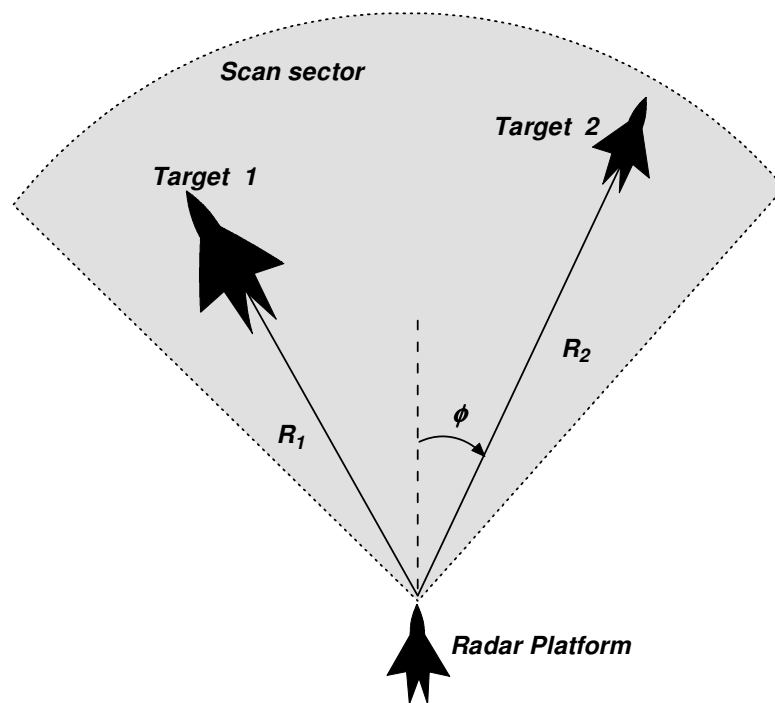


Figure 3-1: Depiction of the simulated radar scenario.

Depending on the range of a target, the received power backscattered from the target varies. The received power as a function of range (and hence, as a function of delay time) is shown Figure 3-3. There is a slight slope to each line due to the varying range as the antenna scans the sector.

The received power is given by

$$P_r = \frac{P_t G^2 \lambda^2 \sigma}{(4\pi)^3 R^4 L} \quad (3.7)$$

where P_r is the received radar signal power in Watts; P_t is the transmit radar signal power in Watts; G is the transmit and receive antenna gain; λ is the radar wavelength in meters; σ is the radar cross section (RCS) in meters square (m^2); R is the target range in meters; and L is the receiver losses. Antenna gain is given as

$$G = \frac{4\pi A_e}{\lambda^2} \quad (3.8)$$

where A_e is the effective antenna aperture area in meters square (m^2). Note that the radar wavelength is given as

$$\lambda = \frac{c}{f_c} \quad (3.9)$$

with c being the speed of light (3×10^8 m/s) and f_c being the radar's operating frequency (Hz). In the simulations, A_e is chosen as 0.1 m^2 and λ is 0.03 m , which yields

$$G = \frac{4\pi A_e}{\lambda^2} = \frac{4\pi 0.1}{0.03^2} = 1.3963 \times 10^3 \quad (3.10)$$

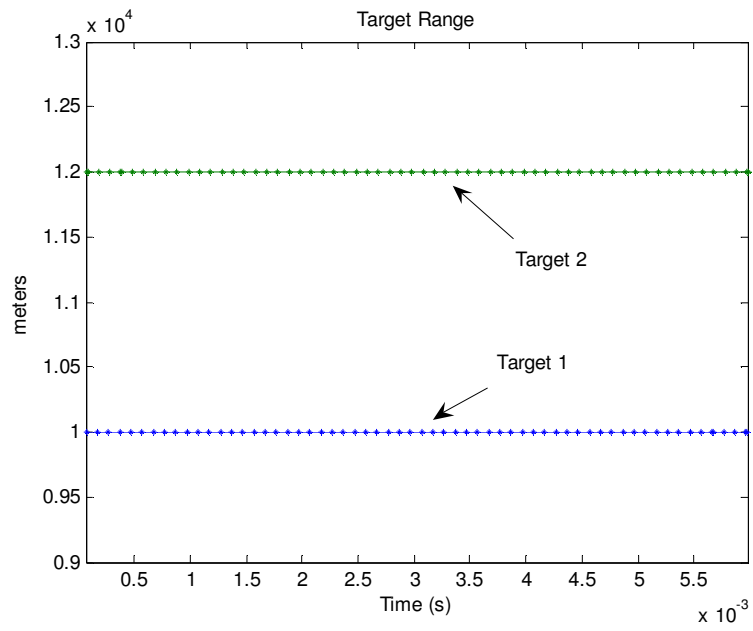


Figure 3-2: Target range within the search period.

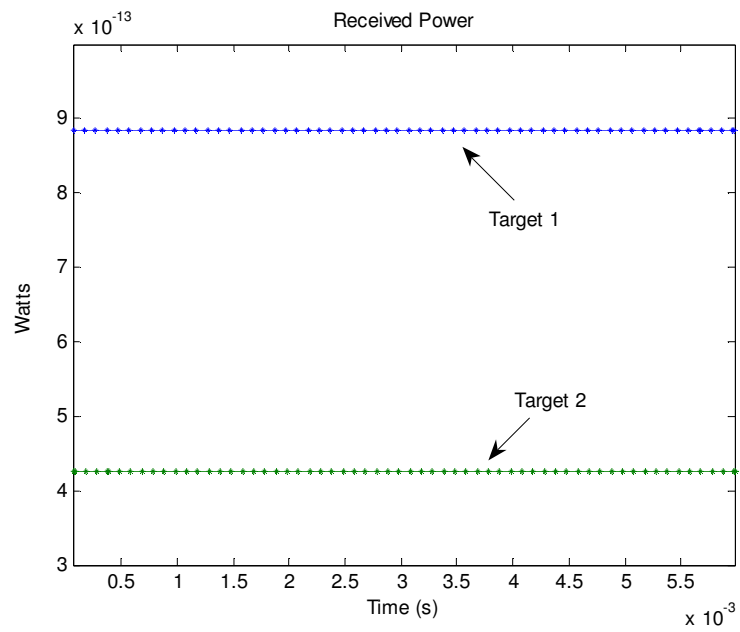


Figure 3-3: Received power in the search period.

As the pulses are transmitted and the backscattered waves travel to the receiver through the receive antenna, receive signal is also subject to the antenna beam pattern. The simulation takes this into account by modeling the antenna pattern and taking into account the target azimuth angles and the antenna look direction at each sampling instant as the antenna is scanned in the search sector. The antenna patterns formed separately for the targets at -10 and 5 degrees of azimuth are shown in Figure 3-4. The antenna's beam width is specified as 5° , and the side lobe level is set to -20 dB below the main lobe.

The simulation of the received signal is performed in the baseband using the complex envelope assuming the receiver stage starting from the IF part and continuing with mixing and match filter stages are already taken into account in formulation.

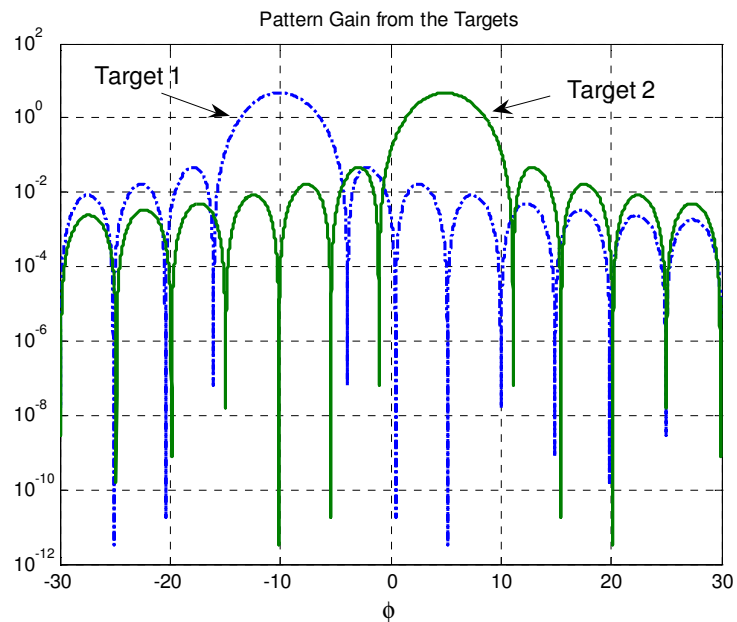


Figure 3-4: Scanning antenna pattern gain in the search period.

The received signal is given as:

$$x(t) = \sqrt{\frac{P_r P_s}{2}} A_p \exp(-j2\pi f_d t) \quad (3.11)$$

where A_p is the pulse amplitude; f_d is the Doppler frequency (Hz); P_r is the received power; and P_s is the scanning antenna gain. Note that the Doppler frequency is given by

$$f_d = \frac{2 V_r f_c}{c} = \frac{2 V_r}{\lambda} \quad (3.12)$$

where V_r is the target's radial velocity in m/s. The received signal with white Gaussian thermal noise is shown in Figure 3-5. The noise power is calculated by

$$N_o = kTBF \quad (3.13)$$

where k is the Boltzman constant, 1.38×10^{-23} (joule/degree Kelvin); T is the effective noise temperature in degree Kelvin; B is the receiver bandwidth (Hz); and F is the receiver's noise figure. Here, the receiver bandwidth is 1 MHz; noise figure is specified as 5; and noise temperature is set to 20 degrees Celcius.

With given received power and noise power, the output signal-to-noise ratio (SNR) can be calculated as

$$SNR_o = 10 \log_{10}(P_r / N_o) \quad (3.14)$$

With the above parameter settings, the output SNR for the targets are about 16.4 and 13.2 dB (change due to P_r throughout the scan is very small).

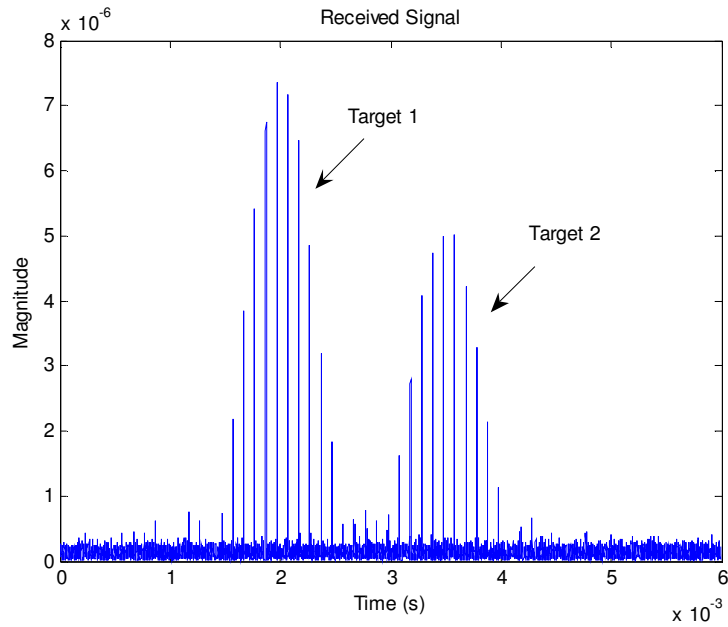


Figure 3-5: Received radar signal with white Gaussian noise.

3.2 Delay-Doppler Detection

For delay and Doppler frequency measurements, a time-frequency distribution of the received signal is computed using power spectral density (PSD) estimation [16]. Note that delay and Doppler frequency correspond to the range and radial velocity (Doppler velocity) of a target, respectively. In the following, the computation of the PSD and the detection in delay-Doppler domain is explained.

3.2.1 Computation of the power spectral density

For PSD computation, Welch's method of windowed and averaged periodograms is used [16]. The Welch method uses overlapped data segments. Each data segment is

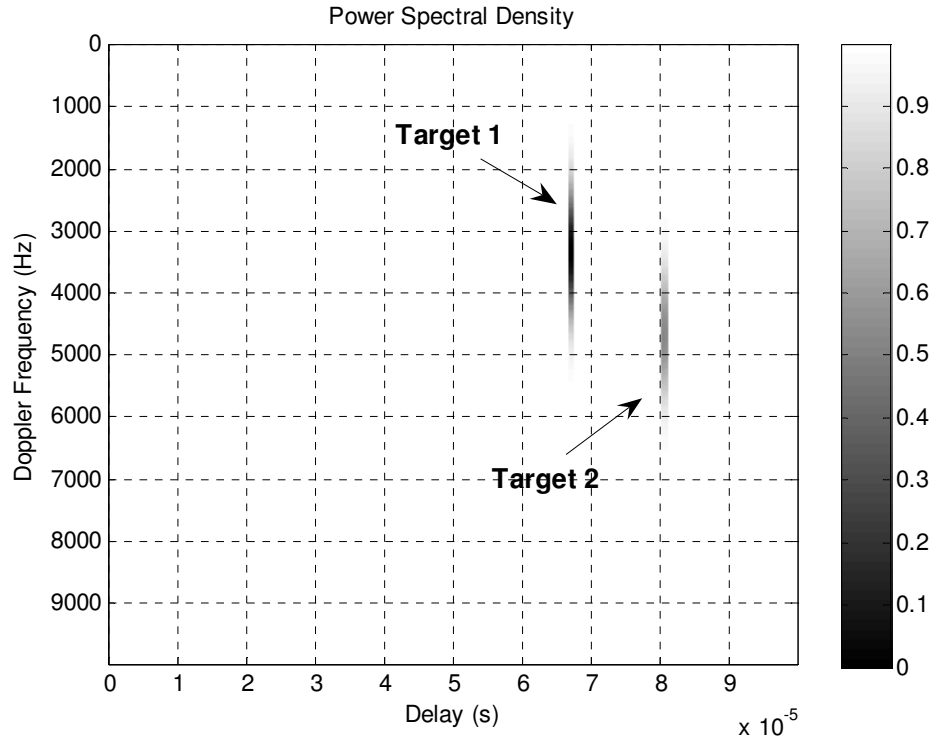


Figure 3-6: Power spectral density of the received pulses as a function of delay and Doppler frequency.

windowed prior to computing the periodogram. The window size corresponds to the number of pulses that are received during time-on-target (illumination time). The PSD of the received pulses during the search scan (6 ms, 60 PRI's) is shown in Figure 3-6. The energy concentrations for the targets are marked on the figure.

The mathematical form of Welch method can be summarized as follows. Let the j th data segment be y_j , which is given as

$$y_j(t) = y((j-1)K + t), \quad t = 1, \dots, M \quad \text{and} \quad j = 1, \dots, S \quad (3.15)$$

Then $(j-1)K$ is the starting point for the j 'th sequence of observations. If $K=M$, then the sequence do not overlap and the sample splitting used by the Bartlett

method is obtained. Bartlett method leads to $S=L=N/M$ data subsamples. On the other hand, the value recommended by Welch method for K is $K=M/2$ in which case $S \cong 2M/N$ data segments with 50% overlap between successive segments.

The windowed periodogram corresponding to $y_j(t)$ is computed as

$$\hat{\phi}_j(w) = \frac{1}{MP} \left| \sum_{t=1}^M v(t) y_j(t) e^{-iwt} \right|^2 \quad (3.16)$$

Here, $v(t)$ is a temporal window such as Hamming, Blackman, rectangular etc., and P is the power of the temporal window $v(t)$:

$$P = \frac{1}{M} \sum_{t=1}^M |v(t)|^2 \quad (3.17)$$

The Welch estimate of PSD is determined by averaging the windowed periodograms as follows

$$\hat{\phi}(w) = \frac{1}{S} \sum_{j=1}^S \hat{\phi}_j(w) \quad (3.18)$$

In the Welch method, the variance of the estimated PSD is decreased by allowing overlap between the data segments and hence by getting more periodograms to be averaged.

3.2.2 Detection using PSD

Detection in delay dimension is performed using certain thresholds on the projection of the PSD onto delay axis (projection along the Doppler dimension). The projection is obtained simply by performing a column sum on the PSD data. Such a projection is shown in Figure 3-7.

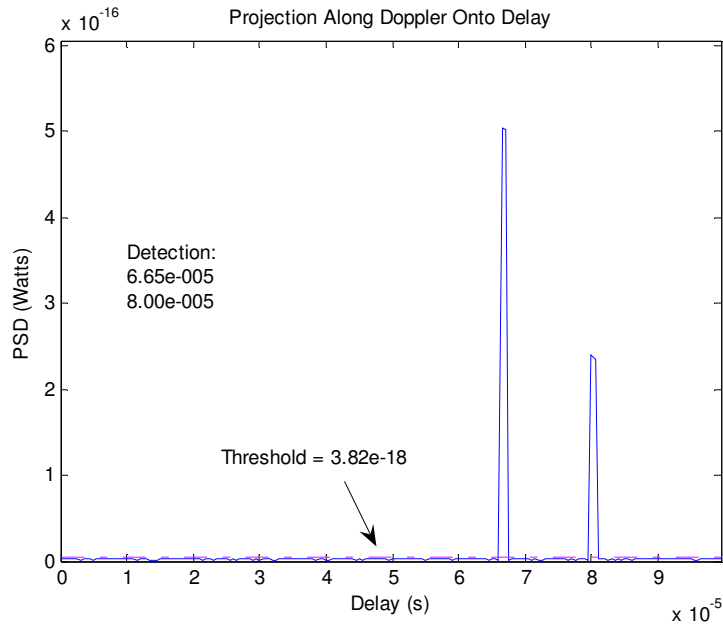


Figure 3-7: Projection of PSD along the Doppler axis onto the delay axis.

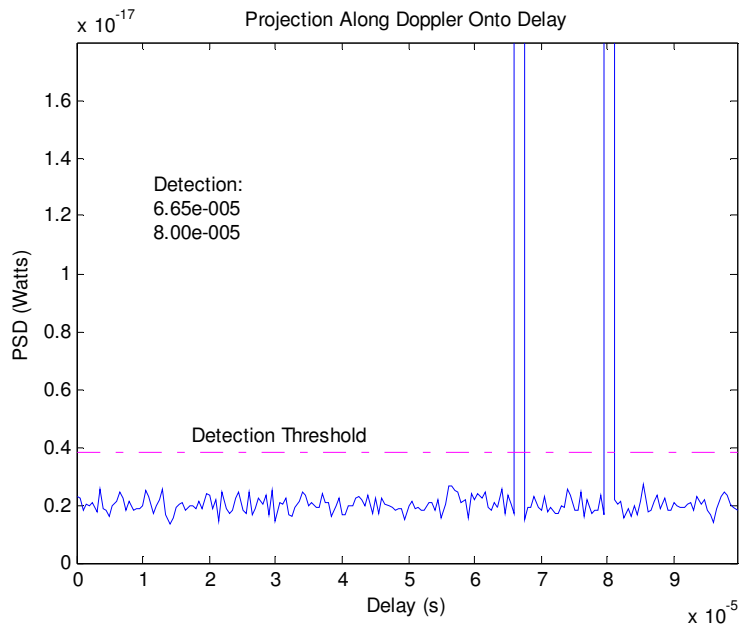


Figure 3-8: Magnified version of Figure 3-7. Detection threshold is indicated.

A magnified version of Figure 3-7, shown in Figure 3-8, indicates the detection threshold. By applying a proper threshold the delay (hence, the range) of each target can be determined using a simple peak detection algorithm.

The computed delays 6.65×10^{-5} s and 8.0×10^{-5} s correspond to 9975 m and 12000 m respectively. Those are close to the figures 10000.0033 m and 12000.005565 m, which are the true ranges of targets at the time of the target illumination. Note that the size of a range cell is 150 m (with a 1 μ s pulse width).

The Doppler frequency detection is then performed along the detected delay values. The cross-section of the PSD along Doppler dimension at delay 6.65×10^{-5} s and 8.00×10^{-5} s is shown in Figure 3-9. Thresholding and peak detection is performed for computing the Doppler frequency corresponding to the peaks in the figure.

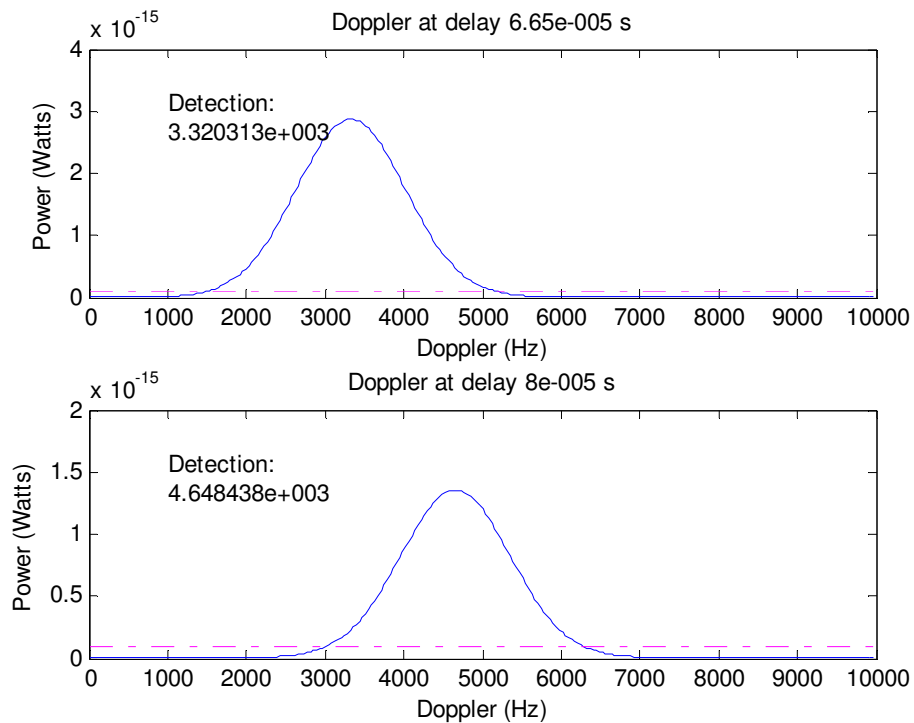


Figure 3-9: Doppler frequency reading from the cross section of PSD.

Note that the bandwidth values (widths at -3 dB down the peaks) in Figure 3-9 correspond to Doppler resolution, which is inversely proportional to both the number of samples in the Welch window used in PSD computation and the pulse repetition interval. The size of the Welch window is limited by the number of pulses on target in the search mode. In the track mode, however, the length of the Welch window can be set to be larger since each pulse collected within a snapshot is on-target.

In the simulations, the following parameters relevant to PSD are used: Hamming window as the temporal window; a Welch window size of 10 samples for both search and track mode, which is equal to the number of pulses on target in the search mode; window overlap with 1-sample shift, that is, 9-sample overlap; and an FFT length of 256 samples. The number of PRI's used as the input data for PSD computation is 60 in the search mode, and 20 in each snapshot in the track mode. Those correspond to 6 ms and 2 ms of radar data, respectively. With those settings, the Doppler resolution is about 1.4 kHz, and the frequency sample resolution, Δf_d , is 39.0625 Hz as given in the previous sections.

The threshold values are computed taking into account the noise power and the false alarm rate. Such a time-domain threshold can be obtained by using the fact that the envelope of a zero-mean Gaussian noise sequence is Rayleigh distributed. By computing the point that satisfies a certain probability of false alarm in the case of only noise as the received signal, a time-domain threshold can be obtained as

$$Y_t = \sqrt{2N_0 \ln\left(\frac{1}{P_{FA}}\right)} \quad (3.19)$$

which varies with the false alarm rate, P_{FA} , and the noise power, N_0 . Note that this is based on the time-domain envelope of the received signal.

There is a certain conversion factor γ_c between the power of the envelope and the standard deviation of PSD in the frequency domain due to the Fourier

transformations and windowing effects in the computation of PSD. This conversion factor can be analytically derived or can be empirically computed. Here the conversion factor γ_c for the current radar parameter settings is empirically computed to be 1.05×10^{-4} . The threshold used on the PSD is thus can be given as

$$Y_f = \gamma_s \gamma_c Y_t \quad (3.20)$$

where γ_s is a scaling factor used with delay detection on the projection in Figure 3-8 and Doppler detection on the cross-sections of PSD as in Figure 3-9. The value of γ_s is determined empirically for the simulations. The value used in the simulations that follow is 0.04 for delay and 1 for Doppler dimensions, respectively. The parameters that are empirically determined in the simulations need to be set through a calibration process in a real radar operation.

3.3 Azimuth Angle Detection

For the azimuth angle detection for each target, the received signal that is obtained through the antenna scan of the sector in the search mode is used. Due to the antenna beam pattern, the received signal contains reception from the targets only when the antenna is directed towards the vicinity of the target. Using the amplitude structure of the received signal, it is possible to find the azimuth angle of each target. A typical received signal is shown in Figure 3-10 and a magnified version of it in Figure 3-11.

First a threshold is applied to separate the received pulses from the noise floor. Then the data points shown in the figures are computed as the maximum of the received pulse samples within a pulse width. Then it is possible to operate on those samples as if they are consecutive samples of a sequence. After second thresholding and curve fitting, the location of the peaks of the fitted curves to each consecutive data segment is determined as the detected angle.

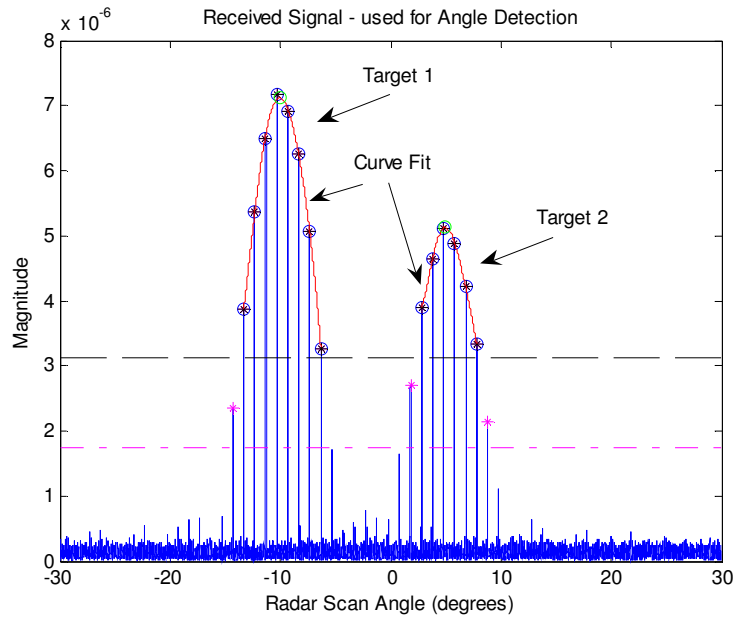


Figure 3-10: Received signal as a function of the radar scan angle is used for angle detection.

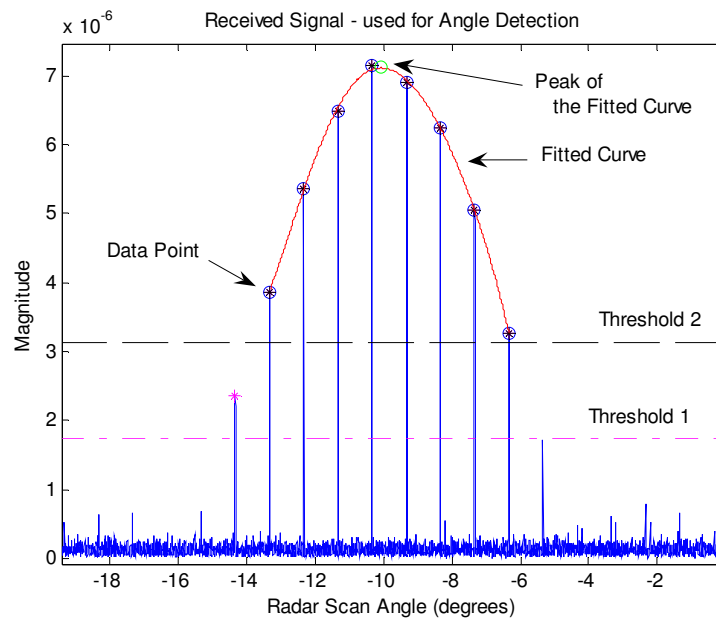


Figure 3-11: Angle detection is performed using curve fitting.

The threshold values are proportional to the threshold Y_t . The first (lower) and second (higher) thresholds can be determined as

$$Y_{LO} = \gamma_1 Y_t \quad (3.21)$$

$$Y_{HI} = \gamma_2 Y_{LO} \quad (3.22)$$

where γ_1 and γ_2 are scaling parameters. In the simulations presented in this thesis, they are both set to 1.8.

Note that the range-Doppler measurements and the azimuth angle measurements need to be associated by each other if there is more than one target present. That is performed by using the received pulse amplitudes within the PRI in the curve fitting regions in Figure 3-10. For instance around -10 degrees, the received pulse amplitudes from Target 1 at 10 km range is larger and the received pulse time-of-arrival is earlier since its range is closer than that of Target 2, which is 12 km. That piece of information makes it possible to associate azimuth angle measurements to range, and hence Doppler measurements.

3.4 Tracking

After the detection of targets in the search mode of the radar, the radar turns its antenna towards the azimuth angle of the single target to be tracked. Since the radar model here is not a phased array, nor a TWS modality is assumed, tracking of multiple targets is not possible since the radar cannot direct its antenna instantaneously towards multiple target angles. Thus, the radar tracks only one of the targets in a continuous tracking fashion. Note that the targets modeled here have only radial velocity. Thus, the look direction stays constant during tracking. If however, the targets had tangential velocity, than it would be necessary to update the look direction of the radar antenna during tracking.

Tracking involves estimation of the target's next *state* (range and velocity) and updating the measurements. Measured range and velocity information at the detection stage is used for target's future state prediction. For this purpose, a constant-coefficient alpha-beta (α - β) tracking filter is utilized. This filter is suitable for the simulated target model.

Tracking also involves a detection stage to produce updated measurements of range and velocity. As the measurements are updated by the detection process, they are input to the tracking filter together with the previous state estimates. That in turn produces updated estimates for range and velocity. The estimates are used for range gating so as to save from computation. For good tracking performance, the error between the state prediction from the tracker and the actual measurements from detector should be small and they should be close to the true range and velocity values.

In this thesis, the radar receiver is assumed to be in a single-target-detection mode during tracking. This amounts to detecting the most prominent return as from the target being tracked. Since the target look direction is directed to a fixed angle; the antenna beam width is relatively small; and the targets assume only a radial velocity; this is a plausible assumption for the purposes of the current analysis.

The data collection in the track mode is performed in a snapshot fashion. Note that this type of data collection is adopted to save from computation. In real radar operation, however, the data is collected and processed in a continuous fashion. A depiction of snapshot data collection is shown in Figure 3-12. After the data collection in the search mode, the radar collects data in the track mode within each snapshot and does not collect data between snapshots. The data collected within a snapshot is used by the radar receiver to produce range and velocity measurements and hence used for the measurement update. Each snapshot consists of a number of PRIs, that is, transmit pulses and the radar returns corresponding to each transmit pulse. In the simulations, the snapshot duration is set to be 20 PRIs, which is 2 ms with a 100 μ s PRI. The offset duration between snapshots is set to be 50 ms. Within

the tracking loop, the start time and the true target range are updated at the beginning of each snapshot. Depending on the simulation, the number of snapshots is varied.

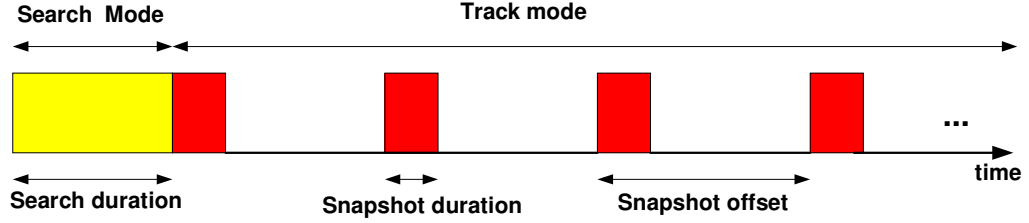


Figure 3-12: Data collection of the radar in the search and track modes.

3.4.1 Tracking Filter

The alpha-beta (α - β) tracking filter assumes that the target is in linear motion. Let $r(n)$ and $v(n)$ be the actual position and velocity of a target at sampling instant nT , where T is the update interval. Then the state equations of the target can be written as

$$r(n+1) = r(n) + T\underline{v}(n) \quad (3.23)$$

$$v(n+1) = \underline{v}(n) \quad (3.24)$$

or in matrix notation

$$\underline{x}(n+1) = \underline{\Phi} \underline{x}(n) \quad (3.25)$$

where the state vector is $\underline{x}(n) = [r(n) v(n)]^T$ and the one-step state transition matrix is given as

$$\underline{\underline{\Phi}} = \begin{bmatrix} 1 & T \\ 0 & 1 \end{bmatrix} \quad (3.26)$$

Double bars beneath a variable indicate a matrix; a single bar indicates a vector. In tracking a target, the actual state of the target is not known and is predicted from noisy radar measurements. Let $r_m(n)$ be the measured range of a target. The measured range of a target is related to its actual range by

$$r_m(n) = r(n) + w(n) \quad (3.27)$$

where $w(n)$ represent the measurement noise. This can be written as

$$r_m(n) = [1 \ 0] \begin{bmatrix} r(n) \\ v(n) \end{bmatrix} + w(n) = \underline{G} \underline{x}(n) + \underline{w}(n) \quad (3.28)$$

In the α - β filter, the next state of the target is given by the prediction equations

$$\hat{r}(n) = \bar{r}(n-1) + T \bar{v}(n-1) \quad (3.29)$$

$$\hat{v}(n) = \bar{v}(n-1) \quad (3.30)$$

where a caret is used over a variable to indicate a predicted estimate, and a bar is used to indicate a filtered estimate. Once a measurement is made the predictions can be updated by using the update equations:

$$\bar{r}(n) = \hat{r}(n) + \alpha [r_m(n) - \hat{r}(n)] \quad (3.31)$$

$$\bar{v}(n) = \hat{v}(n) + \frac{\beta}{T} [r_m(n) - \hat{r}(n)] \quad (3.32)$$

The filtered estimates are smoothed estimates that try to approximate both measurements and previous knowledge about the target. The prediction and update equations can be written in matrix form as

$$\hat{x}(n) = \underline{\underline{\Phi}} \bar{x}(n-1) \quad (3.33)$$

$$\bar{x}(n) = \underline{\underline{H}} \hat{x}(n) + \underline{\underline{K}} r_m(n) \quad (3.34)$$

where

$$\underline{\underline{H}} = \begin{bmatrix} 1-\alpha & 0 \\ -\beta/T & 1 \end{bmatrix} \quad (3.35)$$

$$\underline{\underline{K}} = \begin{bmatrix} \alpha \\ \beta/T \end{bmatrix} \quad (3.36)$$

Then by substitution,

$$\bar{x}(n) = \underline{\underline{A}} \bar{x}(n-1) + \underline{\underline{K}} r_m(n) \quad (3.37)$$

where

$$\underline{\underline{A}} = \underline{\underline{H}} \underline{\underline{\Phi}} = \begin{bmatrix} 1-\alpha & T(1-\alpha) \\ -\beta/T & 1-\beta \end{bmatrix} \quad (3.38)$$

When a target is first detected, the filter states are initiated as

$$\bar{r}(1) = \hat{r}(2) = r_m(1) \quad (3.39)$$

$$\bar{v}(1) = 0 \quad (3.40)$$

$$\bar{v}(2) = \frac{r_m(2) - r_m(1)}{T} \quad (3.41)$$

The corresponding system transfer functions can be derived as, [8]:

$$\begin{bmatrix} h_r(z) \\ h_v(z) \end{bmatrix} = \frac{1}{z^2 - z(2-\alpha-\beta) + (1-\alpha)} \begin{bmatrix} \alpha z \left(z - \frac{(\alpha-\beta)}{\alpha} \right) \\ \frac{\beta z(z-1)}{T} \end{bmatrix} \quad (3.42)$$

The two poles of the transfer function can be made the same at $z = \xi$ by choosing

$$\alpha = 1 - \xi^2 \quad (3.43)$$

$$\beta = (1 - \xi)^2 \quad (3.44)$$

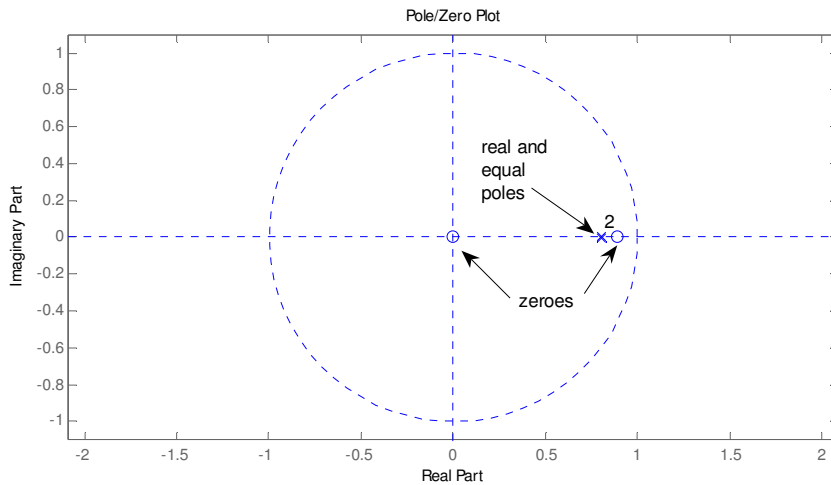


Figure 3-13: Pole-zero plot of the tracking filter with $\xi = 0.8$.

The poles lie inside the unit circle in the z -plane as long as $z = \xi < 1$ making the filter stable. The parameter ξ is called smoothing factor and may be chosen depending on the tracking requirements. The two poles are real and equal; thus, the filter is a critically damped (fading memory) filter, [17]. The pole-zero plot of the filter is shown in Figure 3-13.

In the simulations, the smoothing factor is set to be 0.8. With that setting the filter has been run separately for simulated input and the convergence results are shown in Figure 3-14 and Figure 3-15. The simulated input vector consists of the true range measurements for a target with a constant radial velocity of 50 m/s and the

true velocity measurements (constant, 50 m/s). The result for 100 iterations with an update interval of 0.05 s is shown in Figure 3-14 and Figure 3-15. The initial range and velocity estimates are set to be off by 50 m and 10 m/s, respectively. That perturbation serves to display the convergence of the filter. The range error converges to about 2.5 m, and velocity error converges to 0.

The convergence rate depends on the update interval and the smoothing coefficient. For more frequent updates and/or smaller values of the smoothing coefficient, the convergence becomes faster.

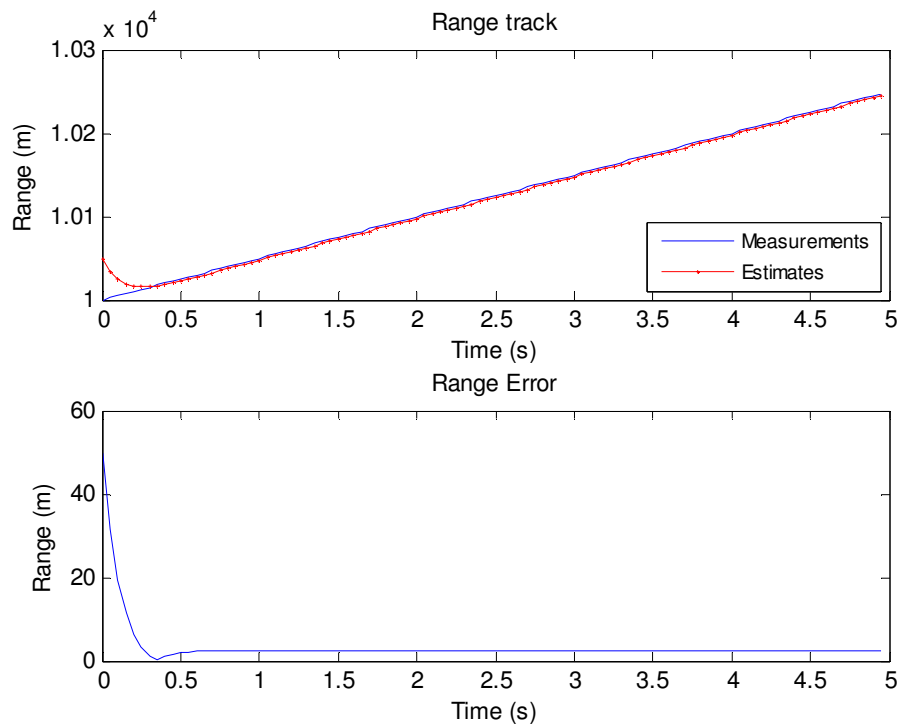


Figure 3-14: Range performance of the tracking filter; update interval is 0.05 s; smoothing coefficient is 0.8.

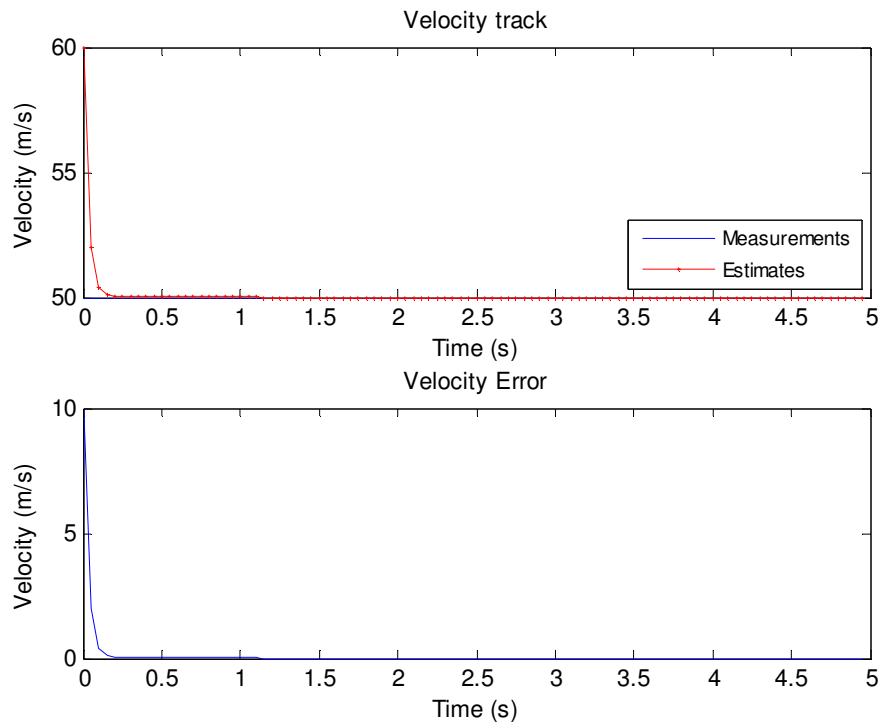


Figure 3-15: Velocity performance of the tracking filter; update interval is 0.05 s; smoothing coefficient is 0.8.

3.5 Tracking Performance under No Jamming

A reference run of the developed radar simulator program is presented in this section. The scenario here does not include jamming pulses or jamming noise. Only a target return and thermal noise is considered. Simulations for the jamming scenarios are discussed in detail in Chapter 4.

Received signal during the first snapshot of the track mode is shown in Figure 3-16. Note that the search mode ends and track mode starts at time instant of 6 ms. Since

the radar antenna is directed to the target direction determined in the search mode, the received pulses have about the same gain.

The initial tracker estimate (range and velocity) is obtained for the simulation by adding a perturbation to the measurements obtained from the search mode. The objective of adding a perturbation is to let the tracker to start far from the initial measurements so as to let the convergence be observed as the tracking filter converges to a neighborhood of further measurements. A perturbation of 75 m for range and 10 m/s for velocity is used.

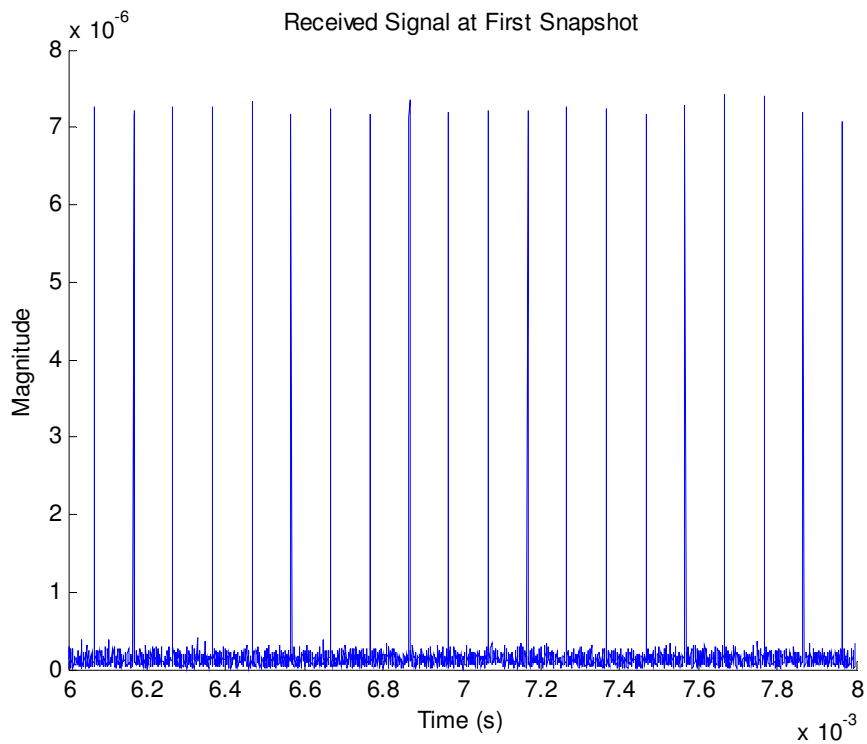


Figure 3-16: Received signal and thermal noise during the first snapshot.

The range gate is determined by the initial estimate. The delay measurement is performed within the range gate as shown in Figure 3-17. The threshold in the figure is 3.83×10^{-18} . The delay is measured to be 6.65×10^{-5} s. Note that the peak detection algorithm detects the peak in the PSD projection in the lower half of the figure. Due to noise, however, the location of the peak can vary within the neighborhood of the true delay of the target. For high input SNR, generally, the data points above the threshold are the ones due to the samples of the target return pulse. Thus, the width of that pulse determines the extent of such a neighborhood.

The Doppler measurement is shown in Figure 3-18. The threshold value used for Doppler detection is 1.0×10^{-16} .

The tracking loop runs until all the snapshots are processed. The number of snapshots was set to 100 for this particular simulation. The total time span is then 5 s. As a criterion, if the detection stage cannot produce measurements for 3 snapshots (age-out count) in a row, the track is dropped.

Note that the thresholds are determined by using the threshold formula based on the false alarm rate given by Y_t and Y_f . The detection threshold is computed such that the radar receiver maintains a constant pre-determined probability of false alarm (P_{FA}). The constant false alarm probability in this simulation was set to 10^{-10} . The value of the false alarm rate is not critical for the analysis here. A lower or a higher false alarm rate could be used. Increasing the false alarm rate decreases the threshold levels and more false alarms can appear.

Since the noise power may change during radar operation due to changes in the environment or due to noise jamming, the threshold is continuously updated based on the estimates of noise variance for providing a constant P_{FA} value. The process of continuously changing the threshold value to maintain a constant P_{FA} is called Constant False Alarm Rate (CFAR) [6].

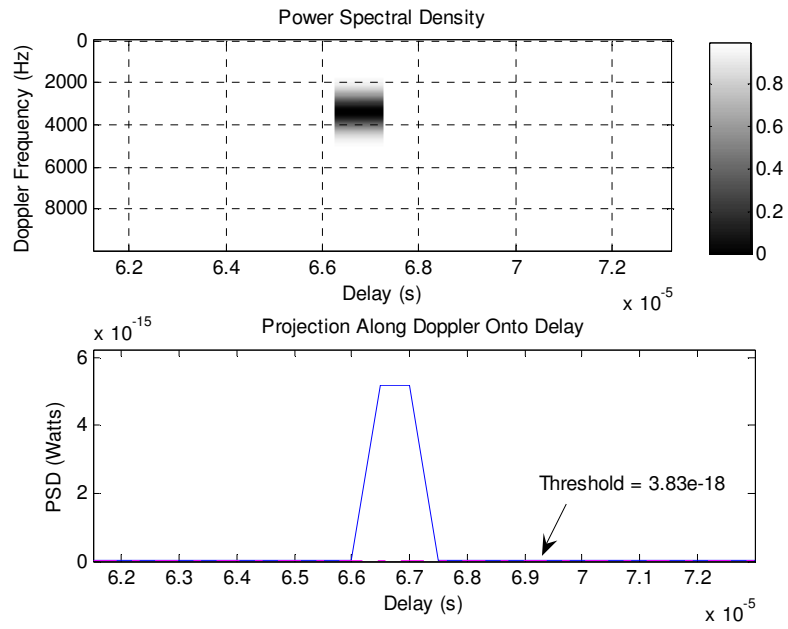


Figure 3-17: PSD of the return signal within the range gate, and its projection on delay axis.

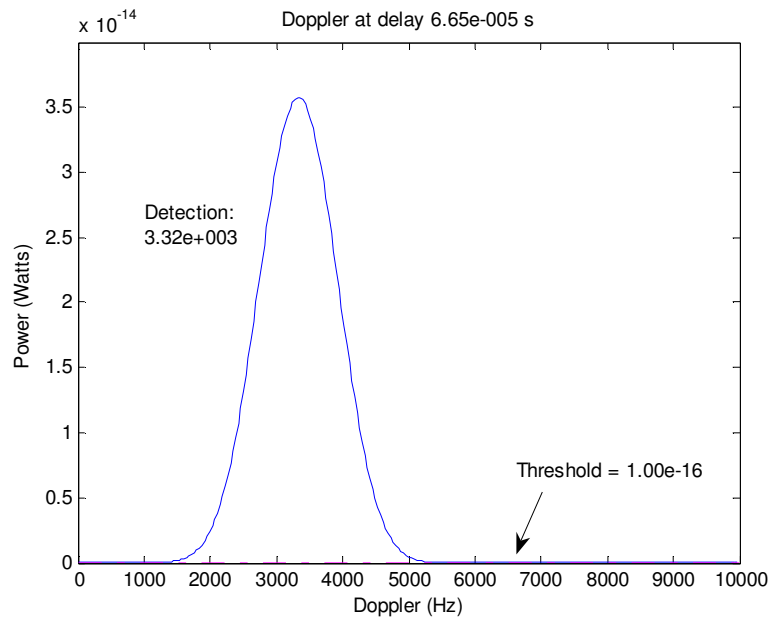


Figure 3-18: Doppler measurement within the first snapshot.

In the radar simulator implemented in this thesis, cell-averaging CFAR is used. Cell averaging is performed on the radar return within the range bins (cells) outside the range gate. The range gate is about 13 range cells, 6 neighboring range cells on each side of the current cell. The number of neighboring range cells in a range gate is a parameter in the simulator program. A CFAR estimate is obtained from the remaining range cells outside the range gate. With the current settings, a range cell is about 150 m. Then about 87 remaining range cells outside the range gate in a PRI are used for the CFAR computation.

The CFAR estimates throughout the snapshots are shown in Figure 3-19. The noise produced by a random number generator for the simulation had a variance of 2.02×10^{-14} . The CFAR estimates are very close to the true value of the noise power.

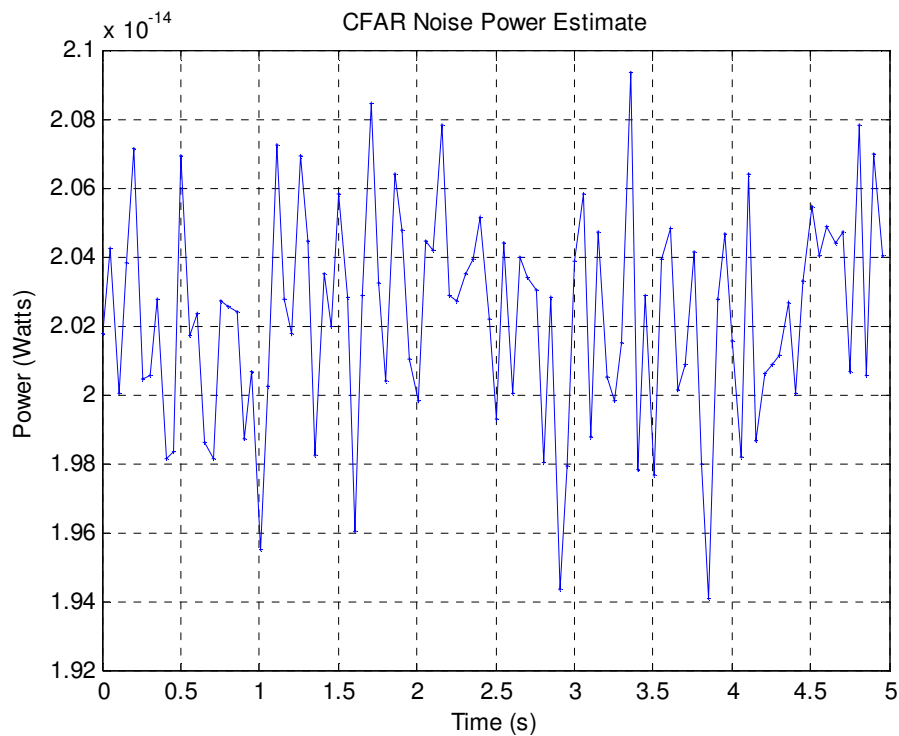


Figure 3-19: CFAR noise power estimate throughout the snapshots.

Tracking results for the no-jamming case are displayed in Figure 3-20 through Figure 3-23 together with true range and velocity of the target. The range measurements and estimates are shown in Figure 3-20. The target's true range starting at about 10 km is indicated. The measurements are about the true range and the estimates follow the measurements. The velocity measurements and estimates are shown Figure 3-21. The velocity measurements are at about 49.8 m/s, which is close to the target's constant velocity of 50 m/s within the velocity resolution dictated by the parameters. The estimates converge to the value of the measurements. Figure 3-22 and Figure 3-23 display the error in range and velocity tracks with regard to the true target range and velocity.

The error performance can be quantified by using the root mean square error (RMSE). RMSE is formulated as follows:

$$RMSE = \sqrt{\frac{1}{N_s} \sum_{k=1}^{N_s} |x_k - \bar{x}_k|^2} \quad (3.45)$$

where x_k is the observed value (a range/velocity measurement or estimate), \bar{x}_k is the true value (true value of range or velocity) and N_s is the number of measurements (that is, snapshots).

For this reference run, the root mean square error (RMSE) of range and velocity estimates is 38.9 m and 1.17 m/s respectively and of range and velocity measurements are 55.1 and 0.2 m/s respectively. RMSE for both quantities are in the resolution boundaries. Note that the RMSE values are from a single run of the simulator program. Even though the figures are consistent, a Monte-Carlo simulation should be run for a large number of noise realizations if more reliable RMSE figures are desired.

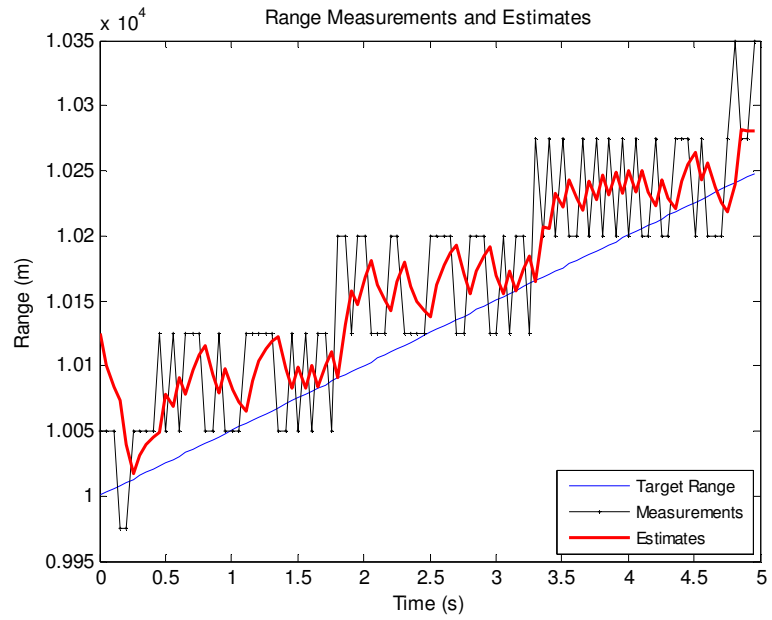


Figure 3-20: Range estimates/measurements for no-jamming tracking scenario.

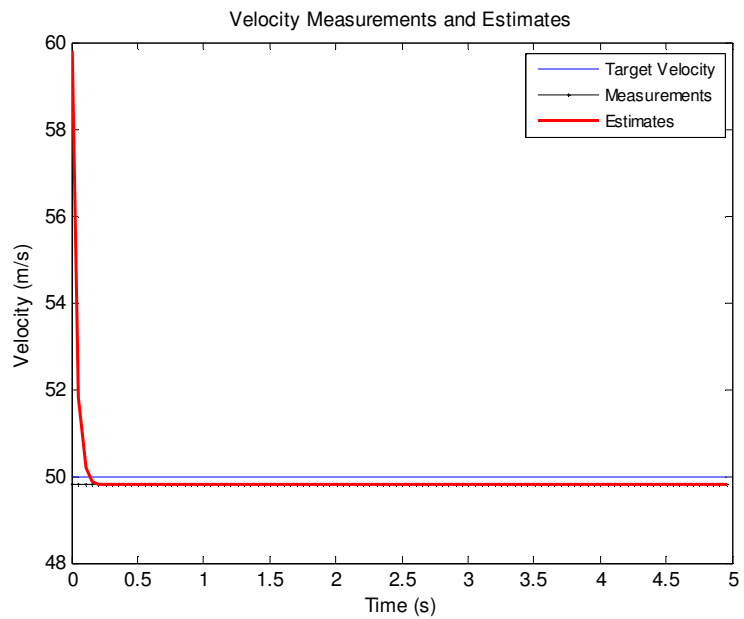


Figure 3-21: Velocity estimates/measurements for no-jamming tracking scenario.

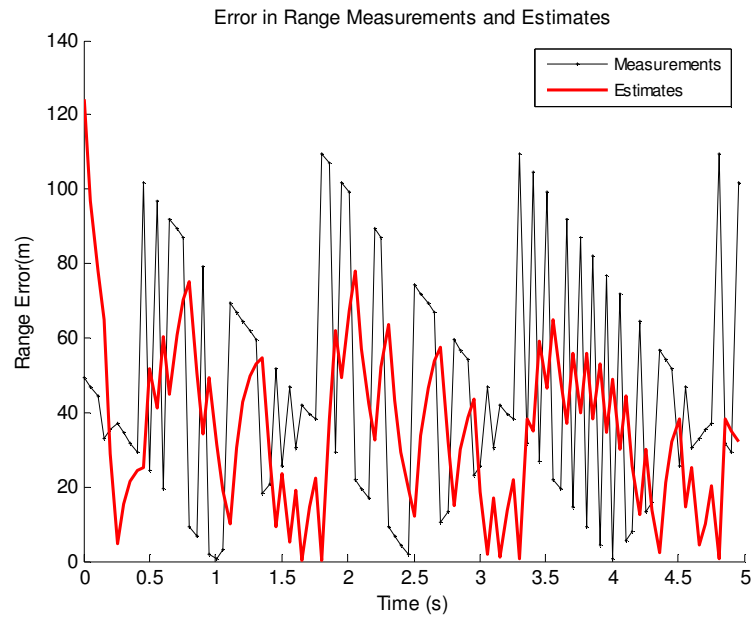


Figure 3-22: Error of range measurements/estimates for no-jamming tracking scenario.

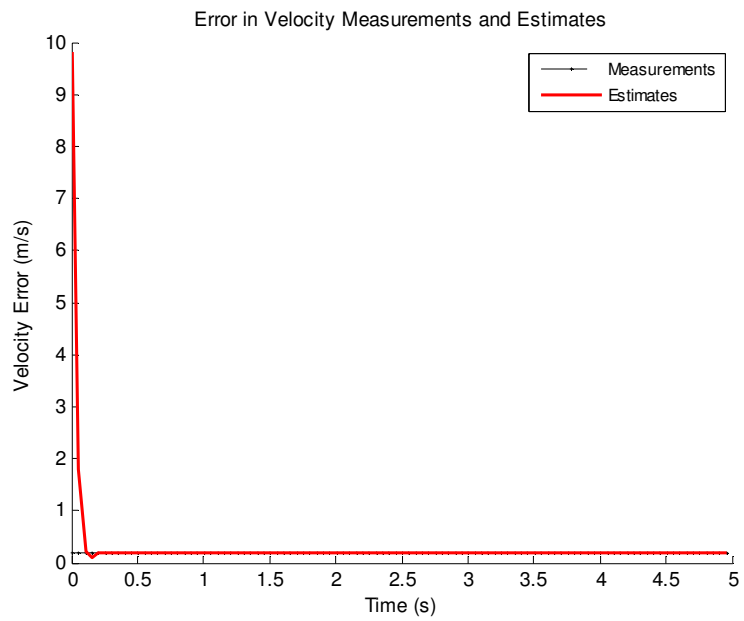


Figure 3-23: Error of velocity measurements/estimates for no-jamming tracking scenario.

Note that the true range is computed by using the initial range and the constant velocity of the target. In that respect, it is the theoretical range and velocity of the target. The simulated target return can be of slightly different range and velocity values than those from such a calculation due to the quantization errors in the simulation stage. For instance, a range value of 10 km assigned to a target would correspond to a return pulse with time-of-arrival index (Matlab indices start from 1) of 134.33 which is rounded to 134 in the simulation of the received signal (target return).

A similar representation error occurs for the velocity of the target as well. Such errors come into picture at the detection stage, that is, they affect the measurements, as if they are errors emanating from the detection stage. The actual detection errors are only due to the presence of noise (either thermal noise or spot noise) in the received signal.

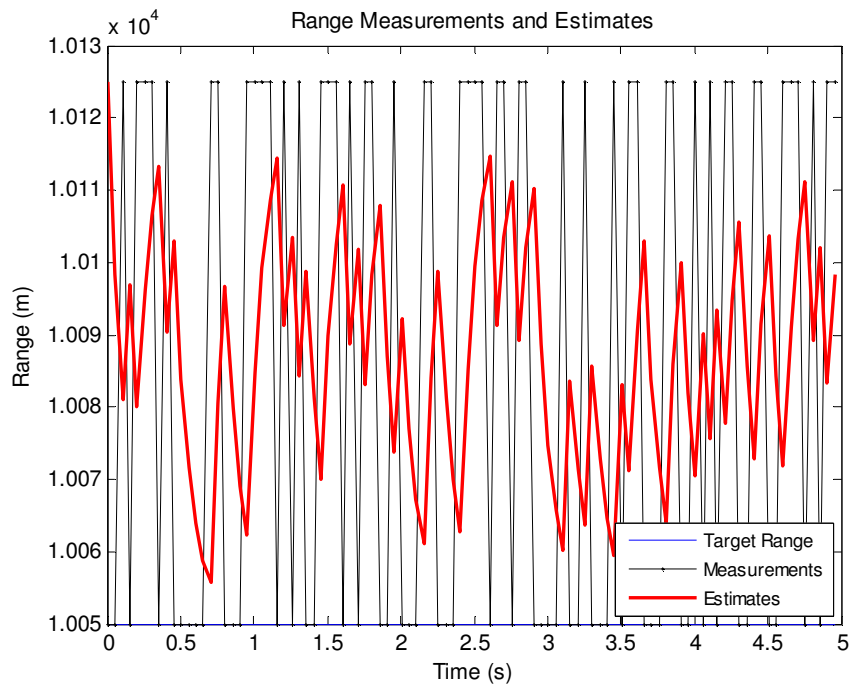


Figure 3-24: Range estimates/measurements for a stationary target at 10050 m.

To illustrate this point a stationary target at 10050 m is tracked. The range measurements and estimates are shown Figure 3-24. The range measurements hop between 10050 m and 10125 m. The hopping is due the peak detection algorithm as explained about Figure 3-17. However, there is no range representation error since the target range, 10050 m, in this example is a multiple of 75 m which is the range represented by a sampling interval in the simulation. The velocity measurements (not shown here) are all 0 and estimates converge to the measurements.

A similar simulation is performed for a stationary target at 10075 m, which is not a multiple of 75 m. The result is shown in Figure 3-25. This time the measurements still hop between 10050 and 10125 m since the received pulse still is represented by those sample points in range.

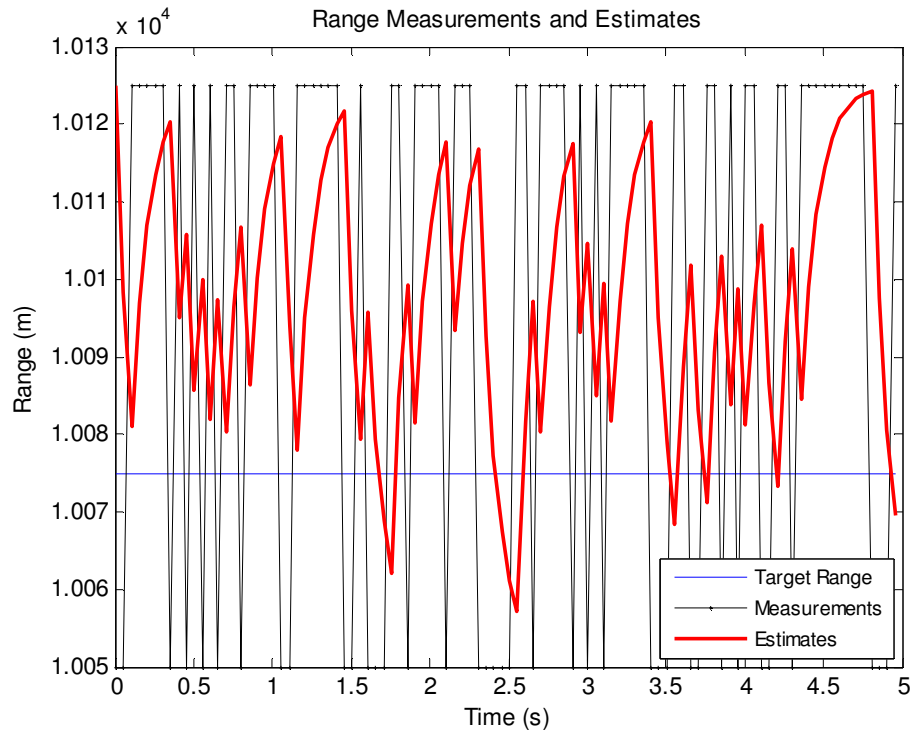


Figure 3-25: Range estimates/measurements for a stationary target at 10075 m.

To illustrate that the velocity measurement errors in Figure 3-21 are due to the reason explained above (the same reason, but for the Doppler frequency dimension), a simulation is performed similar to that produced results in Figure 3-20 through Figure 3-23, but with velocity set to 50.9765625 m/s. This is a multiple of the Doppler velocity ΔV that corresponds to the frequency sample resolution Δf_d represented by the 256-point FFT used in the simulations and the current radar settings. The velocity measurements and estimates are shown (magnified) in Figure 3-26. The measurements are the same as the true value. Thus the delay-Doppler detection used in the radar receiver simulator produces correct measurements, but within quantization errors due to the discrete nature of the simulated target return, and within errors due to noise (thermal noise or spot-noise as will be investigated in the next section).

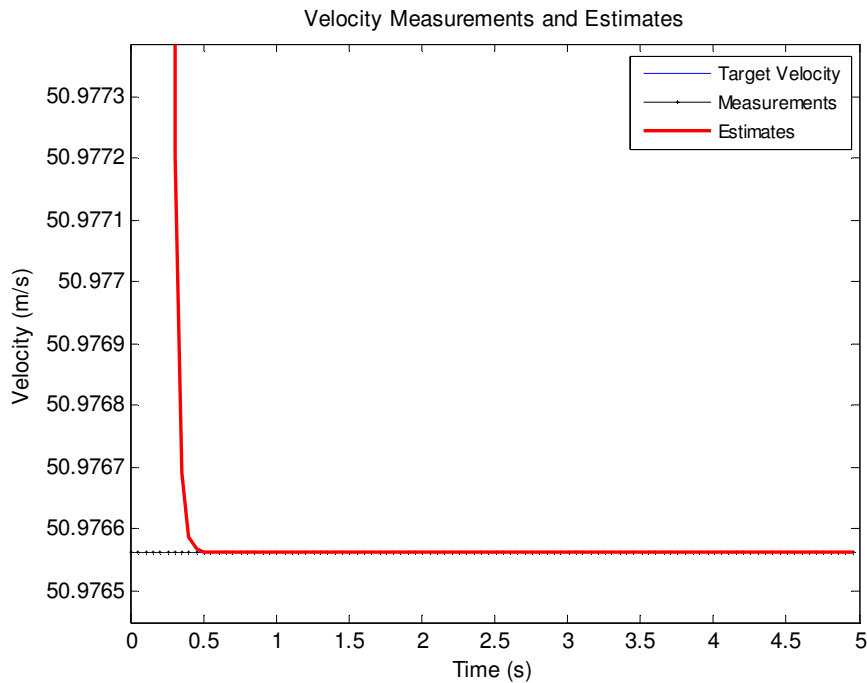


Figure 3-26: Velocity estimates/measurements for a target with no velocity representation error.

CHAPTER 4

JAMMING AND ITS EFFECTIVENESS

4.1 The Jamming Concept

Electronic Countermeasure techniques are applied against the radars in order to jam or deceive the radar receivers. For these purposes, two basic methods are used in the simulator. These methods consist of noise and range deception which is known as repeater technique.

4.1.1 Noise Technique

The noise technique is chosen as spot noise which is a narrowband noise technique. In the simulations, the noise bandwidth is chosen as 5 MHz. The noise is chosen as Gaussian distributed white noise with variance being equal to the half of the self protection jammer's skin paint. The noise is additive on the amplitude of the received signal. As this simulation model is based on base band, the noise model has also complex parameters as the received radar signal. The jammer signal skin paint power is calculated by using the JSR value as specified in the following formula:

$$P_{ssj} = P_r 10^{JSR/10} \quad (4.1)$$

Here, P_r is the received radar echo power and JSR is the jamming to signal ratio in dB, given as

$$JSR = 10 \log \left(\frac{P_{ssj}}{P_r} \right) \quad (4.2)$$

In addition, the jammer's peak power is calculated as:

$$P_j = P_{ssj} \frac{(4\pi)^2 R_j^2 B_j}{G_j G \lambda^2 B} \quad (4.3)$$

Here, R_j is the radar's lethal range at which the self protection jammer starts the jamming process. B_j is the jammer's operating band width; G_j is the jammer antenna gain. G is the radar's receive antenna gain, and B is the radar's operating bandwidth. During the simulation process G_j is set to $G/1000$, and B_j is set to 5 MHz.

The effects of jamming on the radar's detection and tracking process are observed for different JSR values. The change of jammer's peak power also observed for checking validity of these power values as they are assumed as coming from a jammer transmitter.

4.1.2 Range Gate Pull Off (RGPO)

The other basic technique modeled against the simulated radar is RGPO. The main difference between the RGPO and the noise techniques is the original signal source. In the noise technique, the signal source is noise generator while it is the original signal itself in the RGPO. RGPO uses a DRFM in order to process the stored signal by using processes such as delaying the signal, amplifying the signal, directly repeating the signal, overlapping two amplified and delayed signals, etc.

RGPO is self screening ECM technique for use against automatic range tracking radars that capture the victim radar's range gate, pull (walk) it off in range, then turns off, leaving the range gate with no signal.

Automatic tracking radars, which are used for weapon guidance and fire control applications, generally employ early and late tracking gates that straddle the return echo. The gates are removed by a range servo, which follows the target by predicting its future position using a range gate or velocity estimate developed in the range tracker. All other returns, except those returned within the tracking gates, are excluded by the range tracking circuit. This prevents spurious signals from entering the range tracking circuitry and distorting the range estimate, but it also offers the opportunity for a deception jammer to operate in a range stealing or track breaking mode.

RGPO technique causes the radar to get false target range information. This false target range information can result in significant aiming guidance errors for anti-aircraft guns and for missiles that use command guidance because the ground-based computation of weapon lead angle is strongly influenced by the target range as determined by the radar. However, the tracking radar angle circuitry still functions to point the radar antenna's boresight in the direction of the target. This angle information is sufficient for missile guidance, and hence RGPO by itself is not sufficient to prevent hits by the weapon system.

The main purposes of the technique are to break the range track circuit of the range tracking radar.

RGPO is applied against pulsed, automatic, and range tracking radars.

RGPO is generally used with angle jamming techniques. But in the concept of this simulation, spot noise technique is used together with RGPO.

4.1.2.1 Jamming procedure

Following jamming procedure is used for the conventional RGPO technique.

1. Dwell: The victim radar's signal is received, amplified, and is retransmitted with minimum delay to provide a strong beacon signal to the radar. The beacon signal causes the radar receiver gain to decrease because of AGC (Automatic Gain Control) action. As a result, true target RCS signal is suppressed and radar range gate circuit is captured by the strong beacon signal. AGC simulation is not required in the simulations of this study since floating point precision is used in the simulation environment of Matlab. Note that the main purpose of AGC is to fully utilize the available dynamic range. Note also that the simulations of this study are based on single-target tracking via the detection of the prominent target.
2. Pull-off/Walk: The time delay of the repeated signal is progressively increased on a pulse to pulse basis, from true target position out to a time equivalent to many radar range gate widths.
3. Hold: Upon reaching the outer pull-off limit, the ECM repeater is turned off.
4. The program cycle can be repeated if required.

The typical properties of a pull-off period are as follows:

- During the pull-off period, false targets can be created by using RGPO with hold out or overlapped RGPO techniques.
- The maximum acceleration rate must not exceed the victim radar's range tracking limits. In the simulations of this study, constant velocity target are used.

A typical RGPO delay (time offset between the target echo and the jamming pulse) as a function of time is depicted in Figure 4-1.

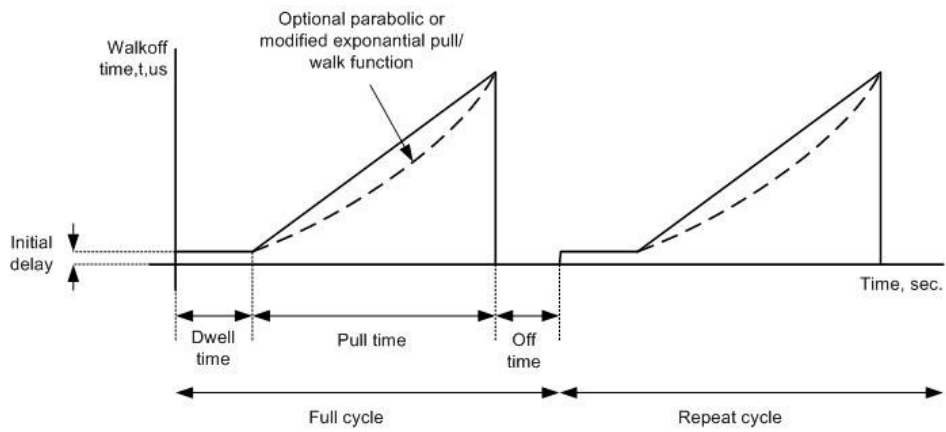


Figure 4-1: RGPO Video Programming Waveforms

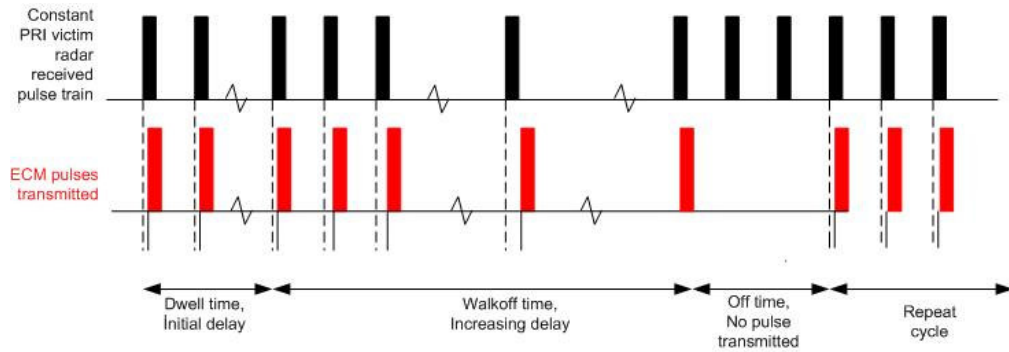


Figure 4-2: RGPO pulse generation

4.1.2.2 ECM parameters

The main parameters in order to define an RGPO technique are as follows:

- Dwell time: This is the time during which cover pulse is to be applied (For each RGPO cycle it can be set to a different value).
- Pull/Walk time: This is the time during which the TOA of received jamming pulses walk. It shall walk away from the echo pulse at least at an amount of ten (10) PW duration. (For each RGPO cycle it may be different)
- Off time: This is the time at which the ECM repeater is turned off upon reaching the outer pull-off limit, (For each RGPO cycle it can be set to a different value).
- Pull/Walk time function (parabolic or linear): This function denotes the change of time delay pattern.
- Number of RGPO cycles: This denotes the number of required RGPO cycles.
- RGPO cycle period: This is the duration of one RGPO program cycle. This may be different for each RGPO program cycle.
- Power increment function (parabolic or linear)
 - Initial power: This is the power of jamming pulses during dwell.
 - Maximum power: This is the maximum power value of jamming pulses gathered at the end of the pull/walk time which should be determined considering the radar receiver limits.
 - Slope of the function: This value is slope of power function.

4.1.2.3 Required radar signal parameters

In order to assign an effective jamming technique against a radar mode, one should know the radar's receiver characteristics. The transmit parameters like RF, PRI, PW and modulation type are also required. These parameters can be listed as follows.

- Pulse width
- RF frequency, RF frequency set
- PRI, PRI set
- Modulation on pulse train (For instance, Frequency Modulation specifies maximum range of radar)
- Radar's range tracking circuit limits.
 - Maximum range gate speed/ acceleration limit
 - Range estimation procedure like Alpha-Beta filter; Alpha-Beta-Gamma filter, Kalman filter.
 - Used information for range tracking like Doppler frequency, angle, and etc.
 - Band Width

4.1.3 Related Techniques

RGPO type related techniques can be classified as RGPI, Overlapped RGPO, and RGPO with Hold out (Hook).

4.1.3.1 RGPI

RGPI simulating an inbound target is applied mostly against leading edge range trackers. In order to apply this technique the repeater should anticipate the reception of the radar pulse and also have sufficient storage capability to store the radar pulse for one pulse repetition interval (PRI). For this purpose, the repeater timing should be initiated from previous received pulse. That is provided by using trackers in the jammer system.

4.1.3.2 Overlapped RGPO

This RGPO program consists of the combination of two RGPO programs one starting with a delay after the first one is started. This technique creates multiple range false targets.

4.1.3.3 RGPO with hold out (hook)

This technique is a combination of a hold-out pulse and an RGPO pulse. The jamming pulse is walked towards the hold-out pulse. When the TOA of the last jamming pulse matches with the TOA of the hold-out pulse, the pull/walk period is completed. Like overlapped RGPO, this technique creates multiple range false targets.

4.2 Tracking Performance under Jamming

In this section, the results of tracking simulations performed using jamming pulses and jamming noise together with the simulated target returns are presented. There are many radar parameters and subsystems that effect the performance of a tracking system. Here, we tried to vary only a few parameters that are most relevant to the respective jamming technique and keep the other parameters the same as of the tracking simulation without any jamming signal described in Section 3.5.

4.2.1 Spot-Noise Jamming

Here a noise signal is used as the jamming signal. The parameter JSR_{spn} indicating the amount of jamming noise is varied and tracking results are observed.

Here the subscript *spn* stands for spot-noise. In RGPO type methods, a jamming pulse (RGPO, RGPI, etc. pulse) and spot-noise are used together for a certain part of the jamming period and only the jamming pulse for the rest of the period. The parameter indicating the jammer-to-signal ratio for the jamming pulses is JSR. It is kept different from JSR_{spn} to enable assigning separate ratios to jamming pulse and jamming noise.

The simulation was first run for $JSR_{spn}=6$ dB. The number of snapshots is 100 and the snapshot offset is 0.05 s. The target return and the jamming noise for the last snapshot and the received signal throughout the snapshots are shown in Figure 4-3. Note the level of jamming noise and thermal noise. Target range and jammer power are shown in Figure 4-4 for all snapshots. To satisfy a given JSR_{spn} value for all instances, the jammer transmit power (and hence jammer received power) is varied in accordance with the target range. Figure 4-5 shows the CFAR estimate for the snapshots. CFAR estimate shows a similar declining trend as of the jammer transmit power.

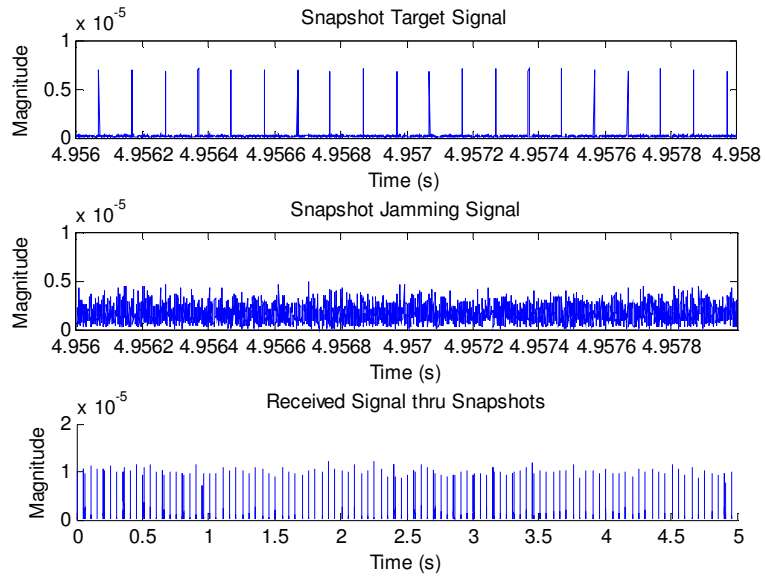


Figure 4-3: Target return and the jamming noise for the last snapshot (Snapshot 100) and the received signal throughout snapshots. Spot-noise, $JSR_{spn} = 6$ dB.

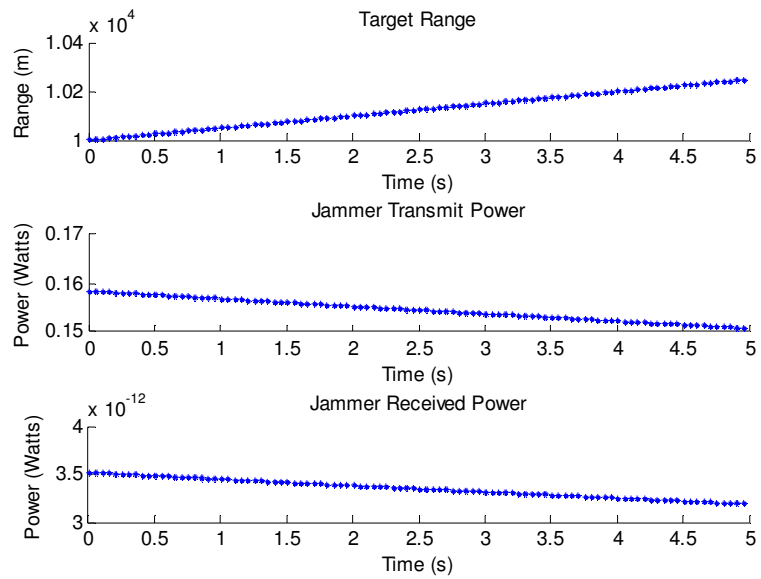


Figure 4-4: Target range, jammer transmit/received power. Spot-noise, $JSR_{spn} = 6$ dB.

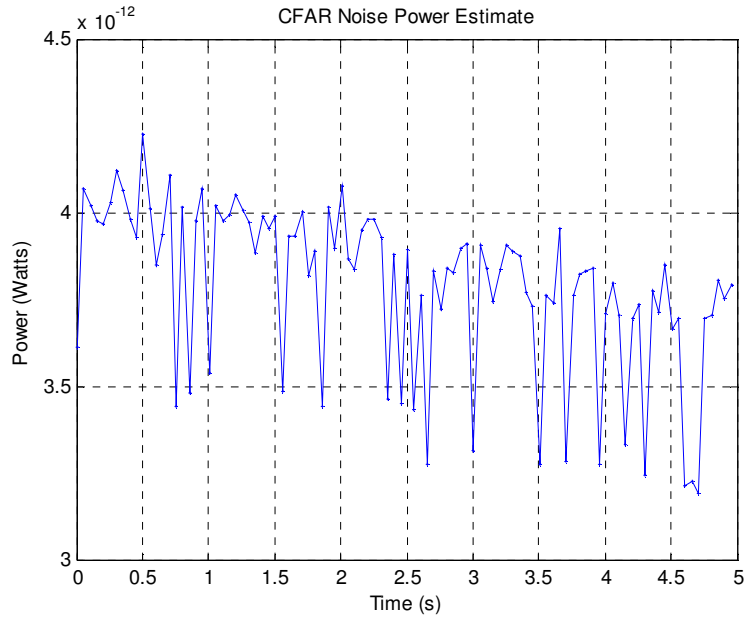


Figure 4-5: CFAR noise power estimate throughout the snapshots. Spot-noise, $\text{JSR}_{\text{spn}} = 6$ dB.

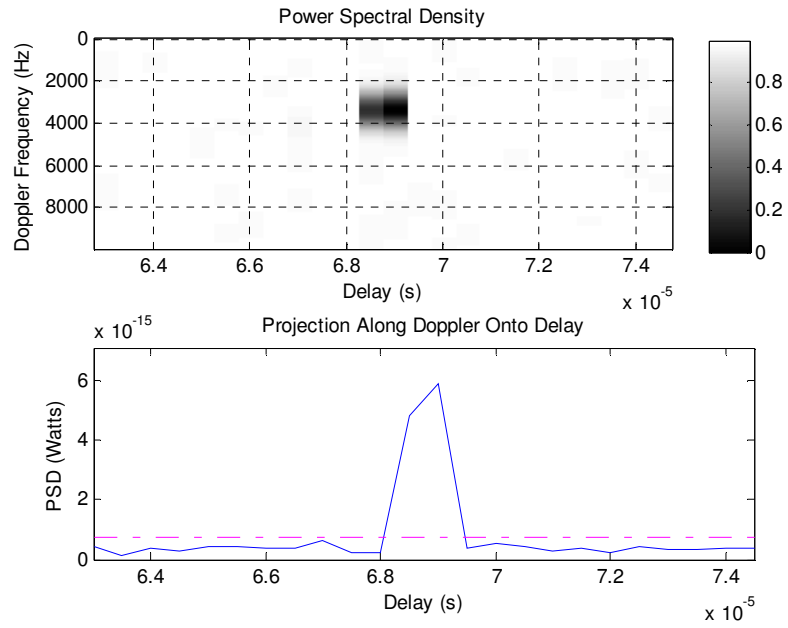


Figure 4-6: PSD for the last snapshot of spot-noise jamming simulation for $\text{JSR}_{\text{spn}} = 6$ dB.

Power spectral density for the last snapshot is shown in Figure 4-6. Note that the level of the threshold 6.87×10^{-16} is much higher than that of the no-jamming case, which is 3.83×10^{-18} . That rise is due to the CFAR estimate of the total noise power (jamming and thermal components, where the thermal component is relatively quite small).

Figure 4-7 through Figure 4-10 display the measurement and estimate tracks for range and velocity. The RMSE for range and velocity estimates are 43.9 m and 1.09 m/s respectively. The RMSE for range and velocity measurements are 58.53 m and 0.28 m/s respectively. Note that the RMSE values are close to those of the no-jamming case, indicating that the target is being tracked.

The measurement and estimate tracks for range and velocity with the setting $JSR_{\text{spn}} = 8$ dB are shown in Figure 4-11 through Figure 4-14. The RMSE are slightly higher but close to that of 6-dB case. For $JSR_{\text{spn}} = 9$ dB, only range tracking result is shown in Figure 4-15. The track was dropped due to the lack of measurement updates consecutively, which in turn is due to rising CFAR noise power estimate that increases the time domain threshold and hence increases the thresholds used in PSD domain for delay-Doppler measurement. For higher JSR_{spn} values greater than 9 dB, track is dropped much earlier.

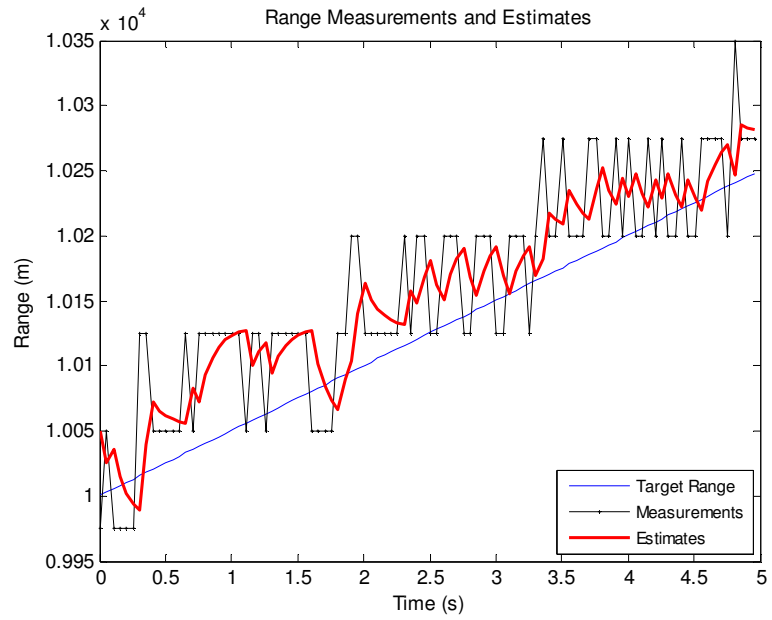


Figure 4-7: Spot-noise jamming, $\text{JSR}_{\text{spn}} = 6 \text{ dB}$. Range measurements/estimates.

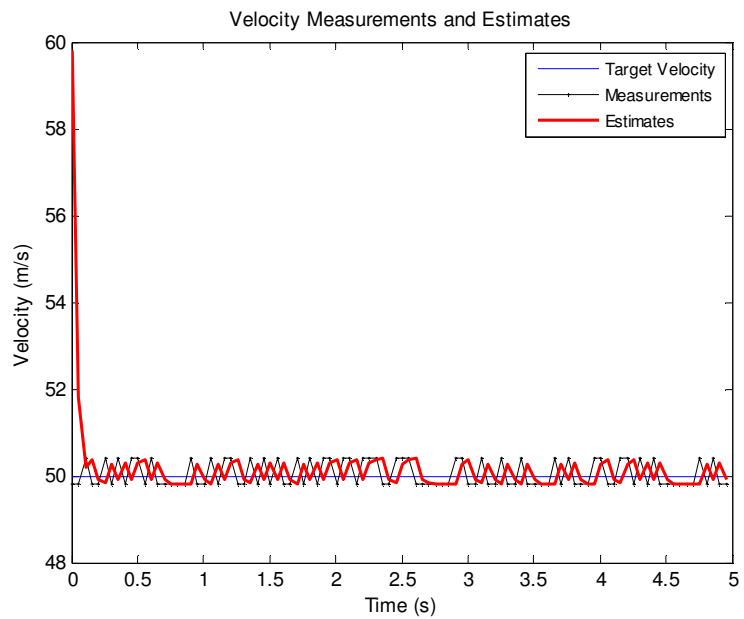


Figure 4-8: Spot-noise jamming, $\text{JSR}_{\text{spn}} = 6 \text{ dB}$. Velocity measurements/estimates.

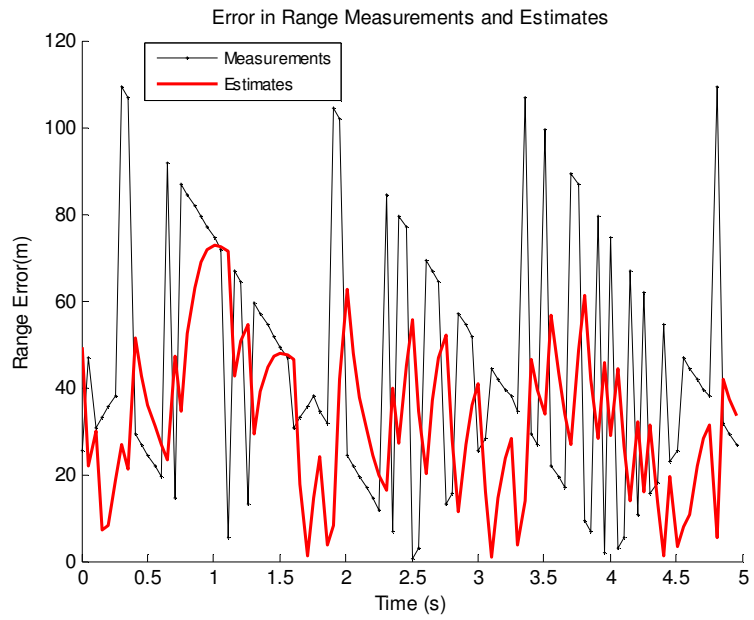


Figure 4-9: Spot-noise jamming, $JSR_{spn} = 6$ dB. Error of range measurements/estimates.

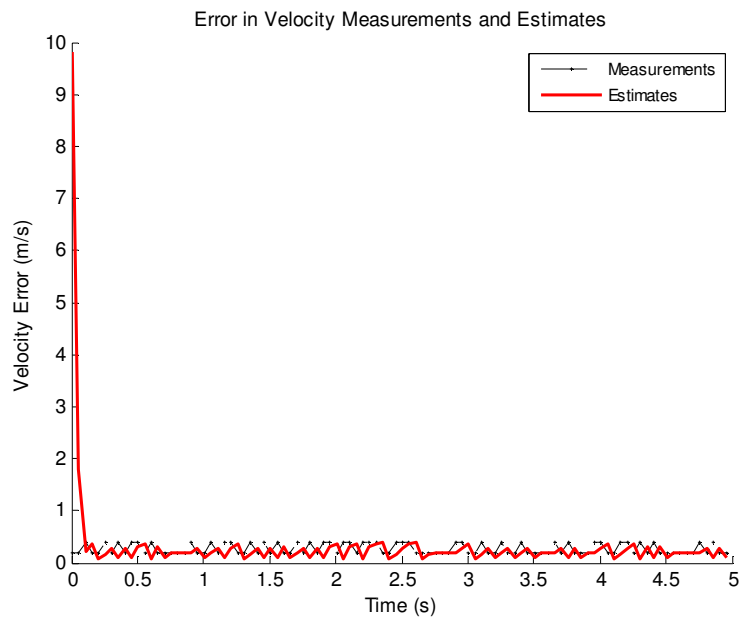


Figure 4-10: Spot-noise jamming, $JSR_{spn} = 6$ dB. Error of velocity measurements/estimates.

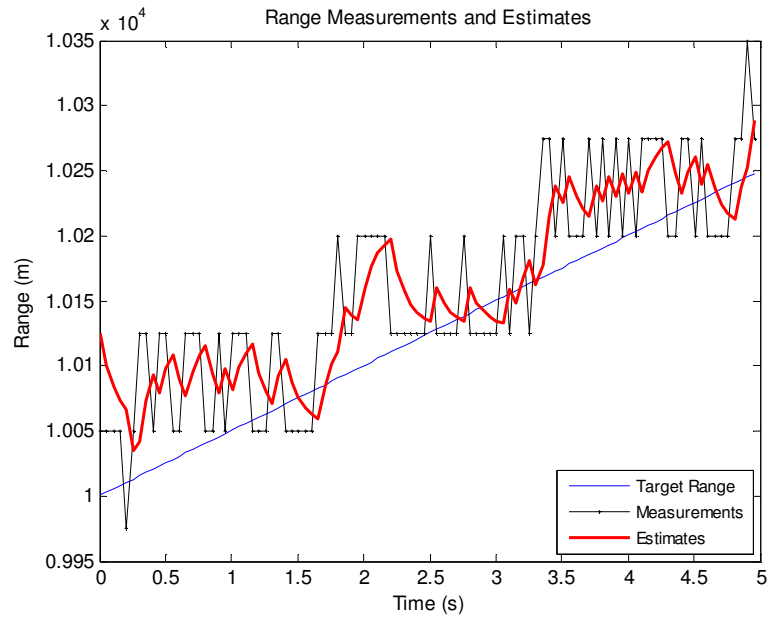


Figure 4-11: Spot-noise jamming, $JSR_{spn} = 8$ dB. Range measurements/estimates.

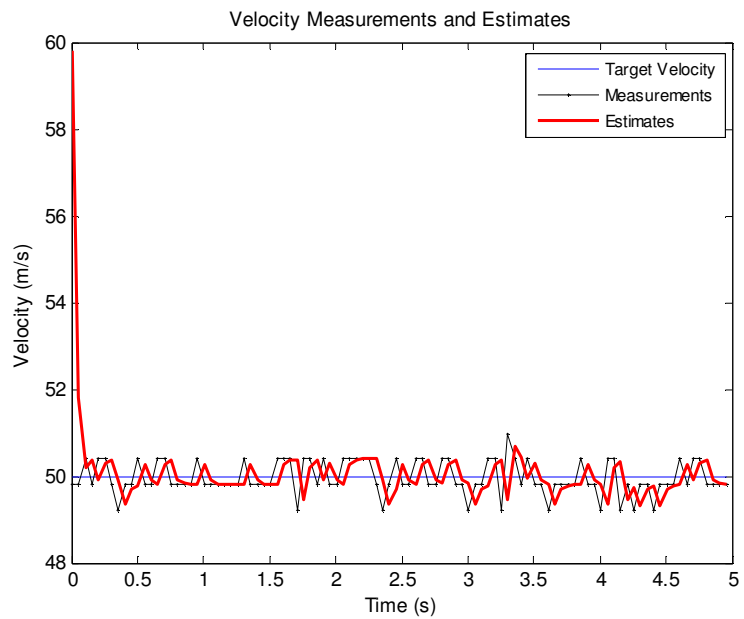


Figure 4-12: Spot-noise jamming, $JSR_{spn} = 8$ dB. Velocity measurements/estimates.

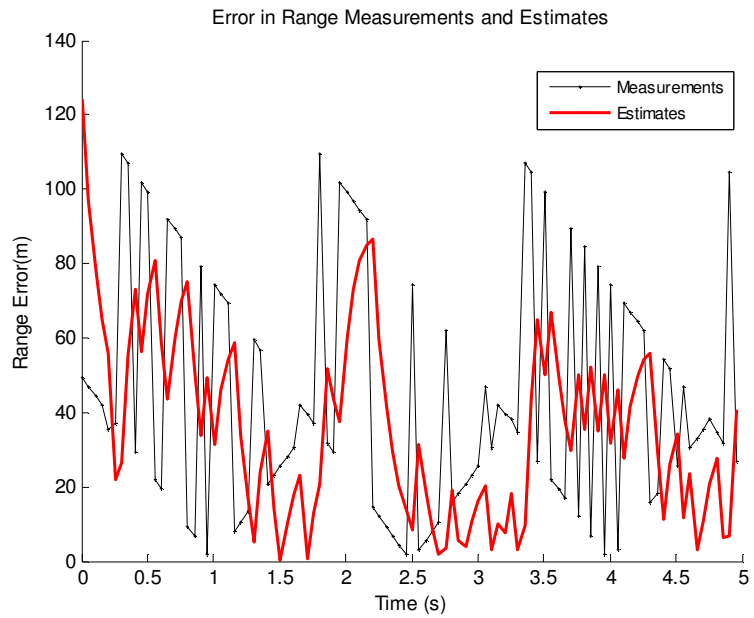


Figure 4-13: Spot-noise jamming, $JSR_{spn} = 8$ dB. Error of range measurements/estimates.

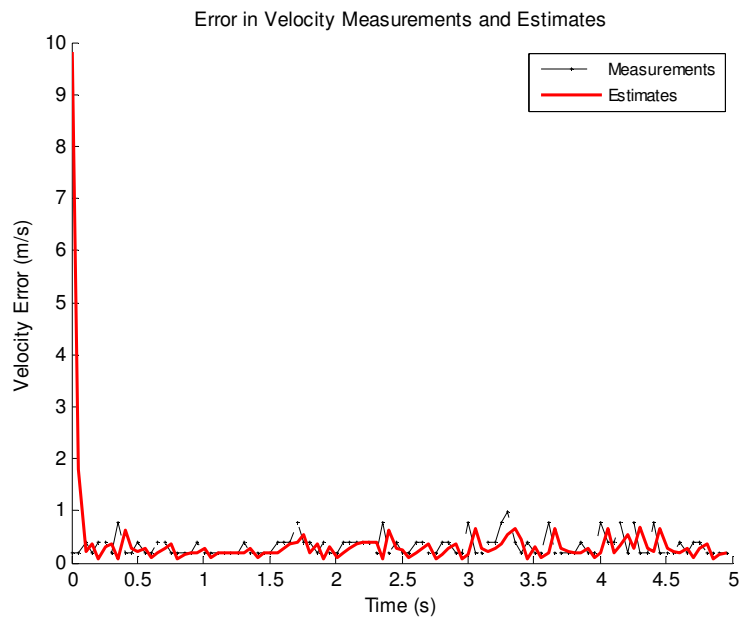


Figure 4-14: Spot-noise jamming, $JSR_{spn} = 8$ dB. Error of velocity measurements/estimates.

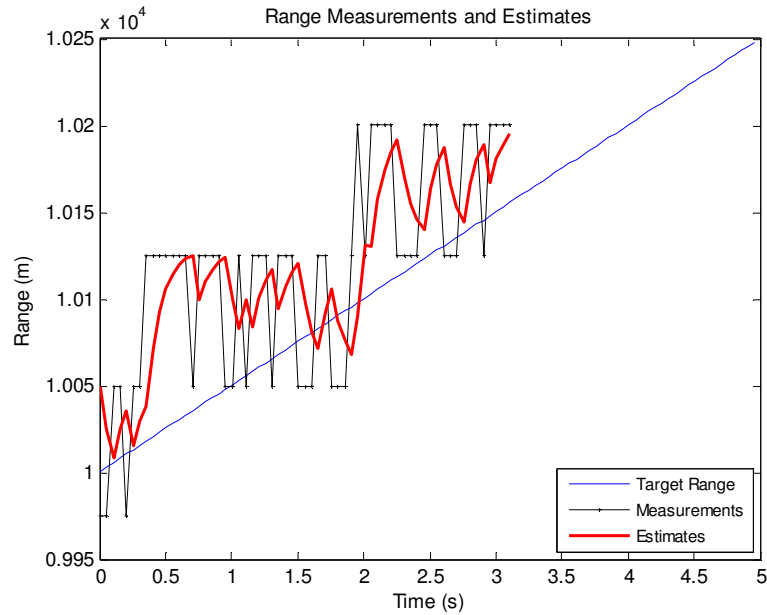


Figure 4-15: Spot-noise jamming, $JSR_{spn} = 9$ dB. Range measurements/estimates. Track is dropped due to the lack of measurement updates.

4.2.2 RGPO

Here, a jamming pulse is used together with jamming noise (spot-noise) as the jamming signal. The jamming pulse first covers the target return (dwell), and then slowly moves away so that the radar tracks the false target (pull-off) and stops after certain time (hold). Spot-noise is utilized only for a certain time covering the dwell and part of pull-off periods. Figure 4-16 displays profiles of such settings as a function of time. Spot-noise gain is either 1 or 0 indicating presence or absence of spot noise, respectively. The actual amount of spot-noise is quantified by the

parameter JSR_{spn} . Similarly, RGPO gain is different from JSR; it is used to assign amplitude for the RGPO pulse.

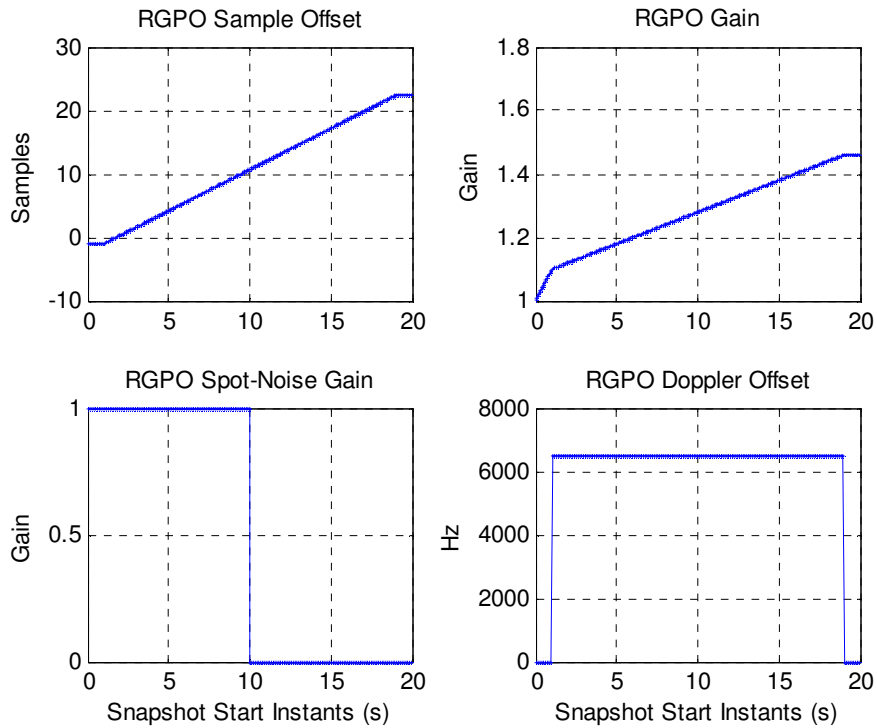


Figure 4-16: RGPO offset and gain profiles.

Sample offset is the number of samples the RGPO pulse's leading edge is displaced with respect to the leading edge of the target return. In the dwell period, the offset is set to -1, and the RGPO pulse width is set to be one sample larger than the target return. Thus an offset of -1 sample lets the RGPO pulse cover the target return fully. In the pull-off period, the RGPO pulse is pulled away from the target return, and in the hold section, it is hold at a constant sample offset relative to the target return.

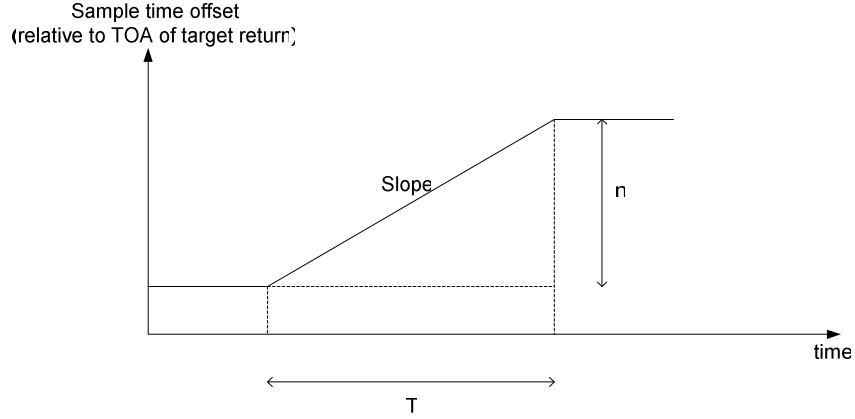


Figure 4-17: A typical RGPO sample-offset profile.

A typical RGPO sample-offset profile is shown in Figure 4-17. Slope in the pull-off period is given by

$$s_{RGPO} = \frac{n}{T} \quad (4.4)$$

The slope is positive for RGPO (and negative for RGPI, which is described in the next section). The amount of range pull-off can be computed as

$$R_{offset} = n T_s \frac{c}{2} \quad (4.5)$$

where T_s is the sampling period. With $T_s = 0.5 \mu s$ and $c = 3 \times 10^8 \text{ m/s}$

$$R_{offset} = n \times 75 \text{ m} \quad (4.6)$$

Then, Doppler velocity and frequency offset are given in terms of the slope as

$$V_{offset} = \frac{R_{offset}}{T} = \frac{n}{T} 75 \text{ m/s} = s_{RGPO} \times 75 \text{ m/s} \quad (4.7)$$

$$f_{d,offset} = \frac{2V_{offset}}{\lambda} = \frac{2 \times s_{RGPO} \times 75}{0.03} = s_{RGPO} \times 5000 \text{ Hz} \quad (4.8)$$

In Figure 4-16, s_{RGPO} is 1.3 samples/s. This corresponds to a frequency (Doppler) offset of 6500 Hz. This is shown in the Doppler offset profile. Note that the range and velocity of the RGPO pulse are coordinated by this setting. The Doppler offset of 6500 Hz corresponds to a velocity offset of 97.5 m/s. Adding the target velocity of 50 m/s to that, the absolute velocity of the false target created by the RGPO pulse is found to be 147.5 m/s. This corresponds to an absolute Doppler frequency of 9833 Hz, which is the frequency to be measured in the delay-Doppler detection stage.

For this simulation, the number of snapshots is set to 400 with snapshot offset of 0.05 s, making the total tracking time of the simulation 20 s. The simulation was first run for $JSR_{spn} = 6$ dB and $JSR = 6$ dB. Figure 4-18 through Figure 4-21 display the PSD in dwell, pull-off and hold periods. Note that the Doppler frequency of the jamming pulse in PSD suits the Doppler offset profile.

The CFAR estimates throughout the snapshots in Figure 4-22 indicate the presence of spot-noise for the duration it was applied, thermal noise (the reading around 2×10^{-14} from the plot matches the actual noise power used) and the target return moving out of the range gate as the radar receiver follows the RGPO pulse.

The measurement and estimate tracks are shown in Figure 4-23 and Figure 4-24. The pull-off in the range dimension was successful. The resulting RMSE was about 961.4 m and 92.3 m/s for range and velocity estimates, and 968.1 m and 92.4 m/s for range and velocity measurements. The RMSE values also indicate a successful false target creation using the RGPO jamming. Note that the estimates closely track the measurements.

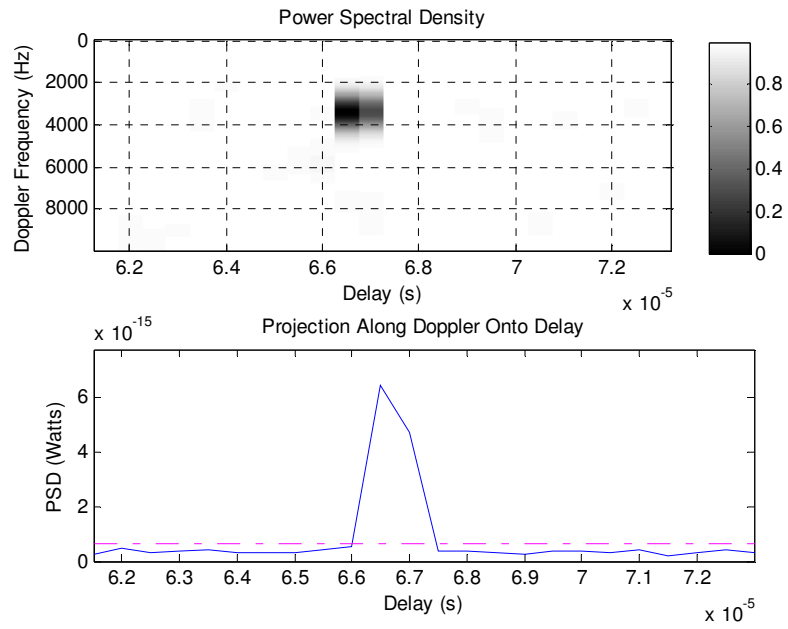


Figure 4-18: RGPO. Snapshot 1, cover pulse. Spot-noise present. $s_{RGPO} = 1.3$ samples/s.

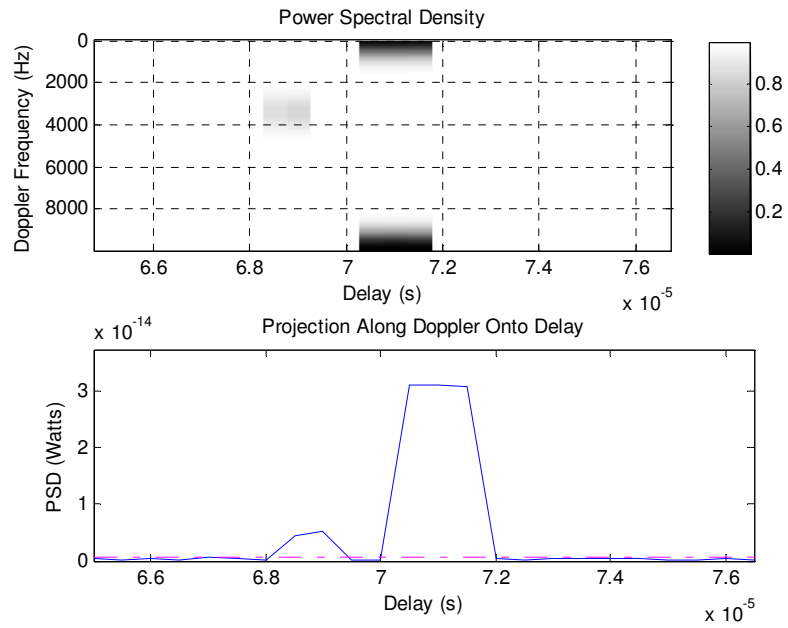


Figure 4-19: RGPO. Snapshot 108, jamming pulse starts pull-off. Spot-noise present. $s_{RGPO} = 1.3$ samples/s.

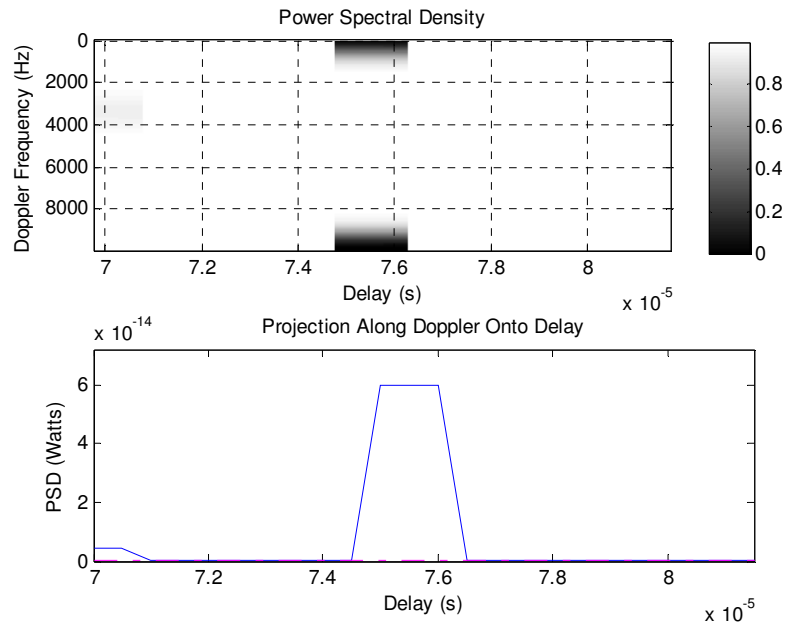


Figure 4-20: RGPO. Snapshot 203, further in pull-off. Spot-noise not present. $s_{RGPO} = 1.3$ samples/s.

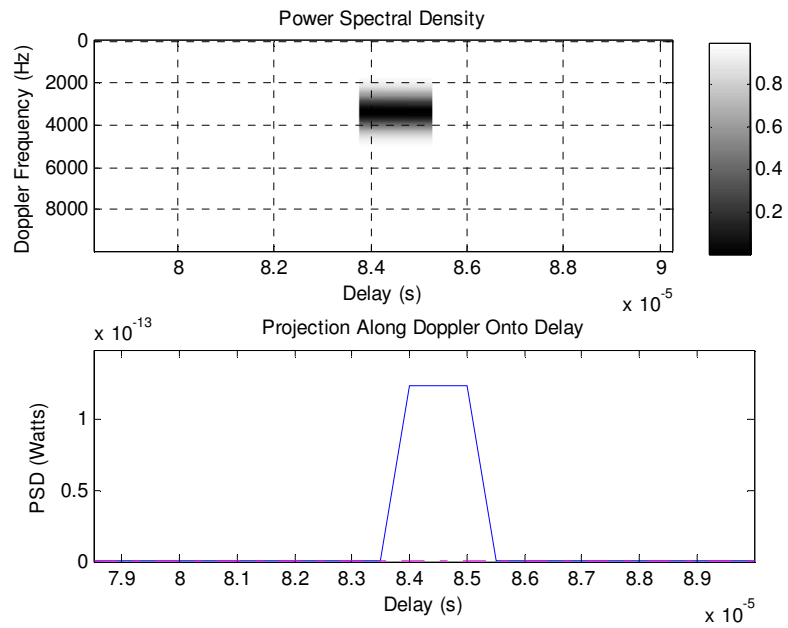


Figure 4-21: RGPO. Snapshot 384, hold period. Spot-noise not present. $s_{RGPO} = 1.3$ samples/s.

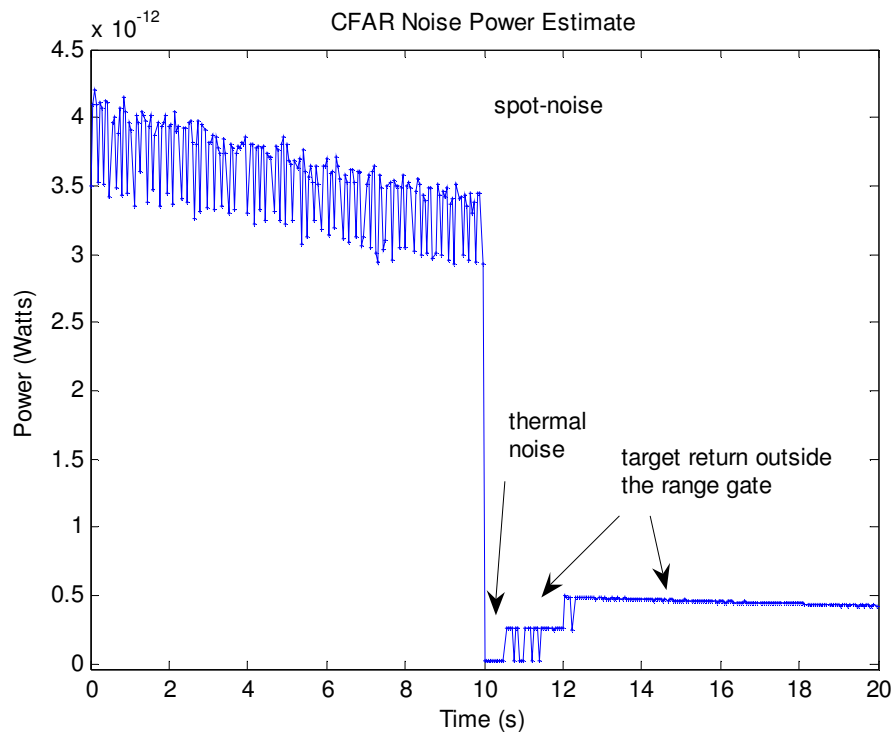


Figure 4-22: RGPO. CFAR noise power estimate. $s_{RGPO} = 1.3$ samples/s.

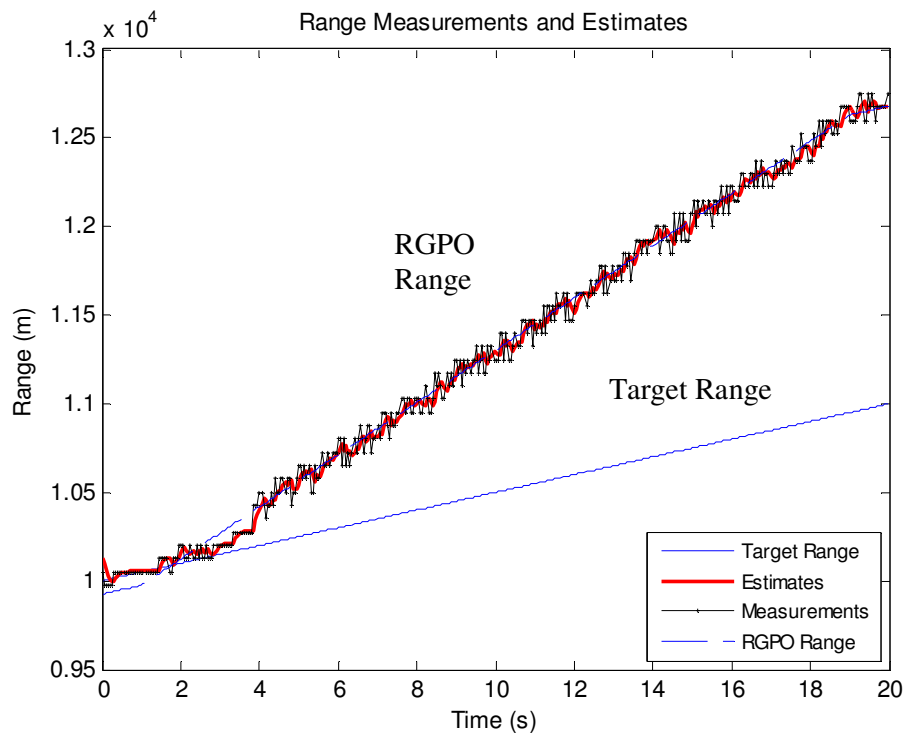


Figure 4-23: RGPO. Range measurements/estimates. $JSR_{spn} = 6$ dB, $JSR = 6$ dB, $s_{RGPO} = 1.3$ samples/s.

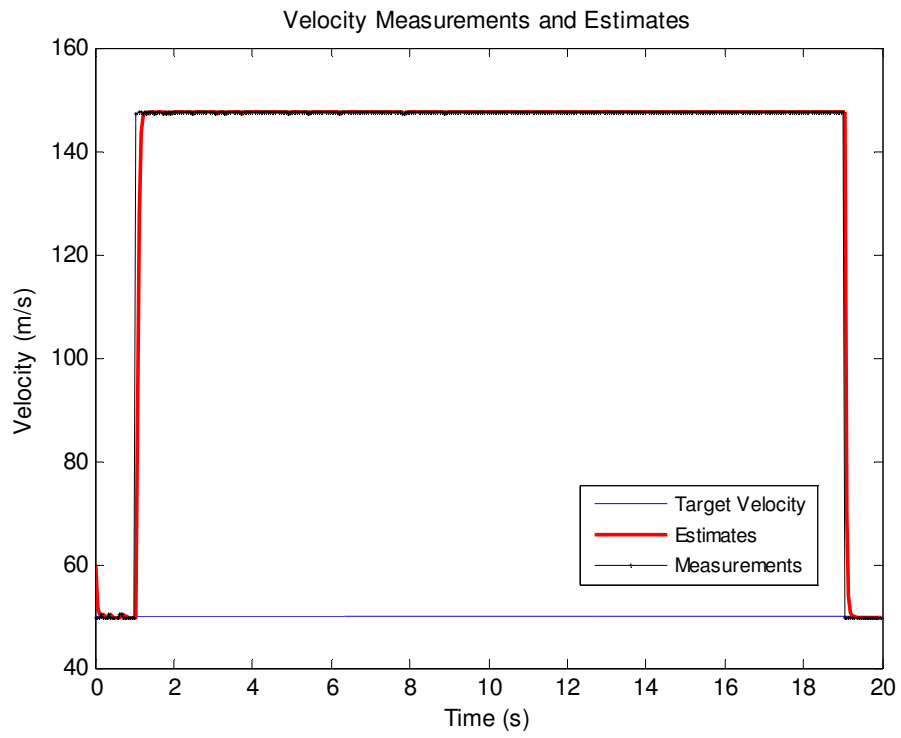


Figure 4-24: RGPO. Velocity measurements/estimates. $JSR_{spn} = 6$ dB, $JSR = 6$ dB, $s_{RGPO} = 1.3$ samples/s.

A similar simulation was performed but with $\text{JSR} = -6$ dB. The range tracking performance is shown in Figure 4-25 and Figure 4-26. The radar tracks the actual target for a while and starts to track the false target as the false target's pulse amplitude becomes higher than that of the target return. The same tracking behavior is observed for velocity in Figure 4-27.

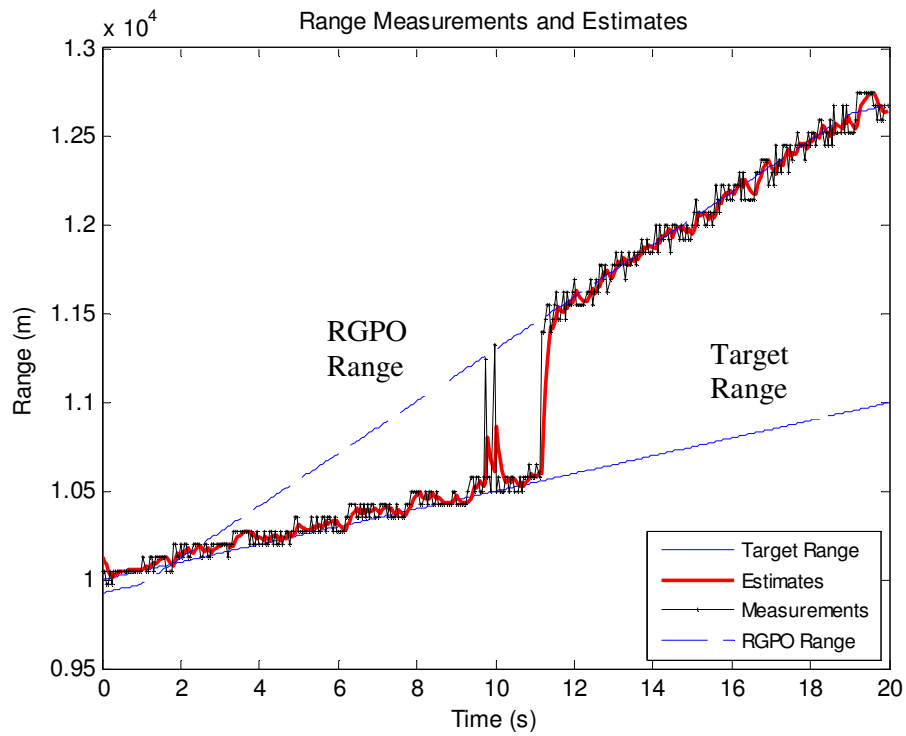


Figure 4-25: RGPO. Range measurements/estimates. $\text{JSR}_{\text{spn}} = 6$ dB, $\text{JSR} = -6$ dB, $s_{\text{RGPO}} = 1.3$ samples/s.

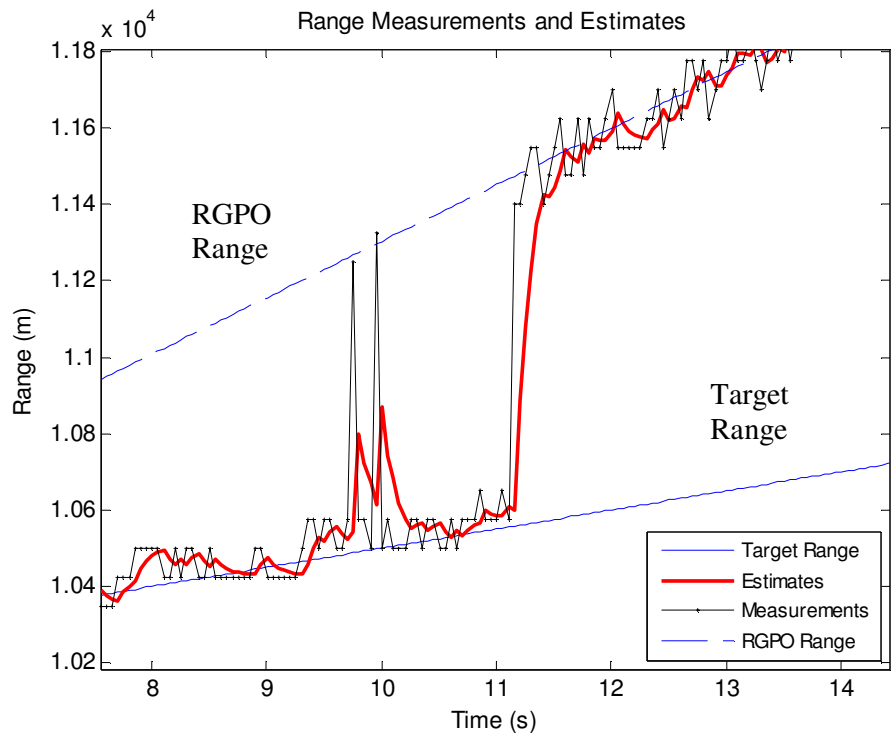


Figure 4-26: Close-up of Figure 4-25.

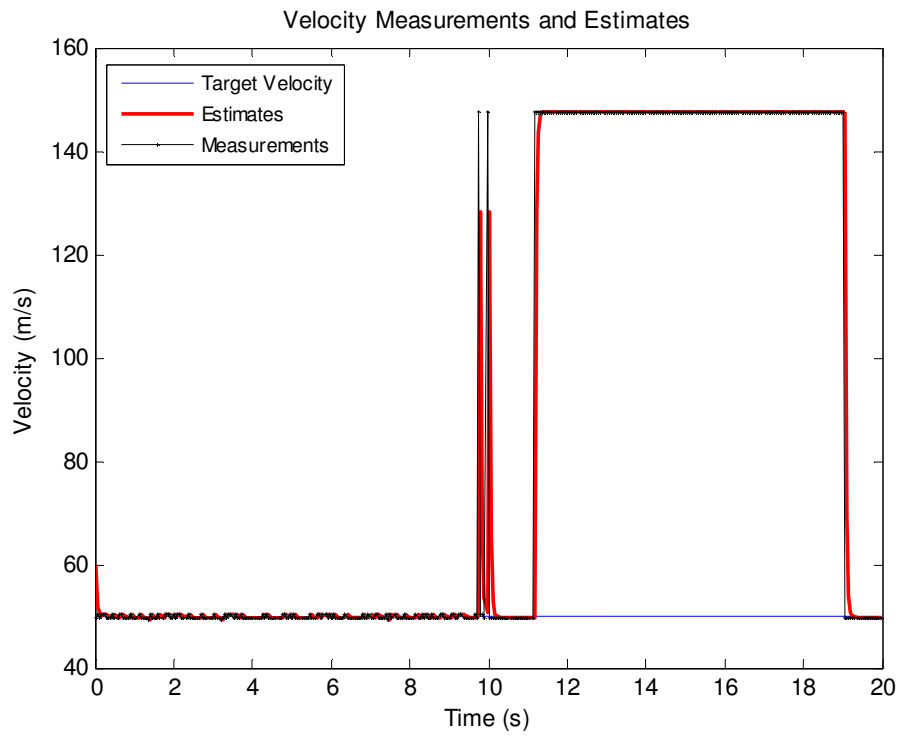


Figure 4-27: RGPO. Velocity measurements/estimates. $JSR_{spn} = 6$ dB, $JSR = -6$ dB, $s_{RGPO} = 1.3$ samples/s.

The results of a simulation with all the same parameters but with JSR = -7 dB is shown in Figure 4-28 and Figure 4-29. The jamming pulse is now even smaller than the actual target return, and the radar tracks the actual target.

Note the effect of spot noise used in the first 10 s of tracking is apparent in Figure 4-29. This is because the detected peak in this case is that of the target return and the target return is relatively smaller in amplitude with respect to spot noise than the jammer pulses of the previous cases.

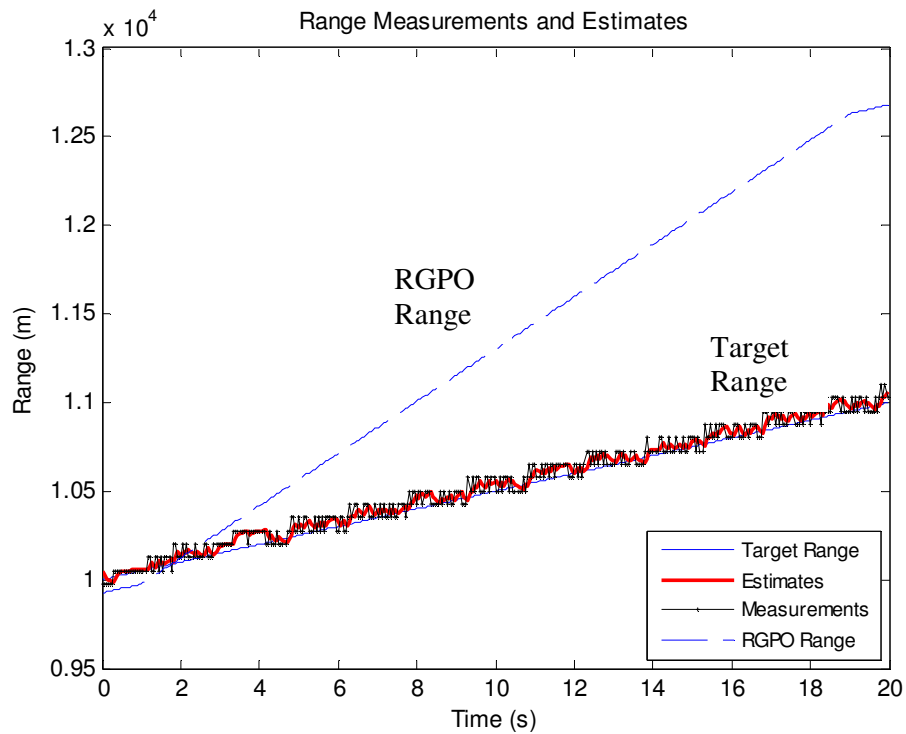


Figure 4-28: RGPO. Range measurements/estimates. $JSR_{spn} = 6$ dB, $JSR = -7$ dB, $s_{RGPO} = 1.3$ samples/s.

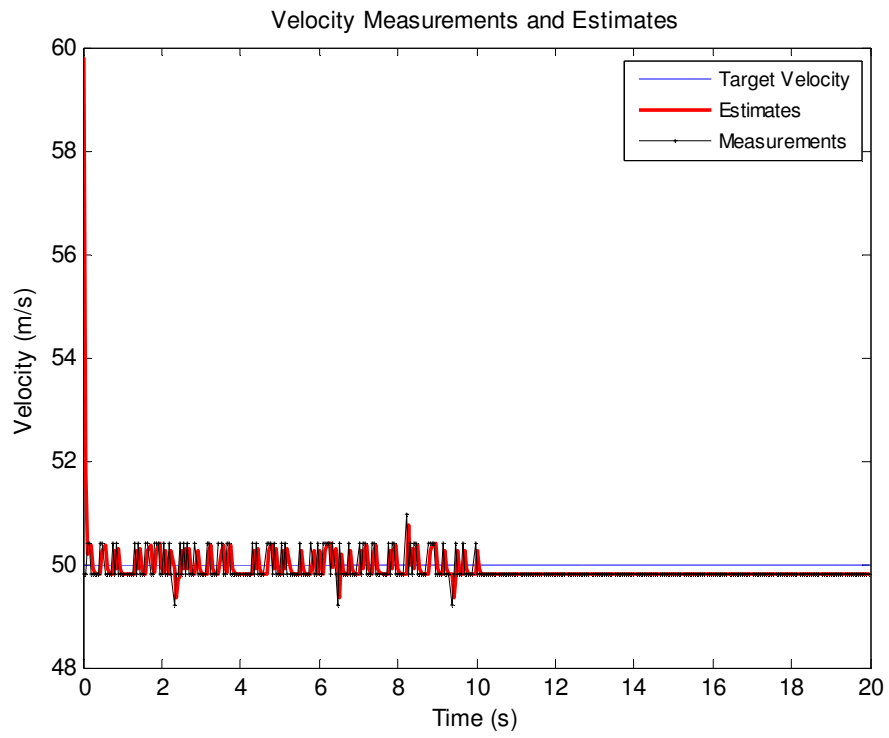


Figure 4-29: RGPO. Velocity measurements/estimates. $JSR_{spn} = 6$ dB, $JSR = -7$ dB, $s_{RGPO} = 1.3$ samples/s.

The results of a simulation with all the same parameters but with $s_{RGPO} = 2.7$ samples/s and $JSR = -3$ dB is shown in Figure 4-30. Compare that with Figure 4-25 where $JSR = -6$ dB and $s_{RGPO} = 1.3$. It is observed that the radar tracks the target for $JSR = -4$ dB and lower for $s_{RGPO} = 2.7$. For faster pull-offs (higher RGPO slopes), the break point for JSR where the target is tracked instead of the false target is higher.

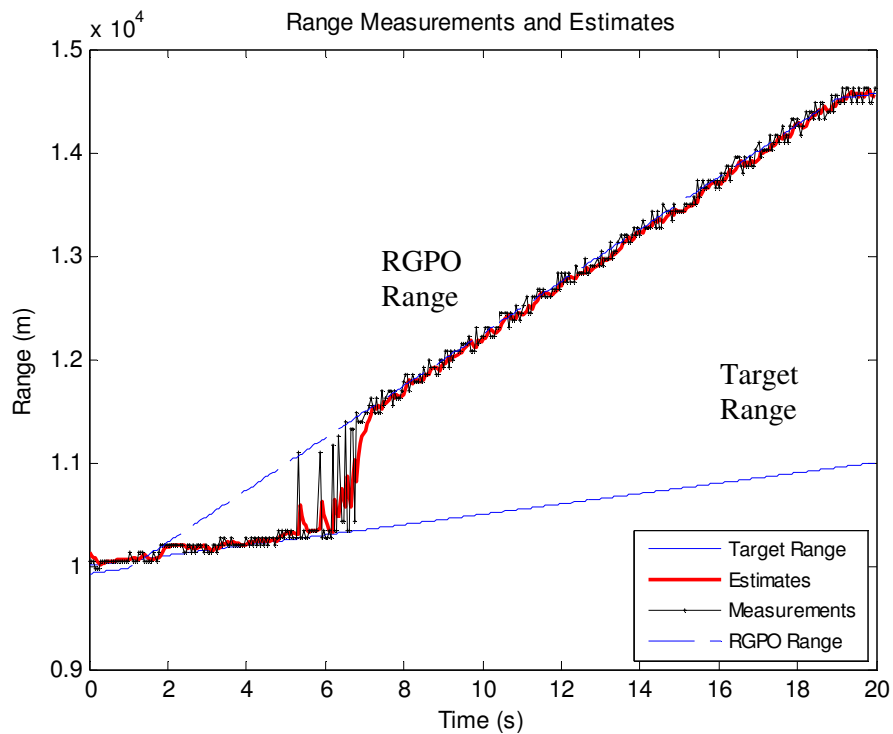


Figure 4-30: RGPO. Range measurements/estimates. $JSR_{spn} = 6$ dB, $JSR = -3$ dB, $s_{RGPO} = 2.7$ samples/s.

The effect of increasing the spot-noise power is discussed in Section 4.2.1 for spot-noise jamming alone. Track is dropped at JSR_{spn} greater or equal to 9 dB. Here however, the break point of JSR_{spn} is higher since the RGPO pulse has more power

than the target return. In a simulation with all the parameters the same as that of Section 4.2.1, this break point was observed to be $JSR_{spn}=12$ dB.

On the other hand, varying the parameter JSR has almost no effect as far as the jamming pulse is higher in peak amplitude in the PSD domain than the target return. This is because of the modeled radar receiver which detects the prominent return (single-target-detection) as the target to track.

In general, it is important how fast the RGPO pulse is pulled off and whether the tracking filter can follow. The former depends on the steepness of the sample-offset slope, that is, s_{RGPO} ; and the latter depends on the tracking filter's smoothing coefficient and the measurement update interval. If a large (close to 1, e.g. 0.98) smoothing coefficient together with a large update interval (e.g. 0.4 s) is used, the tracking filter is slow in convergence. The slope s_{RGPO} about 3 samples/s is a fast pull-off and it is observed that the track is dropped. In the simulations presented in this section, a smoothing coefficient of 0.8 and an update interval of 0.05 s are used. Thus the filter is fast enough not to cause any track-drops with even much higher s_{RGPO} values than 3 samples/s.

It is also observed that for even higher values of the slope (e.g. 30 samples/s) and with a fast-converging tracking filter, the radar cannot track the fast false target, but instead locks on the actual target.

4.2.3 RGPI

RGPI is very similar to RGPO. The jamming pulse is pulled in instead of being pulled off. A simulation was performed for the case with offset and gain profiles shown in Figure 4-31 and $JSR_{spn}=6$ dB and $JSR=6$ dB. Note the RGPI slope is negative and is -1.3 samples/s. Note also that the Doppler offset is wrapped around

as $10 \text{ kHz} - 1.3 \times 5000 \text{ Hz} = 3500 \text{ Hz}$. This corresponds to a velocity offset of 52.5 m/s; and an absolute velocity of 102.5 m/s, with the target's true velocity being 50 m/s.

The PSD for Snapshot 108, 170 and 384 is shown in Figure 4-32, Figure 4-33, and Figure 4-34, respectively. The measurement and estimate tracks are shown in Figure 4-35 and Figure 4-36. The radar tracks the false RGPI target both in range and velocity; and hence the false target creation is successful.

The results of similar simulations but with JSR set to -5 dB and -6 dB are shown in Figure 4-37 and Figure 4-38, respectively. For -5 dB, the radar tracks the target for a while and switches to the false target as the pulse amplitude of the false target gets larger. For -6 dB, the radar tracks the actual target.

The observation on tracking performance with steeper RGPI slopes is the same as of the RGPO in the previous section. With a slowly converging tracking filter and steeper slopes, the track is dropped. Also, for even steeper slopes (e.g. -20 samples/s) and with a fast-converging tracking filter, the radar cannot track the fast false target, but instead locks on the actual target.

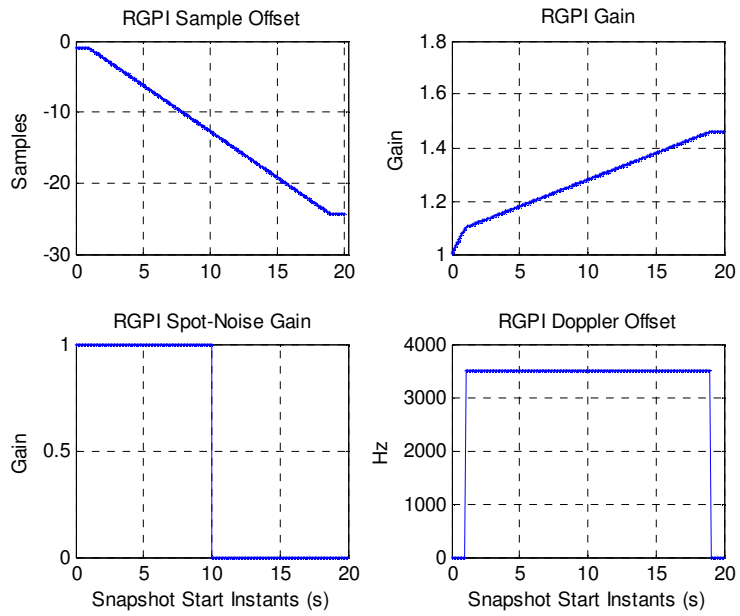


Figure 4-31: RGPI offset and gain profiles.

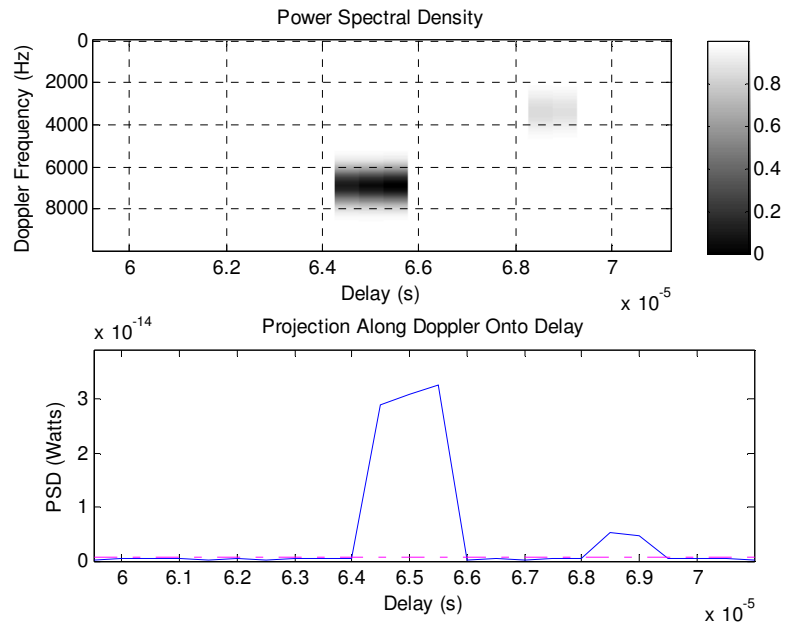


Figure 4-32: RGPI. Snapshot 108, jamming pulse starts pulling in. Spot-noise present. $s_{RGPI} = -1.3$ samples/s.

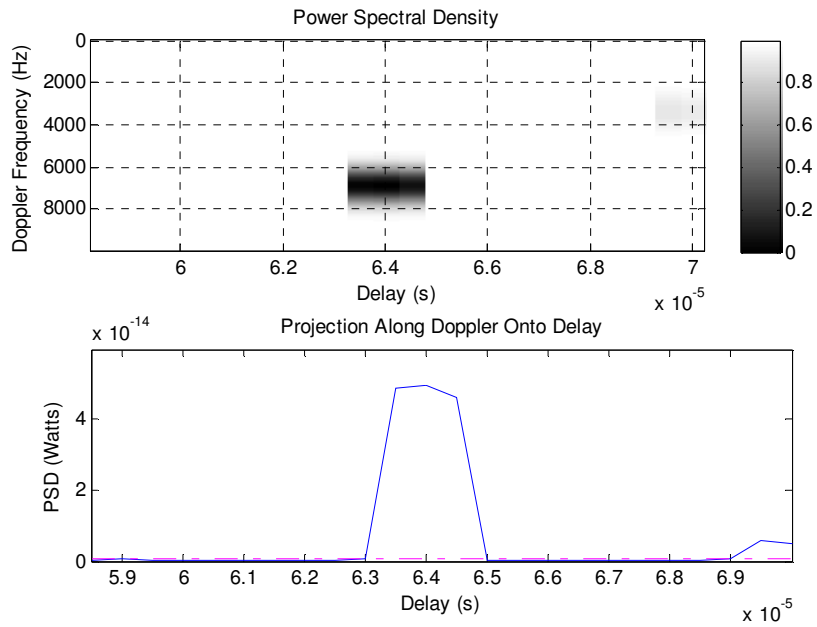


Figure 4-33: RGPI. Snapshot 170, further in pull-in. Spot-noise present. $s_{RGPI} = -1.3$ samples/s.

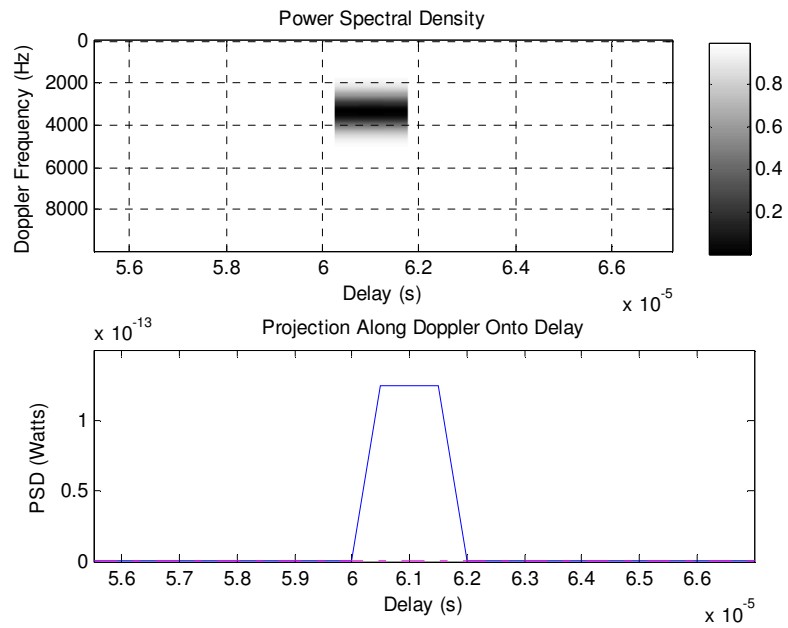


Figure 4-34: RGPI. Snapshot 384, hold period. Spot-noise not present. $s_{RGPI} = -1.3$ samples/s.

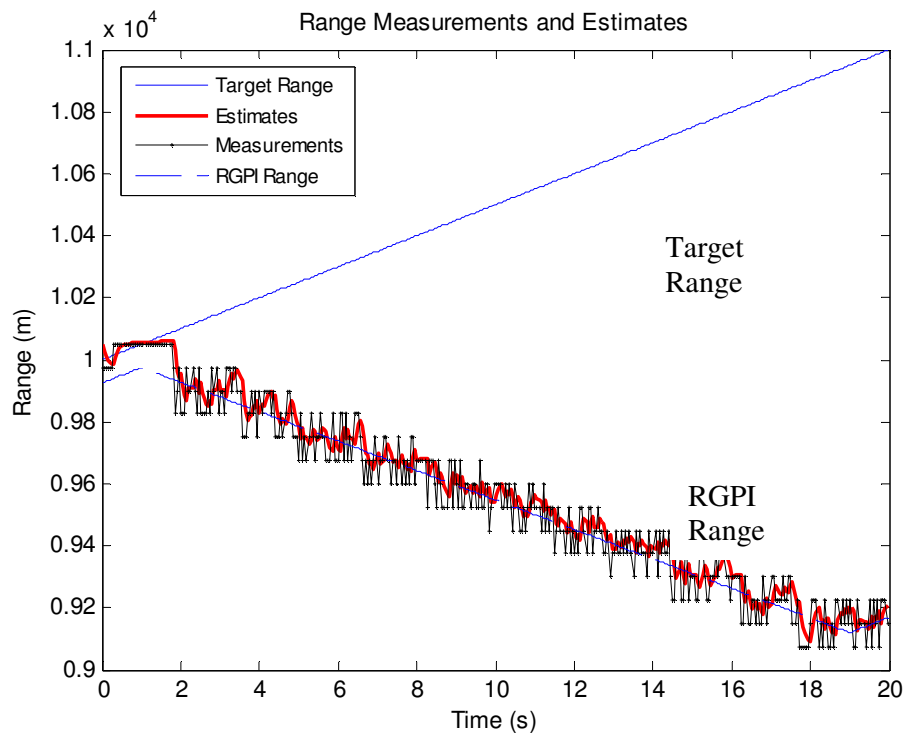


Figure 4-35: RGPI. Range measurements/estimates. $JSR_{spn} = 6$ dB, $JSR = 6$ dB, $s_{RGPI} = -1.3$ samples/s.

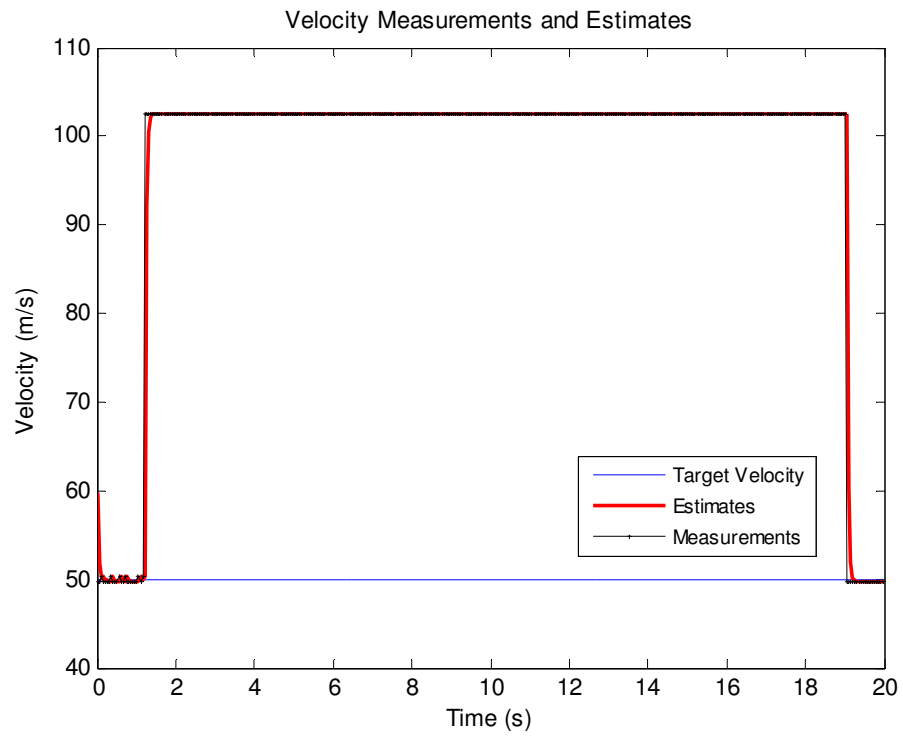


Figure 4-36: RGPI. Velocity measurements/estimates. $JSR_{spn} = 6$ dB, $JSR = 6$ dB, $S_{RGPI} = -1.3$ samples/s.

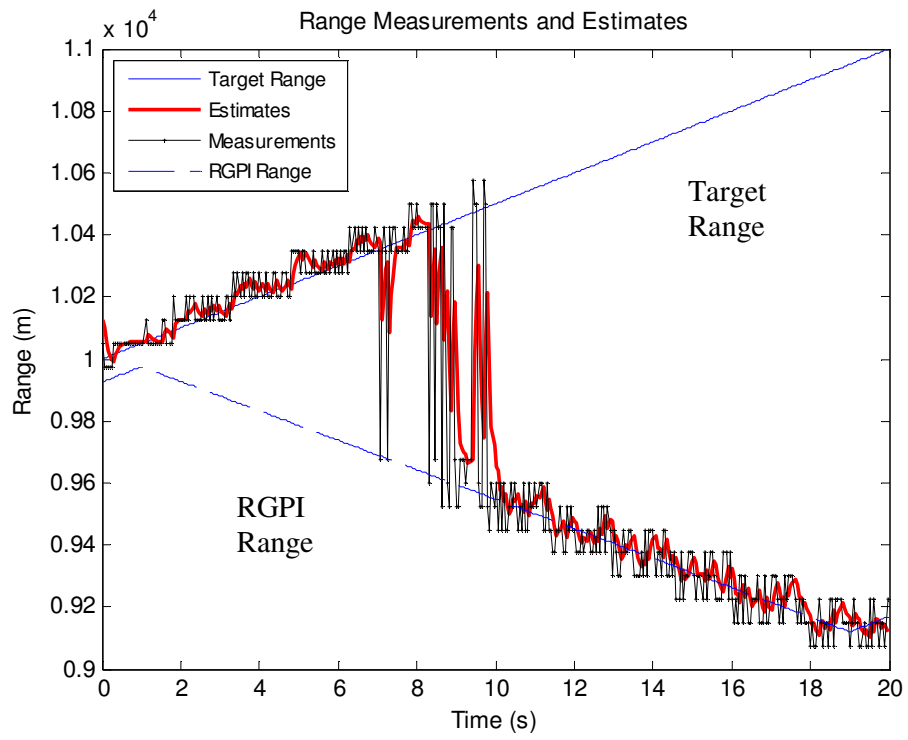


Figure 4-37: RGPI. Range measurements/estimates. $JSR_{\text{spn}} = 6$ dB, $JSR = -5$ dB, $SR_{\text{RGPI}} = -1.3$ samples/s.

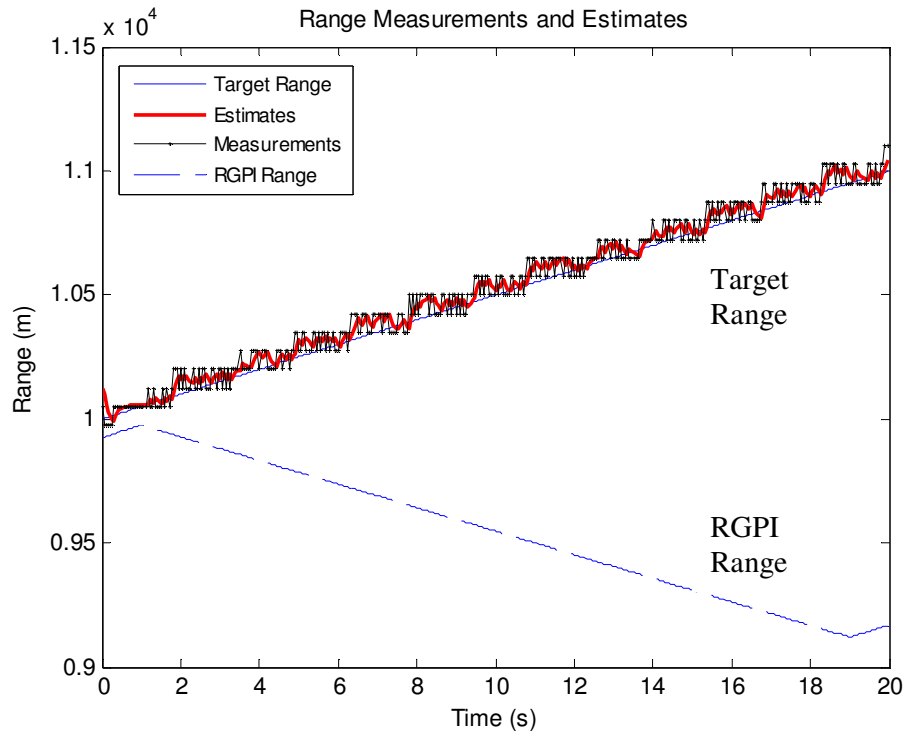


Figure 4-38: RGPI. Range measurements/estimates. $JSR_{spn} = 6$ dB, $JSR = -6$ dB, $SR_{RGPI} = -1.3$ samples/s.

4.2.4 Overlapped RGPO

Here two jamming pulses are used instead of one as in RGPO technique. The offset and gain profiles overlap as shown in Figure 4-39, which displays the profiles for the RGPO pulse and Figure 4-40, which displays profiles for overlapping RGPO pulse. Usually the overlapping pulse starts later in time. Here the overlapping pulse appears 0.5 s later than the RGPO pulse since the pulse gain for the overlapping pulse is 0 for the first 0.5 s.

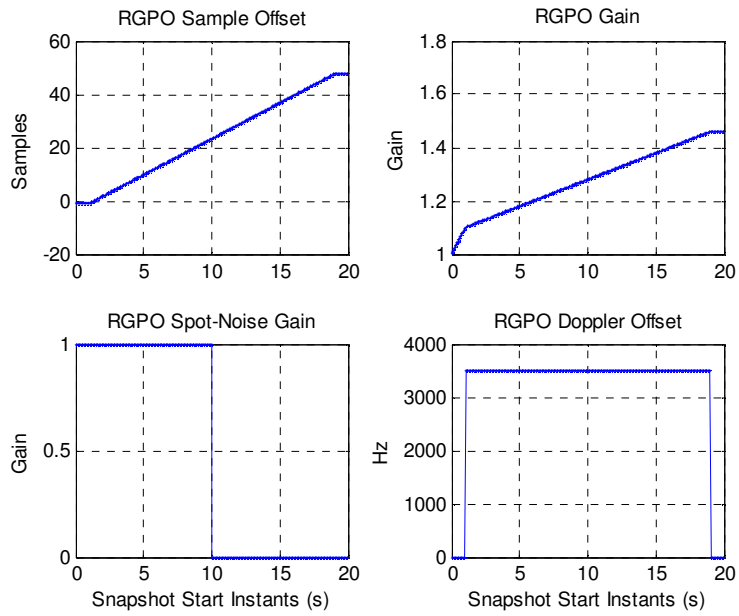


Figure 4-39: RGPO offset and gain profiles. $S_{RGPO} = 2.7$ samples/s.

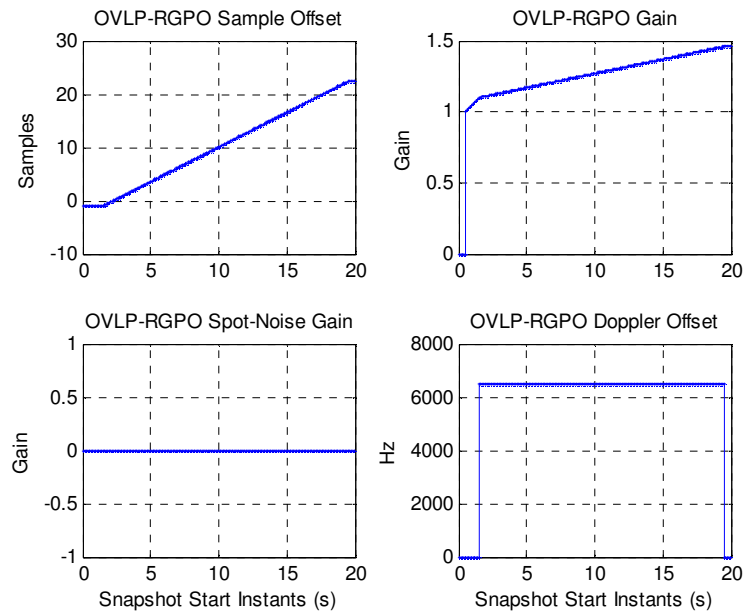


Figure 4-40: Overlapping RGPO pulse's offset and gain profiles. $S_{OVLPGPO} = 1.3$ samples/s.

The slopes in pull-off periods are 2.7 samples/s and 1.3 samples/s for the RGPO pulse and overlapping pulse, respectively. The RGPO pulse is pulled off faster. Note that the Doppler offset profile for RGPO is wrapped around (modulo 10 kHz) in frequency. The velocity offsets for RGPO and overlapping RGPO pulse can be calculated as $2.7 \times 5000 \text{ Hz} - 10 \text{ kHz} = 3500 \text{ Hz}$ and $1.3 \times 5000 \text{ Hz} = 6500 \text{ Hz}$ respectively. The corresponding absolute velocities are 102.5 m/s and 147.5 m/s, respectively. Note that even though the RGPO pulse is pulled off faster, its velocity to be measured is less than that of the overlapping RGPO pulse due to the frequency wrapping in the Doppler frequency dimension.

A simulation was run for $\text{JSR}_{\text{spn}} = 6 \text{ dB}$ and $\text{JSR} = 6 \text{ dB}$. Figure 4-41 and Figure 4-42 display the tracking results for range and velocity, respectively. The radar measurements hop between the RGPO and overlapped RGPO pulses for a while but eventually the radar tracks the false target created by the RGPO pulse in range and velocity.

The reason for the hopping in the measurements is that the overlapped RGPO and RGPO pulses have almost the same but slightly different gains due to the presence of thermal noise and due to the 0.5 s offset between the respective gain profiles. Since the detection stage performs a peak detection (single-target detection), whichever pulse has a higher peak in the PSD domain is assigned to be the one producing the measurement.

Figure 4-43 and Figure 4-44 display the range measurements and estimates for simulations with all parameters the same but JSR set to be -6 dB and -7 dB, respectively. Compare those with Figure 4-25 and Figure 4-28, where similar results for an RGPO pulse with $s_{\text{RGPO}} = 1.3 \text{ samples/s}$ are displayed. Thus, the overlapped RGPO is not much different from RGPO. Depending on the peak value in the PSD in the detection stage, the radar tracks either the target or the false targets created by RGPO or overlapped RGPO pulses.

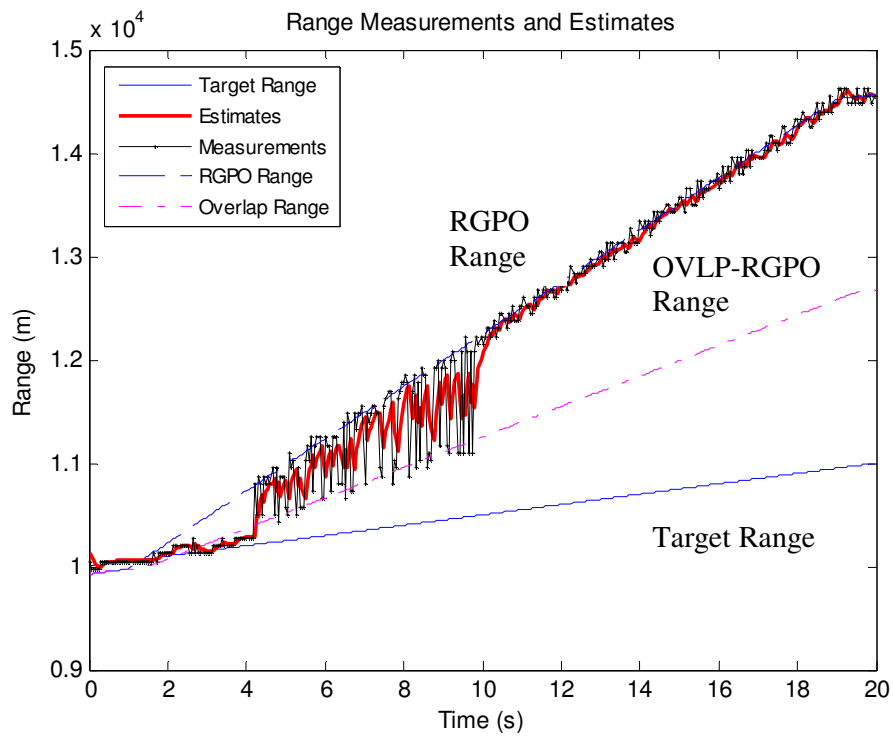


Figure 4-41: Overlapped RGPO. Range measurements/estimates. $JSR_{spn} = 6$ dB, $JSR = 6$ dB, $s_{RGPO} = 2.7$ samples/s, $s_{OVL- RGPO} = 1.3$ samples/s.

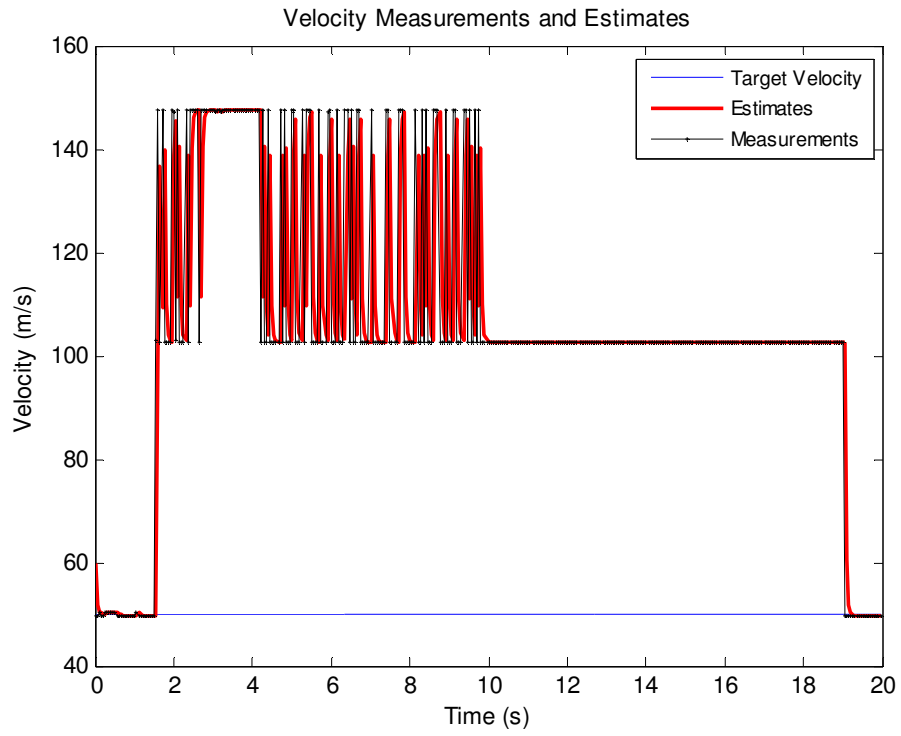


Figure 4-42: Overlapped RGPO. Velocity measurements/estimates. $JSR_{spn} = 6$ dB, $JSR = 6$ dB, $s_{OVLPRGPO} = 2.7$ samples/s. $s_{RGPO} = 1.3$ samples/s.

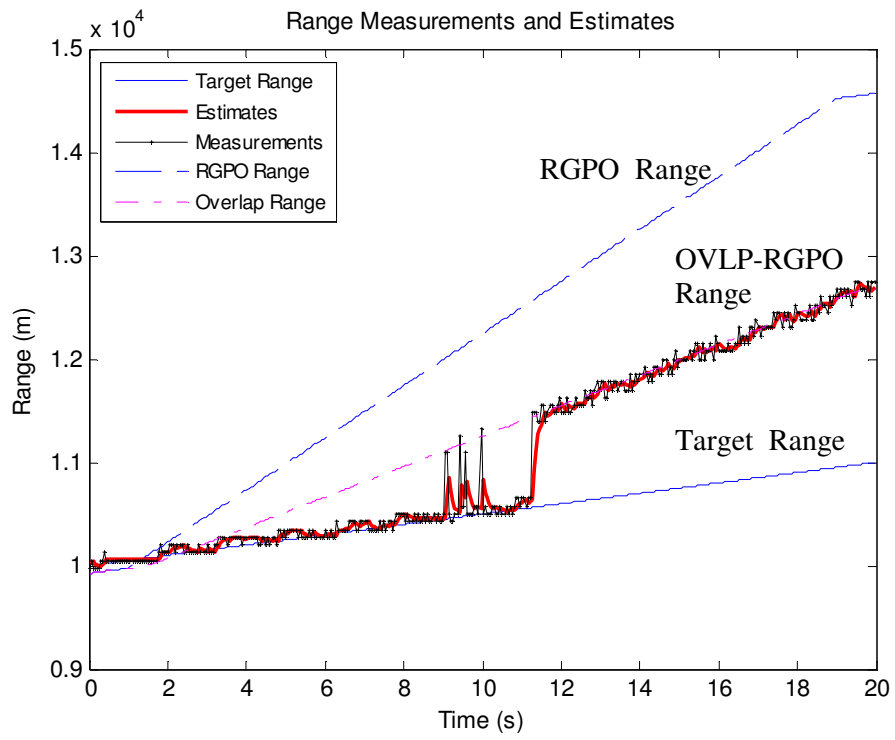


Figure 4-43: Overlapped RGPO. Range measurements/estimates. $JSR_{spn} = 6$ dB, $JSR = -6$ dB, $s_{RGPO} = 2.7$ samples/s, $s_{OVL- RGPO} = 1.3$ samples/s.

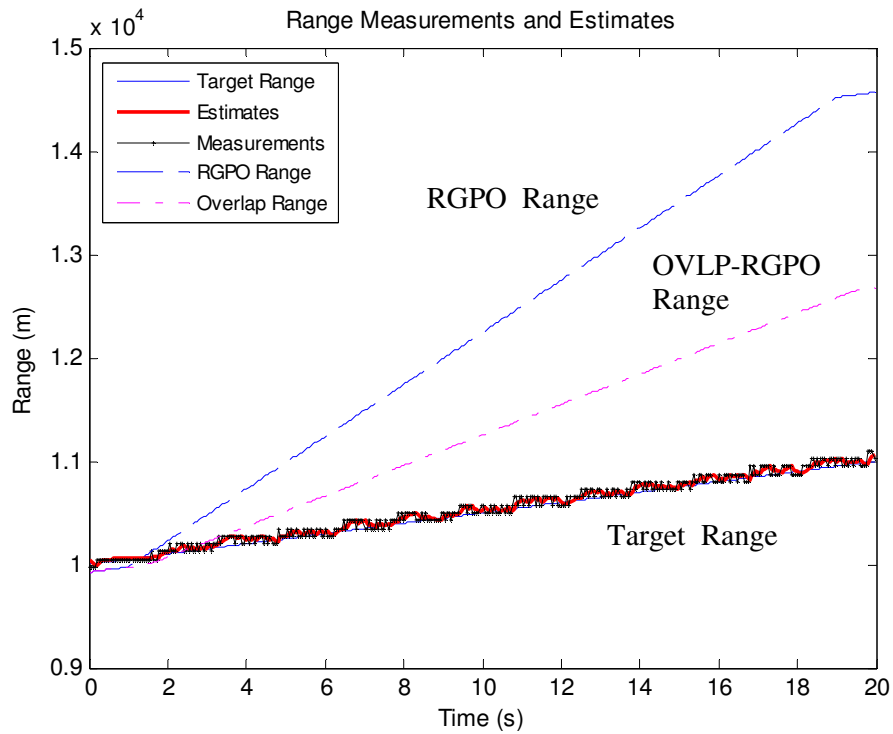


Figure 4-44: Overlapped RGPO. Range measurements/estimates. $JSR_{spn} = 6$ dB, $JSR = -7$ dB, $s_{RGPO} = 2.7$ samples/s, $s_{OVLP-RGPO} = 1.3$ samples/s.

4.2.5 RGPO with hold-out

This technique is similar to overlapped RGPO with the difference that the overlapping pulse stands at the same location and does not move relative to the target return. The RGPO pulse is pulled off towards the hold-out pulse and they fully overlap in the hold period.

A simulation was run for $JSR_{spn} = 6$ dB and $JSR = 6$ dB. The offset and gain profiles are shown in Figure 4-45 and Figure 4-46. The pull-off slope of the RGPO pulse is 1.3 samples/s.

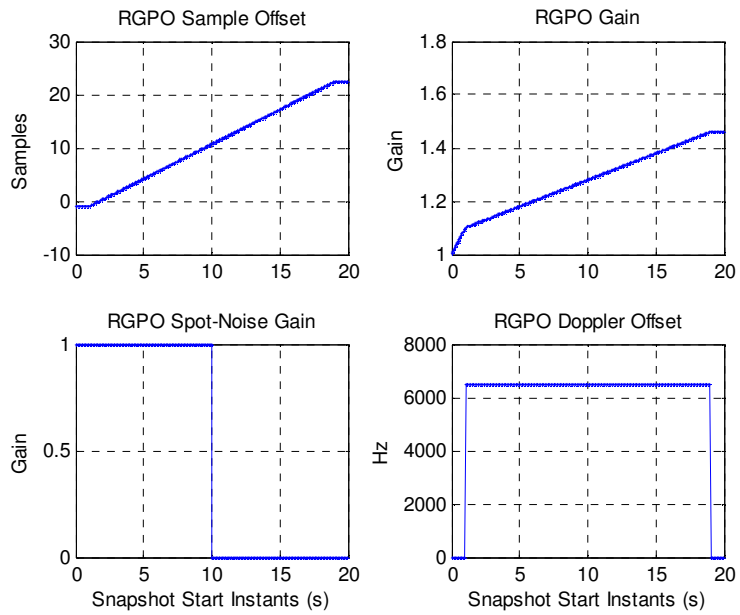


Figure 4-45: RGPO with hold-out. RGPO offset and gain profiles. $s_{RGPO} = 1.3$ samples/s.

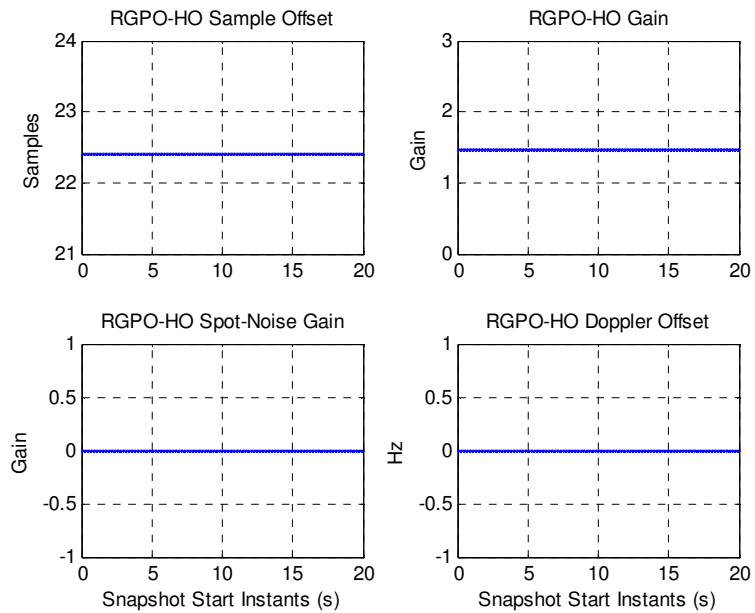


Figure 4-46: RGPO with hold-out. Hold-out offset and gain profiles.

The measurement and estimate tracks are shown in Figure 4-47 and Figure 4-48. As soon as the hold-out pulse moves into the range gate, the radar starts to track the false target due to the hold-out pulse. The hold-out gain is set to be a constant, while the gain of the RGPO pulse slowly increases to that constant. Thus, when the range gate advances to include the hold-out pulse, the gain of the RGPO pulse is lower, and because of the single-target detection implemented in the simulator, the radar detects the hold-out pulse as the prominent target. As long as either the RGPO pulse or the hold-out pulse has higher peaks in the PSD domain than that of the target return, the radar locks on the false target.

Since the hold-out pulse does not move relative to the target return, its relative velocity is 0. Thus, the absolute velocity measurements are 50 m/s, the same as that of the target, as the hold-out pulse is being tracked.

The result of a simulation with all the parameters kept the same but with JSR = -6 dB is shown in Figure 4-49. Similar to the results of the RGPO in Section 4.2.2, the radar tracks the false target after tracking the actual target for a while. However, this time, radar tracks the hold-out pulse as governed by the gains set to RGPO and hold-out pulses. The radar tracks the actual target for JSR = -7 dB and lower. The case with JSR = -7 dB is shown in Figure 4-50.

The result of a simulation with JSR = -3 dB and the pull-off slope of the RGPO pulse set to 2.7 samples/s is shown in Figure 4-51. Compare this to Figure 4-30 for a similar result. Here, the radar tracks the target for a while, switches to the false target due to RGPO pulse and then locks onto the false target due to the hold-out pulse.

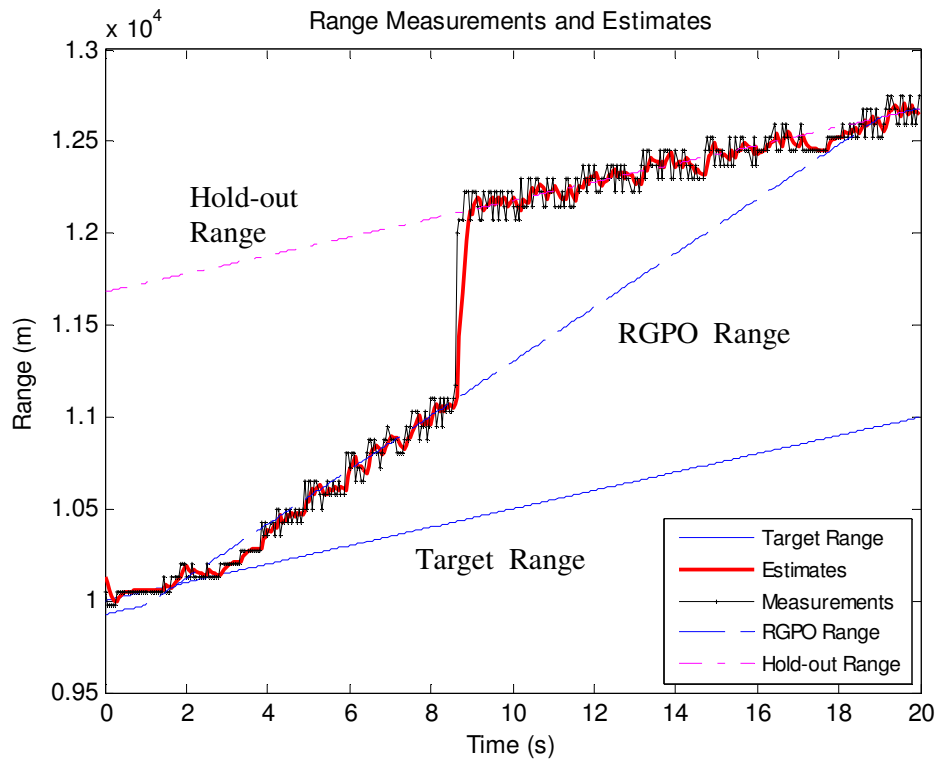


Figure 4-47: RGPO with hold-out. Range measurements/estimates. $JSR_{spn} = 6$ dB, $JSR = 6$ dB, $s_{RGPO} = 1.3$ samples/s.

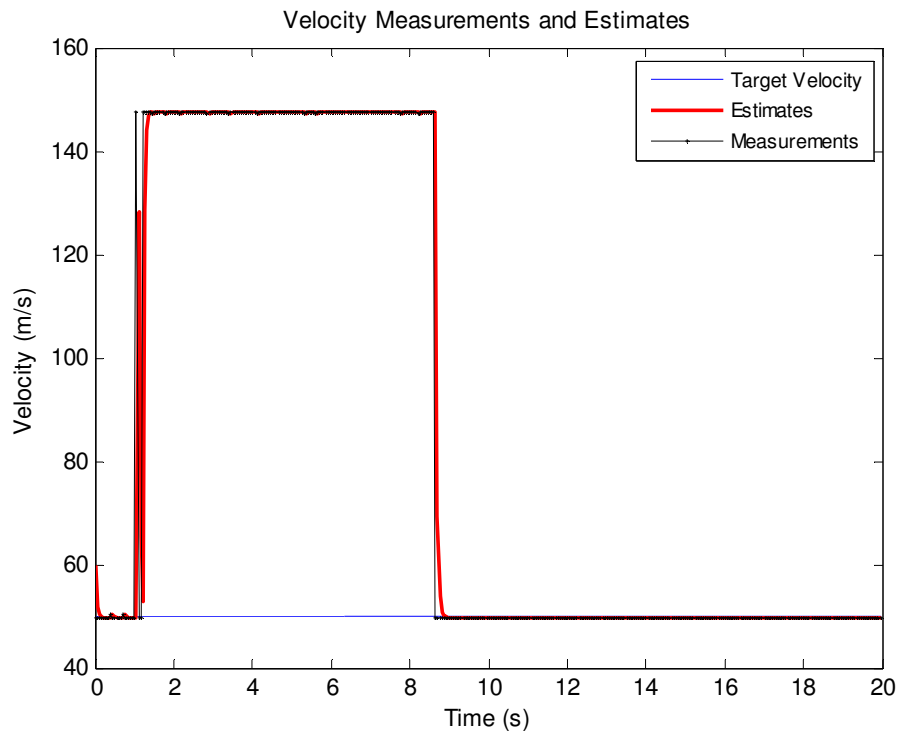


Figure 4-48: RGPO with hold-out. Velocity measurements/estimates. $JSR_{spn} = 6$ dB, $JSR = 6$ dB, $s_{RGPO} = 1.3$ samples/s.

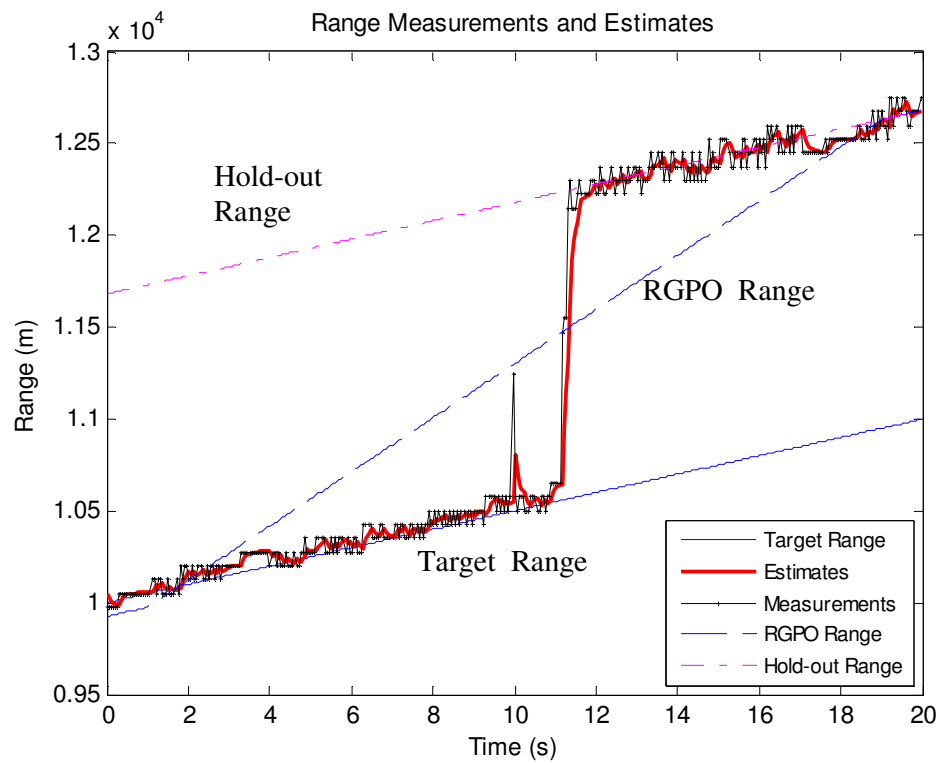


Figure 4-49: RGPO with hold-out. Range measurements/estimates. $JSR_{spn} = 6$ dB, $JSR = -6$ dB, $S_{RGPO} = 1.3$ samples/s.

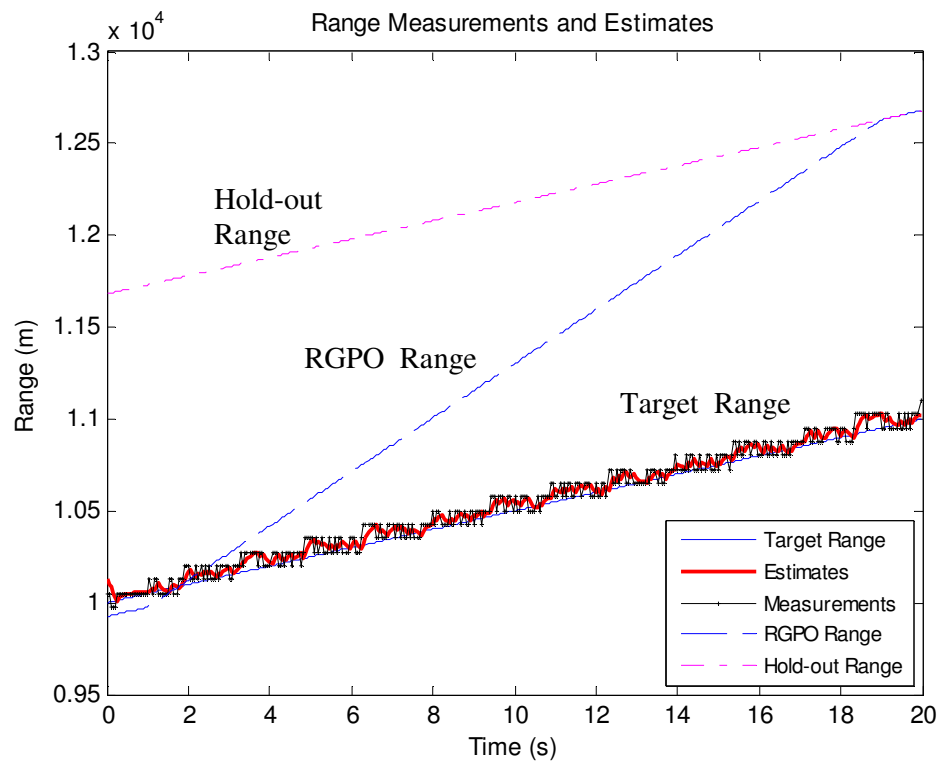


Figure 4-50: RGPO with hold-out. Range measurements/estimates. $JSR_{spn} = 6$ dB, $JSR = -7$ dB, $s_{RGPO} = 1.3$ samples/s.

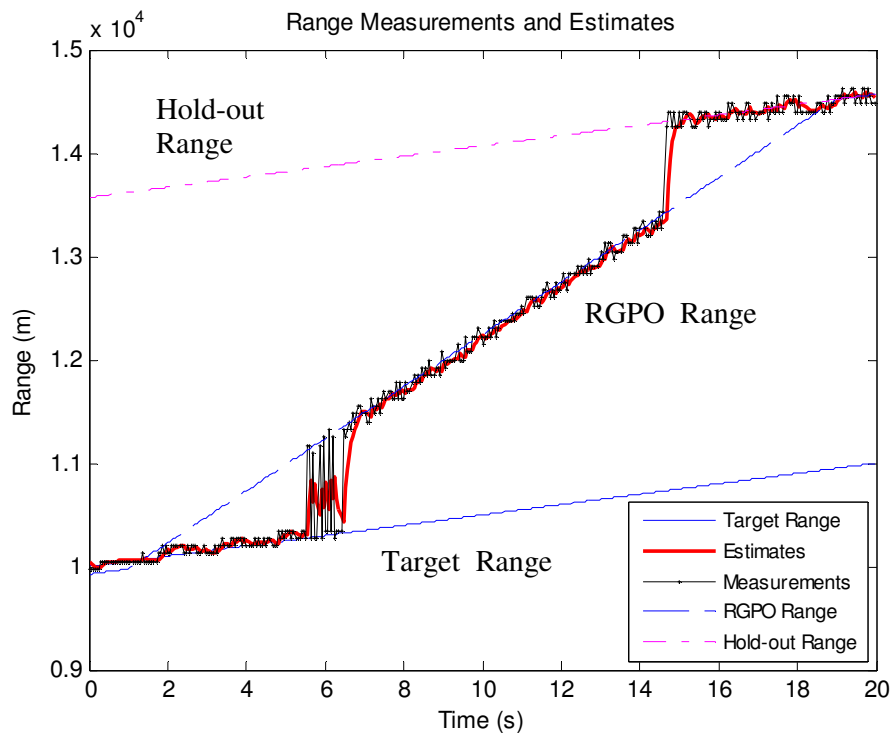


Figure 4-51: RGPO with hold-out. Range measurements/estimates. $JSR_{spn} = 6$ dB, $JSR = -3$ dB, $s_{RGPO} = 2.7$ samples/s.

CHAPTER 5

CONCLUSIONS

Self protection electronic warfare systems require effective jamming techniques. The most critical point in designing a jamming technique is to have detailed information about the receiver characteristics of the threat radars. Simulation of a radar receiver thus enables a fast and comprehensive evaluation of jamming techniques' effectiveness against various threat radars given their receiver characteristics.

In this study, we simulated a radar receiver based on a certain radar model that includes a multiple-target search and single-target track functionality. The simulation also includes a jamming signal simulator that can be used to investigate the effectiveness of a number of different jamming techniques on the simulated radar model in regard to target detection and tracking performance.

The radar model is of pulse-Doppler. A sector scanning receiver antenna in the search mode and a fixed directive receiver antenna in the single-target track mode are assumed. Various radar parameters and the geometry of the scenario such as antenna pattern, received power, range variations of the targets are all included in the model. The detection of targets produces range, Doppler velocity and azimuth angle of each target. The radar turns its antenna towards the direction of one of the targets that is decided to be tracked. Then the tracking algorithm that is incorporated into the simulation tracks the target throughout its course. When the jamming signals are included in the simulation, the effectiveness of the jamming technique

that is being used can be investigated by observing its effects in detection and tracking.

The employed jamming techniques include noise jamming (spot-noise) and RGPO based techniques. Variations of RGPO such as RGPO with hold-out and overlapped RGPO techniques are developed and investigated. RGPO techniques use spot-noise as well in the dwell and in part of the pulse pulling periods. The jamming effectiveness is evaluated for varying jamming-to-signal ratios (JSR). For better identifying the effectiveness of the jamming noise and jamming pulse separately, separate parameters, JSR_{spn} and JSR, respectively, are used to vary the strength of the jammer components.

Jamming performance of spot noise is dependent on the parameter JSR_{spn} . For the parameter larger than a certain value, the track is dropped and the radar cannot track the target. For values smaller than that break point, the radar can track the target. The value of the break point depends on the radar parameters used such as the measurement update interval (snapshot offset) and tracking filter's smoothing coefficient; and can be evaluated easily by using the simulator program developed in this study. With the parameters used in this thesis, the break point is found to be 9 dB.

For the RGPO technique and its variations, the effectiveness is determined by JSR, which determines the strength of the jamming pulse. The pulse amplitudes in techniques of overlapped RGPO and RGPO with hold-out are adjusted by using separate gain coefficients, in addition to a common value of the parameter JSR, for RGPO pulse and the jamming pulse of the respective technique.

For the parameter JSR larger than a certain value, the radar tracks the false target created by the RGPO techniques instead of the actual target. The velocity of the false target is coordinated with its range. Thus false target tracking is achieved both for range and velocity. The break point of JSR for false target tracking is different for each technique and can be evaluated by the developed radar simulator program

for different radar settings. There is not much operational difference between the RGPO variations in regard to that the radar model simulated in this study performs single target detection (single peak detection) and single target tracking and hence tracks the most prominent return. Thus, depending on the amplitudes of the pulses within the range gate, radar tracks the actual target or false targets.

The effect of spot noise used within the RPGO techniques is similar when the spot noise jamming is used alone. Track is dropped when the parameter JSR_{spn} is larger than a certain value. However, this time the break point is higher than that when spot noise is used alone if the amplitude of the RGPO pulse present in the return is higher than the actual target's return.

It is usually difficult to find detailed information about the parameter settings of jamming techniques in the literature, as this can be obtained only through classified defense work. This study however models radar receiver and jamming techniques very realistically making the current investigation important about the jamming effectiveness.

REFERENCES

1. G. R. Curry, *Radar System Performance Modeling*, 2nd Ed., Artech House: Boston, 2005.
2. N. Levanon and Eli Mozeson, *Radar Signals*, Wiley: Hoboken, NJ, 2004.
3. P. K. Willet, "Fixed-Lag Alpha-Beta Filter for Target Trajectory Smoothing," *IEEE Trans. Aerospace and Electronic Systems*, Vol. 40, No. 4, October, 2004, pp. 1417-1421.
4. M. O. Kolawole, *Radar Systems, Peak Detection and Tracking*, Newnes: Boston, MA, 2002.
5. K. Alexiev, "A Matlab Tool for Development and Testing of Track Initiation and Multiple Target Tracking Algorithms", *Information & Security*. Vol. 9, 2002, pp. 166-174.
6. M. I. Skolnik, *Introduction to Radar Systems*, 3rd Ed., McGraw-Hill: New York, NY, 2001.
7. Y. Bar-Shalom, X. R. Li, T. Kirubarajan, *Estimation with Applications to Tracking and Navigation*, Wiley:New York, NY, 2001.
8. B. R. Mahafza, *Radar Systems Analysis and Design Using Matlab*, Chapman & Hall / CRC: Boca Raton, FL, 2000.
9. S. Blackman, R. Popoli, *Design and Analysis of Modern Tracking Systems*, Artech: Norwood, MA, 1999.
10. G. W. Stimson, *Introduction to Airborne Radar*, 2nd Ed., Scitech:Mendham, NJ, 1998.
11. F. E. Nathanson, J. P. Reilly, M. N. Cohen, *Radar Design Principles*, McGraw-Hill: New York, NY, 1990.
12. Nadav Levanon, *Radar Principles*, Wiley: New York, NY, 1988.
13. J. L. Eaves and E. K. Reedy, *Principles of Modern Radar*, Van Nostrand Reinhold:New York, NY, 1987.

14. R. G. Willey, *Electronic Intelligence: The Analysis of Radar Signals*, Artech:Norwood, MA, 1982.
15. August W. Rihaczek, *Principles of High Resolution Radar*, McGraw-Hill: New York, NY, 1969.
16. P. Stoica and R. Moses, *Introduction to Spectral Analysis*, Prentice Hall:New Jersey, 1997.
17. Benjamin C. Kuo, *Automatic Control Systems*, 6th ed., Prentice-Hall:New York, NY, 1991.